Technical Report
TR-15-07
August 2016

Montmorillonite phase behaviour

Relevance for buffer erosion in dilute groundwater

Magnus Hedström
Emelie Ekvy Hansen
Ulf Nilsson

SVENSK KÄRNBRÄNSLEHANTERING AB

SWEDISH NUCLEAR FUEL
AND WASTE MANAGEMENT CO

Box 250, SE-101 24 Stockholm
Phone +46 8 459 84 00
skb.se

SVENSK KÄRNBRÄNSLEHANTERING

ISSN 1404-0344
SKB TR-15-07
ID 1494816
August 2016

Montmorillonite phase behaviour

Relevance for buffer erosion in dilute groundwater

Magnus Hedström, Emelie Ekvy Hansen, Ulf Nilsson
Clay Technology AB

Abstract

During or after a glaciation, water with low salinity may reach the depth of a KBS-3 repository for spent nuclear fuel. Under such conditions the montmorillonite fraction of a bentonite buffer may turn into a liquid colloidal state (sol) at the interface between the thicker clay paste and groundwater. The montmorillonite sol could thus be transported away with the flowing groundwater, leading to erosion of bentonite buffer. As sol formation is largely a problem for sodium-dominated montmorillonite most of the work presented here has been focussed on sodium montmorillonite.

The sol is one of the three major montmorillonite phases that are characterized on a macroscopic scale in the report. The other two phases are termed, paste, and gel. The paste is dominated by osmotic repulsions and expands in contact with excess electrolyte. In aqueous solutions with low ionic strength the paste will eventually turn into a sol as it expands.

In the gel phase the montmorillonite particles are connected through attractive forces that balance osmosis. It is demonstrated that gels do not expand in contact with excess electrolyte. Rotating vane rheometry measurements on gels of montmorillonite extracted from Asha 505 bentonite show that the gels have a yield strength that is higher than expected shear stresses from the seeping water in a future repository.

Phase diagrams for three different sodium montmorillonites are presented. The variables in the phase diagrams were clay concentration and NaCl concentration. The main difference between the three clays is the critical coagulation concentration, CCC, here identified as the NaCl concentration where a gel is observed. Wyoming montmorillonite from MX-80 bentonite has the highest CCC of about 20 mM NaCl, while both Kutch (Asha 505 bentonite) and Milos (Deponit CA-N) have distinctly lower CCC of about 4 and 6 mM respectively.

New evidence is presented that support the notion of positive edge charges and the spillover model, which states that at low salinity the spillover of the negative potential from the face to the edge creates a barrier for edge-to-face interaction. Above the CCC this barrier is overcome and the positive edge of one clay layer is discernible to a second clay layer, which leads to edge-to-face bond formation.

Based on the ideas of percolation theory an experiment was devised in which gel stability was examined at different temperatures. From this experiments, the enthalpy of edge-to-face bond formation was evaluated. While no theory yet exists for how to incorporate edge-to-face interactions into a general model for bentonite expansion and erosion, the knowledge of the magnitude of the binding enthalpy could serve as a guideline for a simplified model beyond the DLVO or primitive model treatment for parallel clay layer.

Erosion experiments in artificial fractures were conducted using Wyoming-Na montmorillonite (Wy-Na) or an equal mixture of sodium and calcium montmorillonite (Wy-Ca/Na). The dry density of the emplaced montmorillonite was nominally 1260 kg/m^3 in all erosion tests. The tests showed that Wy-Na only eroded when the flowing water had NaCl concentration below the CCC. Above the CCC the expansion of montmorillonite into the fracture was limited to a few mm and no montmorillonite was detected in the effluent.

Below the CCC the expansion of the montmorillonite progressed further, but the paste only reached about 1 cm into a 120 µm fracture. Outside the paste there was under stagnant conditions a build-up of a sol-like phase that could be transported away in high flow and that also showed a Rayleigh-Taylor instability, another signature of a liquid phase. The density of this sol was measured to be around 30 g/l. The sol was also found to be eroded by gravity under stagnant conditions.

Erosion was significant below the CCC. At the flow rates tested the build-up of sol around the paste was small. Most of sol was transported away as it was being formed. For Wy-Ca/Na in a horizontal 120µm fracture, the measured erosion rate was 65 $kg/(m^2 \cdot year)$ using 1 mM NaCl (aq) at the lowest tested flow velocity, 850 m/year. Comparable erosion rates were obtained for Wy-Ca/Na using Grimsel water simulant (0.7 mM NaCl and 0.14 mM $CaCl_2$) and horizontal fracture setup.

On the other hand, gravity was shown to have a large impact on erosion rates. Using the same clay and Grimsel water simulant, the unit erosion rate was evaluated to 170 kg/($m^2 \cdot$ year) despite the water being stagnant. Under the assumption of a fracture aperture of 50 μm and that swelling into the fracture in a repository is of the same magnitude as in the artificial fracture tests, that is on the centimetre scale, this unit erosion rate translates to a montmorillonite mass loss of 600 kg over a 10 000 year period. Thus under glacial water conditions large erosion of buffer bentonite as an effect of colloidal sol formation cannot be ruled out.

Erosion rates depend on the fracture aperture and the circumference of the paste-to-sol border which in turn depend on the extent the clay swell into the fracture. The observation in this work is that swelling of paste is limited to the centimetre scale also for ionic strengths well below the CCC. However, if there is a slow expansion, not detected on the timescale of the experiments, actual erosion rates could be higher.

Sammanfattning

Under eller efter en glaciation, kan vatten med låg salthalt nå ned till KBS-3 slutförvaret för använt kärnbränsle. Under sådana betingelser kan montmorillonitfraktionen hos bentonitbufferten omvandlas till ett flytande kolloidalt tillstånd (sol) vid gränsen mellan den fastare lerpastan och grundvattnet. Montmorillonitens solfas kan således transporteras bort med flödande grundvatten, vilket leder till erosion av bentonitbuffert. Eftersom uppkomst av sol i hög grad är ett problem relaterat till natriumdominerad montmorillonit har merparten av arbetet som presenteras här inriktats på natriummontmorillonit.

De tre viktigaste montmorillonitfaserna av vilka solfasen är en, har i denna rapport undersökts och karaktäriserats på makroskopisk skala. De andra två faserna benämns, pasta, och gel. Pastan är en fas som domineras av osmotisk repulsion och den expanderar vid kontakt och tillgång till överskotts-elektrolyt. I vattenlösningar med låg jonstyrka kommer pastan så småningom då den expanderar att övergå till sol.

I gelfasen är montmorillonitpartiklarna sammanlänkade via attraktionskrafter som balanserar den osmotiska repulsionen. I rapporten visas att geler inte expanderar i kontakt med överskottselektrolyt. Reologiska mätningar med roterande vinge på geler bildade från montmorillonit extraherad från Asha 505 bentonit visar att gelerna har en hållfasthet som är högre än förväntade skjuvspänningar från vattenflöden i ett framtida slutförvar.

Fasdiagram för tre olika natriummontmorilloniter presenteras. Variablerna i fasdiagrammen är lerkoncentration och NaCl-koncentration. Den största skillnaden mellan de tre lerorna är den kritiska koaguleringskoncentrationen, CCC, här identifierad som den NaCl koncentration där en gel observeras. Wyomingmontmorillonit från MX-80 bentonit har den högsta CCC på ca 20 mM NaCl, medan både Kutch (Asha 505 bentonit) och Milos (Deponit CA-N) har betydligt lägre CCC på ca 4 respektive 6 mM.

I rapporten framförs nya bevis som stöder idén om en positiv kantladdning och ”spillover modellen”, vilken innebär att vid låg salthalt spiller den negativa potentialen från ytorna över till kantregionen och skapar därmed en barriär för växelverkan mellan kanter och ytor. Ovanför CCC övervinns denna barriär och den positiva kanten hos ett lerflak blir ”synlig” för ett annat lerflak, vilket leder till bildandet av bindningar mellan kanter och ytor.

Baserat på idéer från perkoleringsteori utformades ett experiment där gelers stabilitet undersöktes vid olika temperatur. Ur detta experiment kunde entalpin för bindningen kant-yta utvärderas. Även om det ännu inte existerar någon teori för hur denna växelverkan skall integreras i en generell modell för expansion och erosion av bentonit, skulle ändå kunskapen om denna bindningsentalpi kunna tjäna som riktlinje för en förenklad modell bortom DLVO eller primitiva modellens hantering av parallella lerflak.

Erosionsexperiment i artificiella sprickor genomfördes för Wyoming-Na montmorillonit (Wy-Na) och för lera blandad från hälften natrium och hälften kalcium montmorillonit (Wy-Ca/Na). I samtliga erosionstester var torrdensiteten hos den inplacerade montmorillonitkällan nominellt 1260 kg/m^3. Testerna visade att Wy-Na endast eroderar när det flödande vattnet hade NaCl koncentration under CCC. För NaCl koncentrationer över CCC begränsades utsvällningen av montmorillonit i sprickan till ett fåtal mm och ingen montmorillonit detekterades i det genomflödade vattnet.

Vid koncentrationer under CCC svällde montmorilloniten längre in i sprickorna, men pastan nådde bara in cirka 1 cm då aperturen var 120 µm. Utanför pastan byggdes det under förhållanden av stillastående vatten upp en solliknande fas som kunde transporteras bort med högt flöde. Denna sol uppvisade också Rayleigh-Taylor instabilitet, vilket är ett annat kännetecken på en flytande fas. Densiteten hos denna sol uppmättes till omkring 30 g/l. Tester visade också att denna sol kunde eroderas av gravitation även utan vattenflöde.

Erosion av lera var betydande då vattnets NaCl koncentration var under CCC. Vid de flödeshastigheter som testades var uppbyggnaden av sol runt pastan liten. Merparten av sol transporterades bort i samma takt som den bildades. För Wy-Ca/Na i en horisontellt placerad 120 µm spricka var den uppmätta

erosionshastigheten 65 kg/(m^2 · år) vid 1 mM NaCl (aq) och den lägsta testade flödeshastigheten, 850 m/år. Liknande erosionshastigheter erhölls för Wy-Ca/Na med artificiellt Grimselvatten (0,7 mM NaCl och 0,14 mM $CaCl_2$) flödande genom en horisontellt orienterad spricka. Å andra sidan visade sig gravitation ha stor inverkan på erosionshastigheten. Med samma lera och artificiellt Grimselvatten, uppmättes erosionshastigheten till 170 kg/(m^2 · år) trots att vattnet var stillastående. Under antagande att aperturen är 50 µm och att utsvällningen av lera i sprickor i slutförvaret liknar den som observerats i de artificiella sprickorna dvs. är av storleksordningen centimetrar, motsvarar denna erosionshastighet en montmorillonitförlust på 600 kg över tidsrymden 10 000 år. En ansenlig förlust av buffertlera som följd av bildandet av sol kan således inte uteslutas under glacialvattenförhållanden.

Erosionshastigheten beror av sprickaperturen och omkretsen av pasta-sol gränsen som i sin tur beror av hur långt leran sväller in i sprickorna. Alla observationer i detta arbete tyder på att utsvällningen är begränsad till en storleksordning av centimetrar även vid jonstyrkor väl under CCC. Men om det finns en långsam utsvällning som inte kunnat detekteras på tidskalan för experimenten skulle erosionshastigheten i realiteten kunna vara högre.

Contents

1 Introduction

In the Swedish KBS-3 concept for a geological deep storage, spent nuclear fuel will be placed in copper canisters surrounded by a buffer consisting of bentonite with high montmorillonite content (SKB 2006). Montmorillonite has great affinity for water, which causes build-up of swelling pressure in the confined space of the storage in the presence of water. If there are fractures intercepting the deposition hole, there is nothing to mechanically stop the bentonite from continuous swelling until equilibrium of sorts is reached. At present day conditions, bentonite at the swelling front will coagulate and form a gel as the groundwater is rather saline, thus hindering "unlimited" swelling as well as preventing sol formation. However, during the operational time of the repository, the composition of the groundwater most probably will undergo many changes. In particular during or after a glaciation one cannot exclude the possibility that very dilute groundwater will reach repository depth. Under such conditions the gel at the bentonite groundwater interface may no longer be stable resulting in formation of a colloidal sol that can be eroded. The effects of this process on the repository's safety are still not fully understood. A main goal for the work reported herein is to provide a more profound understanding of the physical forces involved; both their nature and magnitude.

Most of the experimental work reported here has been performed on montmorillonite from three different sources, MX-80 (Wyoming, Wy) Deponit CA-N (Milos, Mi) and Asha 505 (Kutch region India, Ku). We refer to each montmorillonite by their region of origin (Wy, Mi or Ku). Often the montmorillonite has been ion exchanged into homoionic form and then we append the cation to the name, e.g. Wy-Ca (montmorillonite).

1.1 Forces in montmorillonite/bentonite systems

1.1.1 Repulsive forces

Osmotic pressure

As mentioned above montmorillonite has affinity for water which causes the material to swell if unconfined or a swelling pressure is developed under confined conditions. Intuitively, the cause for expansion must originate from a repulsive force. To understand the origin of the repulsive force in smectite clays, a short discussion on the structure of the "fundamental" particles may be helpful. Montmorillonite and other smectite clays consists of ~1 nm thick aluminosilicate layers with lateral dimensions typically in the range 50–500 nm. These so called 2:1 clay layers consists of two tetrahedral silicon oxide sheets sandwiching an octahedral aluminium oxide sheet. The smectite clay layers have a permanent negative charge due to isomorphous substitutions of, e.g., Mg for Al in the octahedral sheet or Al for Si in the tetrahedral sheets. This permanent charge is compensated by exchangeable cations and thus the origin of the cation exchange capacity (CEC). The permanent charge is also the cause of the repulsive force leading to the aforementioned swelling property.

Casual reading of introductory textbooks on colloids may give the impression that the repulsive force is of direct electrostatic nature between the colloidal particles but with a screened Coulomb potential due to the presence of the counterions (Goodwin 2009, Hamley 2007). However, if one scrutinize the expression for the repulsive force that follows from the Poisson-Boltzmann (PB) equation, one finds that it is an expression for osmotic pressure resulting from ion concentrations (Evans and Wennerström 1999, Goodwin 2009, Witten and Pincus 2010). As long as the distance between smectite clay layers is small compared to their lateral dimensions, an often used and well tested approximation to the electrostatic problem is to treat the clay surfaces as infinite parallel planes and solve the PB equation for the ions in the interlayer solution using suitable boundary conditions. This approximation reduces the problem to one dimension and the appropriate variable becomes the separation of the clay layers, i.e., the interlayer thickness h. For $h > 20$ Å and Na^+ or Li^+ as counterions the PB equation gives excellent prediction of swelling pressures (Birgersson and Karnland 2009, Quirk and Marčelja 1997). Large clay layer separations is the relevant condition for approaching the problem of erosion under dilute water conditions, whereas for calculating swelling pressures at high dry densities the inclusion of hydration forces is necessary (Pashley and Israelachvili 1984, Smith et al. 2006). Figure 1-1 illustrates the solution to the PB equation for two parallel charged surfaces that are in equilibrium with an external NaCl bulk solution of concentration

C_{ext} (this enters as a boundary condition (Dubois et al. 1992, Hedström and Karnland 2011, 2012)). From symmetry it is directly evident that there is no electric field on the midplane $x = h/2$ so the only repulsive force (per area) that can be transmitted is the osmotic pressure from the ion concentrations (Evans and Wennerström 1999, Wennerström et al. 1982, Witten and Pincus 2010). Within PB this pressure is calculated from difference in ion concentrations at the midplane and the external concentrations, $P_{PB} = RT\sum_i (C_i(h/2) - C_{i,\,ext})$,where R and T are the gas constant and the absolute temperature, respectively.

Thus, an essential boundary condition for repulsion forces to develop is access to water, and a more fundamental equation for the force/area is given by (Evans and Wennerström 1999)

$$\frac{F}{\text{area}} = -\frac{1}{\text{area}}\left(\frac{\partial G}{\partial h}\right)_T = -\left(\frac{\partial G}{\partial V}\right)_T = -\frac{1}{V_w}\left(\frac{\partial G}{\partial n_w}\right)_T = P_{\text{osm}}, \qquad (1\text{-}1)$$

where G represents Gibbs free energy (per mole), $V = \text{area} \cdot h$, V_W the molar volume of water and n_w the amount of water (mole). The interlayer space is occupied by water and ions and for all practical purposes we may assume that water is an incompressible liquid which allows for the third equality in Equation (1-1). Thus when the two clay surfaces approach each other, water must leave the interlayer space. The last equality follows from the definition of osmotic pressure in terms of the chemical potential of the solvent (water). In the calculation of the osmotic pressure using the PB equation in the case of parallel surfaces, or for a saline solution in general, the contribution to G is purely entropic, the entropy of mixing. There is however nothing in Equation (1-1) that precludes other contributions to G. For small h the size of the hydrated ions would also contribute to the osmotic pressure in Equation (1-1). This would be the free energy of hydration. In the so called primitive model there are no explicit water molecules, instead the solvent is treated as a dielectric continuum (Evans and Wennerström 1999, Forsman 2004). Thus in simulations ions are commonly given a finite radius either as a soft or a hard core that approximately include the hydration shell (Guldbrand et al. 1984, Kjellander et al. 2001). In conclusion, repulsive forces between clay layers are osmotic and thus require access to external water (aqueous solution). Water moves from higher to lower chemical potential. If the clay is confined there will be a build-up of osmotic pressure until the water chemical potential in interlayer equals that of the external solution. If the clay is unconfined water will move into the interlayer causing further and further separation of the clay layers. If the attractive forces are too weak, nothing will prevent clay dispersion, i.e. the formation of a sol. This is a potential problem for the safety function for a repository for spent nuclear fuel, especially during or after a glaciation because of the possibility that dilute groundwater (high chemical potential) may permeate the bedrock. For a complete description, G also contain attractive interactions. The major such interactions are discussed below.

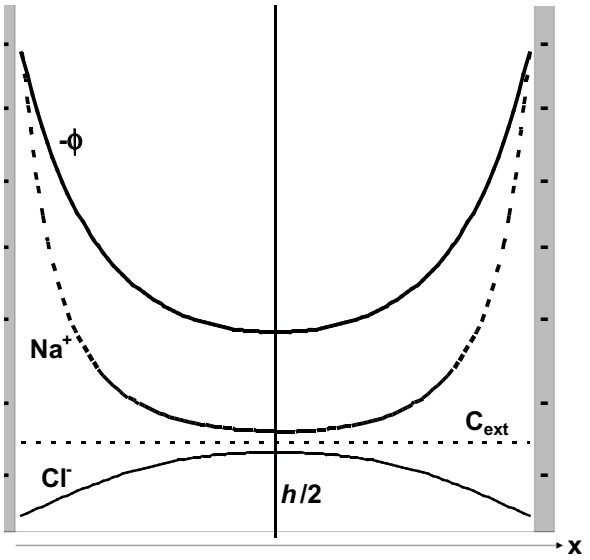

Figure 1-1. *Schematic illustration two parallel montmorillonite layers and the distributions (concentration profiles) of sodium and chloride in the interlayer. The electrostatic potential (multiplied by −1 to become a positive quantity) in the interlayer is also indicated, $-\phi$. The horizontal dashed line specifies the external NaCl concentration C_{ext}. The separation between the clay layers is h. Due to symmetry the electric field, $-d\phi/dx$ vanishes at the midplane, $x = h/2$.*

1.1.2 Attractive forces

van der Waals interaction

In many colloidal systems, the main attractive force is the so called dispersion force and it derives from the van der Waals interaction that operates between any two molecules or atoms. The van der Waals attraction potential between molecules 1 and 2 separated by a distance r is given by $V_{12}(r) \propto -\alpha_1\alpha_2 / r^6$ where α denotes the polarizability at zero frequency. The van der Waals interaction is an example of correlation, the fluctuations in the electron cloud around one molecule perturbs the electron cloud around the other, and these perturbations reinforce each other which gives rise to attractive interactions. Although formally many-body interactions may be significant (Atkins and de Paula 2006), the dispersion interaction between two large molecules or colloidal particles it is often calculated assuming that the interaction is pairwise additive.

Simulations show that for coin-shaped or hexagonal clay layers the dispersion interaction is larger for face-to-face arrangement than for edge-to-face arrangement (Jönsson et al. 2008). For face-to-face arrangement of clay layers the dispersion interaction per area can be found by direct integration of V_{12} where 1 and 2 would refer to volume elements on clay layers 1 and 2, respectively (Evans and Wennerström 1999, Russel et al. 1992). The final result for the interaction energy U_{vdW} is given by

$$\frac{U_{\mathrm{vdW}}}{\mathrm{area}} = -\frac{A_H}{12\pi}\left(\frac{1}{h^2} + \frac{1}{(h+2\delta)^2} - \frac{2}{(h+\delta)^2}\right), \tag{1-2}$$

or in terms of the force

$$\frac{F_{\mathrm{vdW}}}{\mathrm{area}} = -\frac{A_H}{6\pi}\left(\frac{1}{h^3} + \frac{1}{(h+2\delta)^3} - \frac{2}{(h+\delta)^3}\right), \tag{1-3}$$

where δ is the thickness of a clay layer ($\sim$1 nm) and A_H is the effective Hamaker constant that incorporates the material properties of the colloidal particles and the intervening medium. Typical values of A_H for smectite-smectite interactions across an aqueous interlayer is $1\text{–}2 \times 10^{-20}$ J, equivalent to 2.5–5 k_BT at $T = 298$ K (K_B being the Boltzmann constant) (Iwata et al. 1994).

Ion-ion correlation

The PB equation is a mean-field approximation to the primitive model (Forsman 2004). This means that ion-ion correlations are neglected, i.e., the pair correlation function $g_{ij}(\vec{r}_1, \vec{r}_2) = 1$. There are two physical reasons why $g_{ij}(\vec{r}_1, \vec{r}_2) \neq 1$: 1) electrostatics and 2) steric effects (Messina 2009). The latter are implicitly ignored when ions are treated as point charges. Including steric effects lead to excluded volume contributions which are repulsive and can be considered part of the hydration contribution to the osmotic pressure mentioned above.

The electrostatic contribution to correlation is present also when the ions are treated as point particles and becomes increasingly important with increasing valence of the counterions. The Coulomb energy of two counterions of charge Ze separated by a distance R is given by $Z^2e^2/(4\pi\varepsilon R)$ and this quantity divided by the thermal energy defines the Coulomb coupling constant (Grosberg et al. 2002)

$$\Gamma = \frac{Z^2e^2}{4\pi\varepsilon R \cdot k_BT} = \frac{Z^2}{R} l_B, \tag{1-4}$$

where $l_B = e^2/(4\pi\varepsilon k_BT)$ denotes the Bjerrum length which is about 7 Å in water at 298 K. In compacted bentonite at buffer density we may consider the counterions moving in two dimensions as they are always close to the montmorillonite surfaces (h = 6 to 10 Å), thus the average distance between the ions is given by $R \sim (Ze/|\sigma|)^{1/2}$ with σ being the montmorillonite surface charge density. For Wyoming montmorillonite (extracted from MX-80 bentonite) $e/\sigma \approx -144$ Å^2. Thus in the case of Na^+ as counterion Equation (1-4) gives $\Gamma_{Na^+} \approx 0.6$, whereas for Ca^{2+} we obtain $\Gamma_{Ca^{2+}} \approx 1.6$. R decreases with increasing surface charge density, thus ion-ion correlation becomes even more important the higher the CEC. While Equation (1-4) suggests that correlation is substantial for divalent ions in montmorillonite, the value $\Gamma_{Ca^{2+}} \approx 1.6$ does not warrant the use of approximations valid for strongly correlated liquids (Grosberg et al. 2002, Messina 2009). Instead, to assess the magnitude of ion-ion correlations one has to use either simulations (Bratko et al. 1986, Guldbrand et al. 1984, Wennerström et al. 1982) or numerical solutions to advanced integral equation theories for inhomogeneous fluids (Kjellander 1988, Kjellander et al. 1988, Kjellander and Marčelja 1984). Ion-ion correlation in lamellar systems can also be calculated using density functional theory (Forsman 2009, Wang et al. 2011).

Monte Carlo (MC) simulations of the osmotic pressure in a solution between a charged wall ($|e/\sigma| \approx 72$ Å^2) and a neutral wall revealed that PB overestimated the pressure a factor 1.5 in the case of monovalent counterions and about a factor of 12–15 in the case of divalent counterions showing that the ion-ion correlation yields an attractive contribution (Wennerström et al. 1982). When the fluid is confined between two charged walls (Figure 1-1) the attraction due to correlations across the midplane may even outweigh the osmotic repulsion in the case of divalent counterions (Guldbrand et al. 1984, Kjellander et al. 1988). These results are also consistent with X-ray diffraction measurements showing that the basal distance never progresses beyond the three water layer hydrate ($d(001) \sim 19$ Å) for Ca-montmorillonite (Brindley and Brown 1980), whereas for Na-montmorillonite the swelling may be indefinite (Norrish 1954). For Li- and Na-montmorillonite the mean-field theory has been successful (Birgersson and Karnland 2009, Quirk and Marčelja 1997), while for divalent counterions, PB not only give quantitatively wrong swelling pressures but also qualitatively the wrong results as it cannot predict the limited water uptake in the interlayers.

As discussed above ion-ion correlation may in the case of divalent counterions cause several clay layers to aggregate in a face-to-face arrangement. In the present text we will refer to such composite particles as tactoids. Also high salinity, > 1 M NaCl, may promote tactoid formation, as the osmotic repulsion is reduced so van der Waals forces dominate (Norrish 1954).

Electrostatic edge-to-face (edge-to-edge) interactions

The final attractive force of importance in montmorillonite systems is the interaction between edges and faces of the clay layers. At the edge, the 2D crystal structure of the clay layer is disrupted and the covalent bonds are broken. This gives the edge a positive charge as verified in transmission electron microscope images showing how negatively charged gold colloids adhere to the edges but not the faces of clay particles (Thießen 1947). The edge charge is possibly associated with titratable groups and is thus influenced by the pH of the surrounding electrolyte. In the literature there is however, little consensus regarding the pK values for edge site protonation. A recent review of the acid-base properties of clays showed that published pK values spread over 10 pH units (Duc et al. 2005). The most frequently found values were mainly located in three domains, pH 4–5, pH 6–8 and pH 10–11. Acidic pK values were normally attributed to the tetrahedral sites (Si–OH) and the basic pKs to the octahedral sites (Al–$OH_2^{-1/2}$). (Avena et al. 2003) suggest a pK value of 10 for the latter sites, which thus are predominantly positively charged (Al–$OH_2^{+1/2}$) below pH 10. Other authors categorically maintain that positive charges can only develop on the Al-OH edge sites at pH less than about 6.5 (Tombácz and Szekeres 2004). Leaving the discussion of pH aside for the moment, we realize that positive charges on the edges may interact with the negative basal surface, forming edge-to-face associations. With only negative charges on the edge and relatively low NaCl concentrations, simulations of idealized laponite clay particles show that electrostatic edge-to-face interactions are repulsive and are larger than the van der Waals attraction (Jönsson et al. 2008).

The number of isomorphic substitutions is far greater than the number of edge charges so even with a positively charged edge the overall charge of the clay layer is negative. Consequently, the interaction between two Na-montmorillonite layers is repulsive at long distance. This means that there is a barrier separating configurations where repulsion dominates from attractive alignments. Furthermore, it is only above a certain salinity that the positive edge of one clay layer is discernible to an approaching particle. This is due to the spillover of the negative potential associated with the faces into the edge region (Secor and Radke 1985). The spillover hypothesis is discussed further and tested experimentally in chapter 4.

There have been several propositions regarding the geometric arrangement of two interacting clay layers (Van Olphen 1977); the two most commonly discussed configurations that both would lead to voluminous gel structures are shown in Figure 1-2. Experimentally, it has not been settled which structure predominates, the house-of-cards or the band-like structure (Jönsson et al. 2008). Regarding theoretical work, there is no simple expression that embodies the edge-to-face interaction so once again one is referred to simulations. Depending on the assumptions in the simulations one configuration may be preferred over the other. Using a coarse-grained approach (no explicit water or ions) it was found that the overlapping coin configuration gave the global minimum for laponite-sized clay layers (Jönsson et al. 2008). In this simulation the clay layers consisted of a collection of spheres each containing a unit charge, negative on the spheres associated with the faces and positive on the edge.

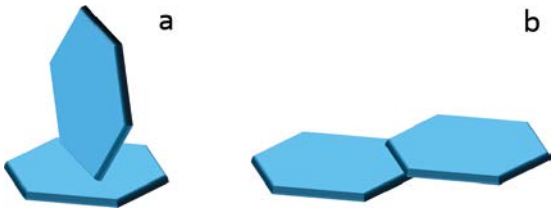

Figure 1-2. *Proposed arrangements for edge-to-face interaction: a) T-shaped configuration, leading to house-of-cards structure. b) Overlapping coins configuration that gives band-like structures.*

The interaction between the charges on different clay layers was described via screened Coulomb potentials. However, in similar simulations involving a larger number of clay layers and at higher volume fractions, a larger variety of different phases was found, including T-shaped interactions giving house-of-cards structures (Delhorme et al. 2012a) as well as several liquid crystalline structures (Delhorme et al. 2012b).

One cannot emphasize strongly enough the importance of edge-to-face interactions for the formation of gels as well as certain types of aggregate formation (Angelini et al. 2014). The other attractive interactions discussed here, van der Waals and ion-ion correlations, both lead to face-to-face arrangements, which essentially are one dimensional and can therefore never give a space-filling gelled structure. A 1D chain is always of finite size (N) because only one bond needs to be broken, and as the chain grows in length the number of positions to break the chain grows so eventually the gain in entropic energy $k_BT\ln N$ for breakage outweigh the loss in binding enthalpy (Ziman 1979). Note that this is an argument based on topology and therefore robust and does not require knowledge of the precise nature of the attractive force. Experimentally, it is confirmed that tactoids formed in suspensions of Ca- or Mg-montmorillonite are of finite size (average number of layers $\leq\sim 20$) and experiments performed on size-fractionated clay show that the tactoid size decreases with decreasing area of the montmorillonite layer (Segad et al. 2012) as expected from the above analysis. The arrangements of clay layers in Figure 1-2 naturally give rise to 3D structures that may percolate, i.e., reach a critical fraction of bonds to yield an infinite structure, given sufficiently strong interaction and high enough volume fraction of clay.

1.2 Montmorillonite phases

1.2.1 Definitions

A schematic phase or state diagram for Na-montmorillonite in contact with NaCl(aq) is shown in Figure 1-3. It contains the phases: sol, gel and repulsive paste (repulsive gel). In principle the same diagram could be used for a mixed Ca/Na system as long as the behaviour is not dominated by the ion-ion correlations, i.e. the amount of Na^+ in the interlayer is $>\sim 20$ %. For the mixed system, the ionic strength has to be set by a mix of $CaCl_2$ and NaCl to avoid exchange. This more complicated type of phase diagram has been discussed previously in terms of the sol-formation zone (Birgersson et al. 2009, 2011).

When discussing the different montmorillonite phases, we will try to adhere to the following definitions as recommended by either the National Institute of Standards and Technology, NIST (Hackley and Ferraris 2001) or by the International Union of Pure and Applied Chemistry, IUPAC (Alemán et al. 2007).

Sol: A liquid *dispersion* containing particles of *colloidal* dimensions (NIST). The IUPAC recommended definition of a sol is “a fluid colloidal system of two or more components”.

Gel: Bicontinuous structure with a solid and a liquid component. The solid network may consist of *particles* or polymers, held together by covalent, ionic or dispersion (physical) forces. The network may be elastic, viscoelastic or plastic. The scale of the mesh of the network (distance between cross links) is of *colloidal* dimensions. (NIST). The recommended definition of a gel by IUPAC is a “non-fluid colloidal network or polymer network that is expanded throughout its whole volume by a fluid”.

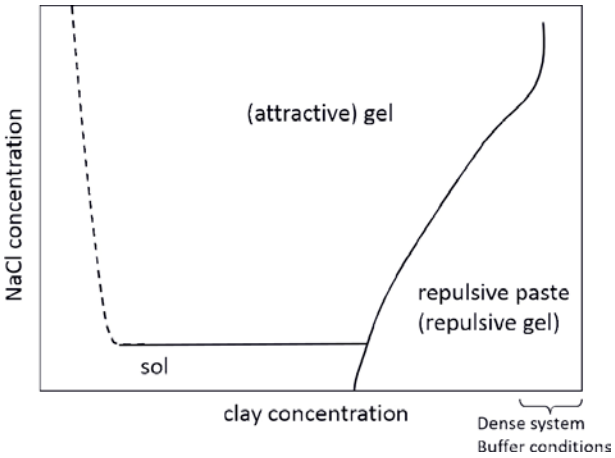

Figure 1-3. *Schematic phase (state) diagram for Na-montmorillonite.*

A different criterion for a gel is that it has a finite yield stress (Everett 1972). This is a phenomenological classification criterion that is bound to lead to inconsistent nomenclature, e.g., both foams and liquid crystals would qualify (Evans and Wennerström 1999). We therefore prefer to follow the NIST and IUPAC definition of a gel as far as possible.

The attractive montmorillonite gel is a gel in the strict sense. In view of the NIST definition, the word attractive may seem superfluous since the particles in a gel are "held together" which implies attraction. Thus the term attractive gel as often used in the literature (Abend and Lagaly 2000) is termed gel in this report.

Repulsive paste: This is a term that we introduce here as a reminder that the phase often labelled "repulsive gel" (Abend and Lagaly 2000) not necessarily is a gel. On short time scale this phase does not flow and it has a yield strength. While it may be possible that a "repulsive" clay gel consists of a particle network, it has not yet been proven. As we have not been able to find any support in the literature for the existence of a particle network dominated by repulsion forces between the clay layers, we will refer to the repulsive systems as pastes. Furthermore, it may be so that there are in fact two states – both repulsive gels and pastes, with the repulsive gel as an intermediate state in between the "attractive" gel and the repulsive paste state. For the purpose of describing the properties and evolution of the clay in a repository we want to interpret these to mean that a paste is a comparatively dense mixture that exhibits a swelling pressure when it has access to water that can enter through osmosis into the paste. Under unconfined conditions the paste will swell.

Critical Coagulation Concentration (CCC): By the CCC we mean the lowest concentration of electrolyte needed to form a gel. The CCC is determined from the observation of the occurrence of a macroscopic gel.

Our definition is different from, e.g., the definition given by NIST. However, the CCC values we have reported earlier (Birgersson et al. 2009) are in line with literature data (Hetzel and Doner 1993, Permien and Lagaly 1994, Swartzen-Allen and Matijevic 1976). In most of these studies the CCC was defined from turbidity measurements; for ionic strengths above the CCC aggregation lead to rapid sedimentation and a significant lowering of the turbidity in the supernatant.

The NIST definition of CCC reads: "The molar concentration of electrolyte, C_0, necessary to induce rapid (diffusion-limited) *aggregation*. Experimentally determined by extrapolation of ln W versus ln C_0 to ln W=0, where W is the *stability ratio*."

The definition based on the stability ratio is largely linked to DLVO theory for spherical particles with only one type of charge (Verwey and Overbeek 1948). At the CCC the repulsive barrier vanishes leading to rapid aggregation. For smectite clays this definition of CCC is less relevant as the clay layers are anisotropic and are carrying both negative and positive patches. Due to this anisotropy, the timescale for the attractive interactions to be decisive may be long. Thus to induce rapid aggregation might require significantly higher ionic strength (more screening of the electric double layer) than needed for the formation of a gel.

Independent of how CCC is defined, one has to realize the role of cation exchange (Jenny and Reitemeier 1935, Kahn 1958). In the present work we will mostly work with homoionic (Na) montmorillonites and avoid the complication of exchange when determining the CCC (generally using NaCl). Kahn (1958) pointed out that "In the flocculation of sodium montmorillonite by polyvalent cations, ion exchange plays a dominant role". Still during more than fifty years following the remark by Kahn, measurements of, e.g., "CCC for Ca^{2+} in Na-montmorillonite" appear in the literature, e.g., Lagaly and Ziesmer (2003), although such statements lack meaning. How to handle and quantify the influence of exchange on gelation has however been fully resolved and tested experimentally for Ca/Na systems (Birgersson et al. 2009, 2011).

Knowledge of the CCC for various sodium montmorillonites is important for the safety assessment of repositories for spent nuclear fuel as it provides concentration limits for the onset of bentonite erosion by dilute groundwater. Many investigations regarding the CCC are performed on very dilute montmorillonite suspensions (Hetzel and Doner 1993, Lagaly and Ziesmer 2003). However, for the assessment of the performance of bentonite in a repository denser systems are more relevant (Birgersson et al. 2009). The CCC of dilute suspensions would be more relevant for the situation when, e.g., a river transports clay particles into the sea or an estuary where they may coagulate. However, in a repository for spent nuclear fuel, the bentonite has a considerably higher density (dry density ~1600 kg/m^3) and in order for erosion to be limited, a gel has to be formed at the interface between the swelling bentonite paste and the groundwater.

Nevertheless CCC values determined for Na-montmorillonites using NaCl appear to be unchanged from the dilute suspension (~0.1 % w/w) to denser systems 1 % w/w (Birgersson et al. 2009, Hedström et al. 2011) and the present work (chapter 3) shows that gels appear at the CCC for clay concentrations up to 4 to 6 % w/w depending on clay origin. Still the notion that CCC determined for dilute suspensions is the relevant parameter for the gelling of montmorillonite at the swelling front comes with a caveat: The CCC for dilute suspensions seem more sensitive to pH, whereas pH has small influence on the NaCl concentration required for gelling of denser systems that are relevant for repositories for spent nuclear fuel (Birgersson et al. 2009, Goh et al. 2011, Hetzel and Doner 1993).

1.2.2 The main phases of (Na) montmorillonite

Repulsive paste

At high clay concentration the repulsive forces (osmotic double layer forces and hydration) dominate the system and the yield stress that the system displays is a consequence of jamming. This phase also displays significant osmotic pressure, particularly in the denser region that is representing the conditions for the buffer. In this dense region salinity has little qualitative effect on the system. Even at high NaCl concentrations (>3M) the osmotic pressure never vanishes (Karnland et al. 2006). At lower clay concentration the repulsive system may show liquid crystalline behaviour and an isotropic to nematic transition has been observed (Michot et al. 2004). Below the CCC the repulsive paste would eventually turn into a sol if it has free access to solvent and the volume is not restricted.

Montmorillonite sol

The sol phase is a suspension of montmorillonite particles (individual layers or aggregates) that are only weakly interacting. We have previously shown that aggregates are formed in the sol phase even when the clay is dispersed in deionized (DI) water (Birgersson et al. 2009) and recent theoretical work suggests the apt term disconnected house-of-card for such structures (Angelini et al. 2014). These aggregates have limited size and do not form a network that span the available space, hence no yield strength. Edge-to-face interaction is most probably the cause for aggregate formation. Over long time periods, aggregates may accumulate at the bottom of a vessel as a sediment. The sediment has no observable yield strength.

Making sols stable has been a major effort in colloid science and technology, and one can readily appreciate the importance when it comes to products such as paints or household cleaners. The sol is stable if the repulsion extend beyond the distance where the attractive potential minimum is about k_BT or less. If we for the sake of argument assume the naïve idea that face-to-face van der Waals interaction is the cause for coagulation in Na-montmorillonite, we can estimate how close two clay layers need to be in order to be bound. A realistic area of a montmorillonite layer is 10^5 nm^2, as found by, e.g., Ploehn and Liu (2006). Using this area and $A_H = 5\ k_BT$, Equation (1-2) then predicts $|U_{\mathrm{vdW}}| < 1\ k_BT$ when $h > 16$ nm. Thus if the range of the repulsive force is longer than 16 nm, the van der Waals interaction will be insufficient to cause coagulation. A separation of 16 nm may seem large, especially

compared to the buffer condition where the interlayers have either two or three layers of water molecules corresponding to separations of approximately 6 or 9 Å, respectively. However, compared to the lateral dimensions of the clay layers, 16 nm is still a small separation as shown by the scale drawing in Figure 1-4. The volume fraction of clay in this case is $\phi_c \approx 1/17$ which correspond to a mass concentration of 160 g/l. At the experimentally determined critical coagulation concentration for Wyoming Na-montmorillonite, ~20 mM NaCl, the calculated osmotic pressure (PB + Equation (1-3)) at $\phi_c \approx 1/17$ is about 1.4 kPa. Thus one can conclude that face-to-face van der Waals interaction contribute marginally to destabilizing Na-montmorillonite sols.

Montmorillonite gels

Gels are formed above a critical concentration of electrolyte. In the present work the influence of NaCl on gelation has been investigated in particular. Above the CCC a gel phase is formed. This gel can be produced by either letting montmorillonite swell in a solution with NaCl concentration above the CCC or by adding NaCl to a montmorillonite sol such that the final NaCl concentration is above the CCC. In the former case the gel would swell until it meets the boundary separating the repulsive paste from the gel (Figure 1-3). At equilibrium the repulsive and attractive forces in the gel exactly balance each other in the gel. In the latter case we have found that a very low density gel can be formed where the average clay concentration may be more than an order magnitude smaller than the clay concentration at which the clay particles can start to rotate freely. Our conceptual view of this gel is a loose percolated network (Tanaka et al. 2004) of clay layers interacting through edge-to-face attraction. An example of such a gel is shown in Figure 1-5. The following can be inferred from this figure: (i) attraction forces must be the cause for keeping the gel together and give it yield strength. Although repulsive interactions can give arrested states (repulsive paste), such a structure would not be stable and occupy only a part of the total available electrolyte volume (note that the vial is filled with electrolyte). The gel in Figure 1-5 has remained unchanged for more than seven years, showing that it withstands both gravity, thermal fluctuations and potential osmotic forces. In this particular case, the osmotic pressure contribution from PB (Figure 1-1) equals zero; (ii) face-to-face van der Waals interactions can be totally ruled out at $\phi_c \approx 7 \times 10^{-4}$; (iii) overlapping coin configurations must to a large extent contribute to the structure, because a gel with only T-shaped configurations would have a much higher ϕ_c.

At sufficiently low clay concentration the clay layer density is below the percolation threshold, i.e. a space-filling network cannot be formed even if the ionic strength is above the CCC. This percolation threshold is indicated with a dashed line in Figure 1-3. The precise location of this border has not been explored in this study. Any smectite gel would collapse under gravity before one actually reach the percolation limit.

Figure 1-4. *Side view of two montmorillonite layers at a separation where the van der Waals attraction is of the order of k_BT.*

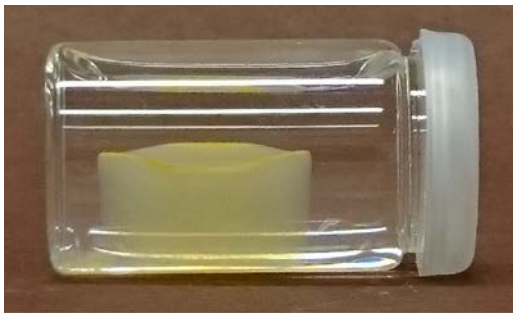

Figure 1-5. *Snapshot of Ku-Na gel taken ca seven years after formation in a mixed NaCl/NaOH solution of ionic strength 15 mM and pH ~ 11. Initially the vial was standing upright and filled with a montmorillonite sol of 2 g clay/l that was settling and slowly gelling and consolidating. After the gel was formed, the vial was placed horizontally and the gel eventually unfastened from the glass and flipped forward. Most of the clay particles actually settled before gelation took place. Based on turbidity we estimate the clay concentration in the gel to be less than 2 g/l, equivalent to a volume fraction of 0.07 %. Note that the gel is fully surrounded by electrolyte.*

As mentioned above, edge-to-face interactions are necessary for gelation of montmorillonite. Measurement on dilute montmorillonite sols, suggests a rather strong pH dependence on the stability ratio (Tombácz and Szekeres 2004) and it seems reasonable that an increase in pH would promote deprotonation of titratable edge groups. However, conclusions often drawn from such experiments, that the edge charge can only be positive below pH 6.5 and at slightly alkaline conditions the edge is negative cannot be generally valid as they would be at odds with the observed effect of pyrophosphate on gelation and rheology.

Pyrophosphate anions have large influence on the formation of montmorillonite gels as the anions bind to the positive edge and thereby block the edge-to-face attraction. The addition of 0.25 % tetra sodium pyrophosphate to 0.5 % w/w Wy-Na suspensions increased the CCC for NaCl by almost an order of magnitude (Birgersson et al. 2009). Similarly addition of pyrophosphate to an existing gel was found to lead to an almost instantaneous disintegration of the gel. These observations are completely in line with recent rheological measurements on bentonite slurries (7 % w/w) where it was found that the addition of polyphosphates totally removed the yield strength over the pH range 5–10 and drastically reduced the yield strength below pH 4 (Goh et al. 2011). Without adding polyphosphate, the yield strength was significant ~30 Pa even at pH 10, which led the authors to draw the inevitable conclusion that: "The nature of the clay particle edge charge must still be positive at this high pH level". Birgersson et al. (2009) tested the influence of pH on the formation of Wy-Na gel and found that CCC remained at 25 mM NaCl up to the highest tested pH value of 9.1. Similarly, in erosion tests using artificial fractures, erosion has not been observed for Wy-Na provided that the NaCl concentration is above 20–25 mM even at pH up to 10 (chapter 6).

1.3 The phase diagram and bentonite erosion

At the time for installation of the bentonite buffer, the salinity in surrounding fractures will be above the CCC. Thus as the bentonite (montmorillonite) swells into the fracture it would eventually turn into a gel at the front. Looking at the phase diagram in Figure 1-3, this means that the swelling front meets the border separating the repulsive paste and the gel at some clay concentration, arriving from the right in the phase diagram, i.e. from higher clay concentration. Provided that the gel can withstand the shear forces from the seeping water in the fracture the buffer is protected from erosion. In principle the a gel should get weaker with decreasing salinity near the CCC possibly leading to erosion also from the gel state as indicated in Figure 1-6. In our studies we have not been able to observe such process, suggesting that the sol to gel transition occurs over a very narrow interval in ionic strength (< 1 mM). In other words, if the ionic strength is ~1 mM above CCC, the yield strength of the gel is already substantial (chapter 5). Thus, the problem with buffer erosion starts when the salinity drops below the CCC. Initially such a lowering of salinity would lead to a transition of the gel to a sol at the front and subsequently to further expansion of the repulsive paste and a paste to sol transition. Recent rheological measurements strongly indicate that direct mechanical erosion from the paste is unlikely (Eriksson and Schatz 2015). Thus we may conceptually view erosion as a process occurring from the sol. Rate limiting factors for erosion would then be repulsive paste to sol transfer rate and the rate by which the sol is removed.

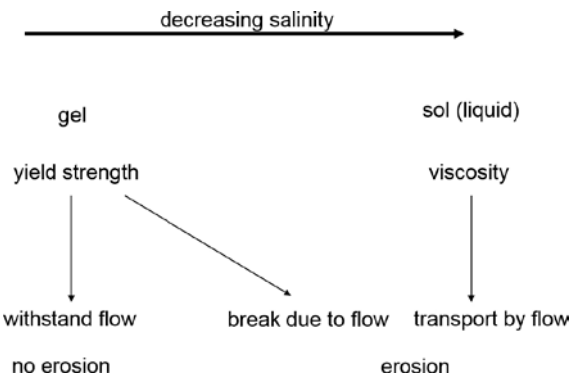

Figure 1-6. *Scenario for colloid erosion from a bentonite buffer in a repository.*

2 Break-up of Ca-montmorillonite by Na-montmorillonite

A possible scenario in the post-glacial evolution of the bentonite buffer used in a KBS-3 repository for spent nuclear fuel is that parts of the buffer may erode due to sol formation. A homoionic Ca-montmorillonite would not pose any problem with respect to colloidal sol formation because it has limited swelling most likely due to attraction forces caused by ion correlations. Thus in earlier studies homoionic Ca-montmorillonite have never been found to spontaneously form a sol (Birgersson et al. 2009, 2011, Hedström et al. 2011).

However mixed Ca/Na-montmorillonite with of more than 10–20 % Na^+ in the interlayer have been shown behave similar to homoionic Na-montmorillonite and is thus sol forming in contact with deionized water (Hedström et al. 2011).

In the work reported in this chapter we use turbidity measurements to study the break-up of clay particles, also called tactoids. In this particular context particle may be an aggregate of several montmorillonite layers, thus break-up refers to the aggregate particle not an individual layer. Turbidity of a solution is proportional to the particle concentration. Different clay suspensions may also show different turbidity because turbidity is also proportional to the square of the tactoid volume. Mixing two different clay suspensions would have a turbidity that is the weighted average of the separate suspensions in case the two types of clay particles do not interact. In case the two types of clay particles interact after mixing, the turbidity could either be higher or lower than the weighted average. In most cases the turbidity was seen to be lower than the weighted average. This is interpreted as a break-up of the larger particles as will be further elaborated in the theory discussion below.

2.1 Theory

According to the Rayleigh-Debye-Gans scattering theory (Garcia-Lopez and Garcia-Rubio 2008) the turbidity, τ which is proportional to the intensity of scattered light, can be expressed as

$$\tau \propto V_p^2 \left[\frac{n_{cw}^2 - 1}{n_{cw}^2 + 2} \right]^2 \cdot \frac{N_p}{V}, \tag{2-1}$$

where V_p denotes the volume of the scattering particle, V the total volume of suspension, N_p the number of scattering particles and n_{cw} is the relative index of refraction of clay (c) to the aqueous medium (w). Equation (2-1) is valid for dilute suspensions in which multiple scattering is negligible. It is also assumed that the tactoid size remains approximately the same for all dilutions under consideration. In concentrated suspensions τ is no longer linear in N_p / V but also higher order terms are needed. Assuming only minor variation of n_{cw} among different montmorillonites, Equation (2-1) can be simplified to

$$\tau = k \cdot V_p^2 \cdot \frac{N_p}{V}, \tag{2-2}$$

where k is a constant. Let ρ_p be the particle density such that the mass of one particle is $m_p = \rho_p \cdot V_p$ and the total mass in volume V is $N_p \cdot \rho_p \cdot V_p$. The clay mass concentration (g/l is a convenient unit) of the suspension can then be written as $C = N_p \cdot \rho_p \cdot V_p / V$. Rearranging Equation (2-2) one finds that for a given type of clay the turbidity is proportional to C according to

$$\tau = k \cdot V_p \frac{C}{\rho_p}. \tag{2-3}$$

For a mixture of several different (clay) particles the above equations can be generalized to

$$\tau = k \sum_i V_{p,i}^2 \cdot \frac{N_{p,i}}{V} = k \sum_i V_{p,i} \cdot \frac{C_i}{\rho_{p,i}} = \sum_i \tau_i \tag{2-4}$$

provided that the properties of one type of clay particles is unaffected by the presence of another. In the present study, suspensions of the same concentration of two different clays were mixed. The clay suspensions contain homoionic montmorillonite and DI water, but no excess salt. The unmixed

suspensions may thus differ in counterion as well as origin of the montmorillonite. If the conditions leading to Equation (2-4) are fulfilled then the turbidity for a mixture of two clays is the weighted average of the turbidities (τ_i) of the two unmixed suspensions according to

$$\tau = \tau_1 \frac{V_1}{V} + \tau_2 \frac{V_2}{V} \qquad (2\text{-}5)$$

where the total volume $V = V_1 + V_2$. If on the other hand the experimental turbidity for the mixed montmorillonite suspension deviates from Equation (2-5) one may conclude that the two montmorillonites interact.

2.2 Material and method

Montmorillonite (<2μm fraction) extracted from three types of bentonite have been used during these investigations: Wyoming-type (Wy) obtained from MX-80 bentonite (American Colloid Co.), Kutch-type (Ku) obtained from the Indian bentonite Asha 505 (Ashapura Minechem Co.) and Milos-type (Mi) obtained from the Greek bentonite IBECO Deponit CA-N (Silver & Baryte Mining Company S.A.). The montmorillonites were purified and ion-exchanged with NaCl to the homoionic form according to the procedure described in Karnland et al. (2006). The purified montmorillonites are referred to as Wy-Na, Ku-Na and Mi-Na, where Na is the counterion.

The chemical formula for an ideal sodium montmorillonite, interlayer water excluded, can be written as $[(Si_{8-\alpha}Al_{\alpha})(Al_{4-\beta}Mg_{\beta})O_{20}(OH)_4]^{(\alpha+\beta)-}Na^{+}_{\alpha+\beta}$, where by definition the tetrahedral charge is lower than the octahedral charge ($\alpha<\beta$) and the sum of tetrahedral and octahedral charges fulfil $0.4<\alpha+\beta<1.2$. The charge distributions of the clays in this study have been determined previously (Karnland et al. 2006) and are summarized in Table 2-1. The values in Table 2-1 are based on ICP/AES measurements on the homo-ionized clay fraction <2μm and calculated according to the procedure described in Newman and Brown (1987). For comparison the measured CEC values (using Cu(II)-triethylentetramine) are also included in Table 2-1. The agreement between measured and calculated CEC was very good for Wy and Ku, whereas the spread in the values was larger for the Milos clay. Measured CEC values suggest that Wy and Mi are rather similar, while the surface charge density for Ku is about 15 % higher. Also quantitative tests according to Greene-Kelly (1953) confirmed the increasing ratio of tetrahedral charge in the series Wy (8 %), Mi (22 %), and Ku (26 %) although less pronounced than the calculated values in Table 2-1 suggests.

Table 2-1. Cation exchange capacity (CEC) and charge distribution of the investigated clays as calculated from ICP/AES data (Karnland et al. 2006). For Wy-Na and Mi-Na the tests were done in duplicates.

	Wy-Na1	Wy-Na2	Mi-Na1	Mi-Na2	Ku-Na
CEC (measured) [eq/kg]	0.86	0.86	0.87	0.82	0.99
CEC (calculated) [eq/kg]	0.87	0.88	0.97	1.09	1.04
Tetrahedral Charge [e]	−0.11	−0.05	−0.15	−0.27	−0.38
Octahedral Charge [e]	−0.54	−0.60	−0.57	−0.55	−0.42
Total Charge [e]	−0.65	−0.65	−0.72	−0.82	−0.79

Batch suspensions of concentrations 0.5 and 1.0 g/l of each homoionic montmorillonite were prepared. For Wy-Na and Wy-Ca, 2.0 g/l suspensions were made and for Ku and Mi in both Ca and Na form, suspensions of concentrations 1.5 g/l were also prepared. The reason for using 1.5 instead of 2.0 g/l is that in the cases of Ku-Ca and Mi-Ca the turbidity of the 2.0 g/l suspensions is outside (above) the range of the turbidimeter. The required amount of montmorillonite was added to 100 ml of DI water. In the case of divalent counterions the suspensions were sonicated for 15 min before being mixed with a magnetic stirrer for 24 h. Without sonication clay particles (aggregates) remained so large that they settled on the timescale of seconds, making turbidity measurements impossible (meaningless). This shows that for a suspension of montmorillonite with divalent counterions the turbidity is not uniquely determined by concentration but depends strongly on preparation. This point will be further illustrated for Ku-Ca below. For monovalent counterions the sonication step was not required to disperse the clay.

In the experiments, suspensions of two different clays were mixed and the turbidities of the resulting suspension were recorded with a portable turbidimeter (TN-100, Eutech instruments). Immediately after mixing, the vials were vigorously shaken and then tapped to remove air bubbles before measuring the turbidity. The light source in the turbidimeter is an infrared-emitting (850 nm) diode. The intensity of the scattered light is directly converted to nephelometric turbidity units (NTU) by the instrument.

2.3 Results and discussion

Previous work has shown that montmorillonites of different origin may give different turbidities with the same counterion and clay concentration (Birgersson et al. 2009). In particular Ku-Na gives significantly higher turbidity than Wy-Na so mixing these two clays offers a good opportunity to test the validity of Equation (2-5). If the clay concentration is the same for both homoionic clay suspensions one may use the fraction $X_1 = V_1 / V$ to label the mixed suspension. Figure 2-1 shows the turbidity variation with X_{Ku}, the equivalent Ku-Na fraction, for mixed Ku-Na/Wy-Na montmorillonite at 1 g/l concentration. The values represent the equilibrium turbidities measured > 2.5 h after the mixing of the suspensions. However, the change from the measurement at 15 min after mixing were at most 2 NTU, i.e. well within the size of the data point markers. Prior to the turbidity measurements the vials with suspensions were shaken because sedimentation may otherwise cause undue influence.

The turbidity of the mixed suspension varies linearly with X_{Ku} in accordance with Equation (2-5), from the value of 129 NTU for homoionic Wy-Na ($X_{Ku} = 0$) to 396 NTU for Ku-Na. Clearly the mixing of these two clays did not induce any change in the particle structure, in particular the volumes V_p for either montmorillonite. Based on Equation (2-2), the particles responsible for scattering of light are 'larger' in the case of Ku-Na than in the case of Wy-Na. It is important to note that natural smectites are polydisperse which means that even for a homoionic Na-montmorillonite that separate into individual clay layers the turbidity is a weighted average of all sizes as described by Equation (2-4). The higher turbidity of Ku-Na compared to Wy-Na should thus be understood in terms of polydispersity – a different distribution is sufficient to give a higher turbidity, so a naïve interpretation that the ratio of the volume of Ku-Na to Wy-Na particles equals the ratio of their respective turbidities should be avoided. The validity of Equation (2-5) for Ku-Na/Wy-Na mixtures as demonstrated in Figure 2-1 is expected since it is known that Na-montmorillonite is more or less completely delaminated in dispersions (Ploehn and Liu 2006). Thus the montmorillonite particles from both clays are individual clay layers and given that the counterion is Na^+ there is no mechanism for aggregation that could change the particle size distributions in de-ionized water. It is important that Equation (2-5) was verified because it gives more confidence to discuss the cause of deviations that may be observed in other mixed clays.

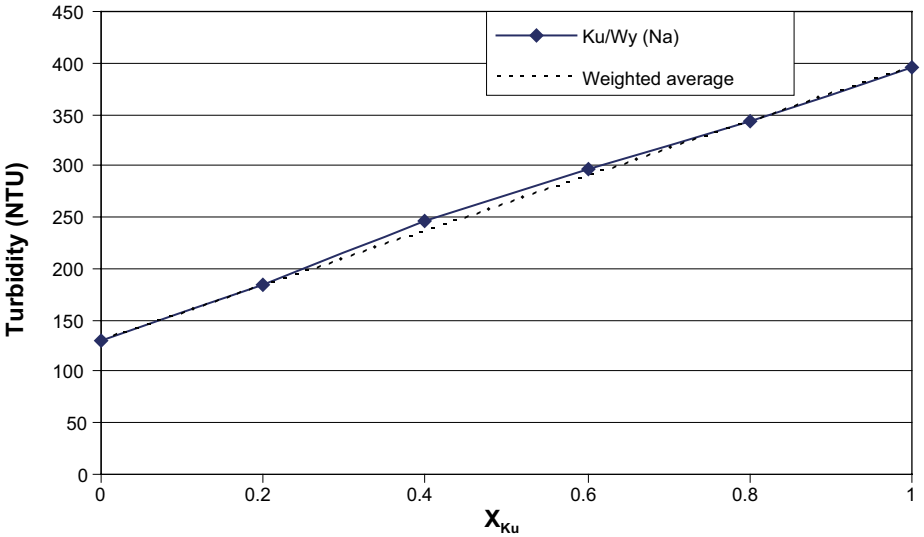

Figure 2-1. *Turbidity of mixed Ku-Na/Wy-Na dispersions at a concentration of 1 g/l. The measured turbidities are very close to the weighted average in accordance with Equation (2-5). In the range 100 to 1000 NTU the instrument resolution is 1 NTU.*

Equation (2-5) was also tested for 1 g/l mixed dispersions of Mi-Ca and Mi-Mg as well as Mi-K and Mi-Na, and the results are shown in Figure 2-2. The turbidity variation with XCa for Mi-Ca/Mg dispersions fully follows the weighted average. The difference in turbidities between homoionic Mi-Ca and Mi-Mg clays is rather small showing that the two clays are similar and that the valence of the counterion determines the particle (tactoid) size. With monovalent counterions the turbidities are significantly lower. Furthermore, exchange of Ca and Mg that must occur for entropic reasons does not influence turbidity, i.e., the particle size distribution. The turbidities for the Mi-K/Na suspensions are slightly lower the weighted average equation, indicating some interaction between Mi-K and Mi-Na particles leading to shift towards lower turbidities. Possibly some of the Mi-K clay is not fully delaminated, and ion exchange into mixed K/Na clay leads to a certain degree of particle break-up.

In the following it is important to bear in mind that the turbidity of, e.g., a Ca-montmorillonite suspension is not exclusively determined by its concentration but also on the preparation as is illustrated for Ku-Ca (1.5 g/l) in Figure 2-3. Two suspensions with 100 ml DI water and 0.15 g Ku-Ca were prepared by 24 h mixing with a magnetic stirrer. Before sonication 10 ml suspension was extracted for turbidity measurement. For suspension Ku-Ca1 eight intervals of 15 minutes sonication followed. After each interval the suspension was stirred on the magnetic stirrer for 60 s before 10 ml was extracted for turbidity measurements. The extracted suspensions were stored and turbidity was once more measured 70 h later (Ku-Ca1 +70 h). For the suspension labelled Ku-Ca2, the first five sonication intervals were 5 minutes each, then followed a final interval of 1.5 h. After 120 minutes accumulated sonication time both suspensions have similar turbidity, while at shorter times the turbidity of Ku-Ca1 is up to 3 % higher than that of Ku-Ca2. For both suspensions the turbidity is significantly lower prior to any sonication. This is because there are many clay aggregates that are large enough to settle during the time the sample vials are placed in the turbidimeter. The turbidity has a maximum after a certain accumulated sonication time because the larger tactoids are then small enough to stay in suspension. Further sonication promotes additional fragmentation of the tactoids leading to lower turbidity. Letting the sonicated suspensions rest for 70 h did not influence the turbidity. Thus the particles did not re-aggregate during this time. The last point is made because it is conceivable that after supplying enough energy, the aggregate or tactoid distribution may be shifted from the equilibrium towards smaller particles.

Turning our attention to the mixing of divalent and monovalent montmorillonite suspensions we first study the time development of turbidity. As stated above, after mixing, the vials were forcefully shaken and then tapped to remove air bubbles before the turbidity was measured. Prior to each subsequent turbidity measurement the vials were again shaken and tapped. In Figure 2-4 the turbidities at different times after mixing Wy-Ca and Wy Na suspensions (1 g/l) are shown. Within 10–12 minutes the turbidities have reached their equilibrium values showing, that the Ca/Na exchange process is very rapid. It is also interesting to note that there is no excess salt in the suspension, essentially only the counterions are present. The graph in Figure 2-4 indicates that Wy-Ca/Na behaves similar to Wy-Na for XCa $\leq$0.6 while the turbidity is significantly above the Wy-Na value for XCa $\geq$0.8. This is in accord with earlier studies of sol formation in mixed Ca/Na-systems (Birgersson et al. 2009, Hedström et al. 2011).

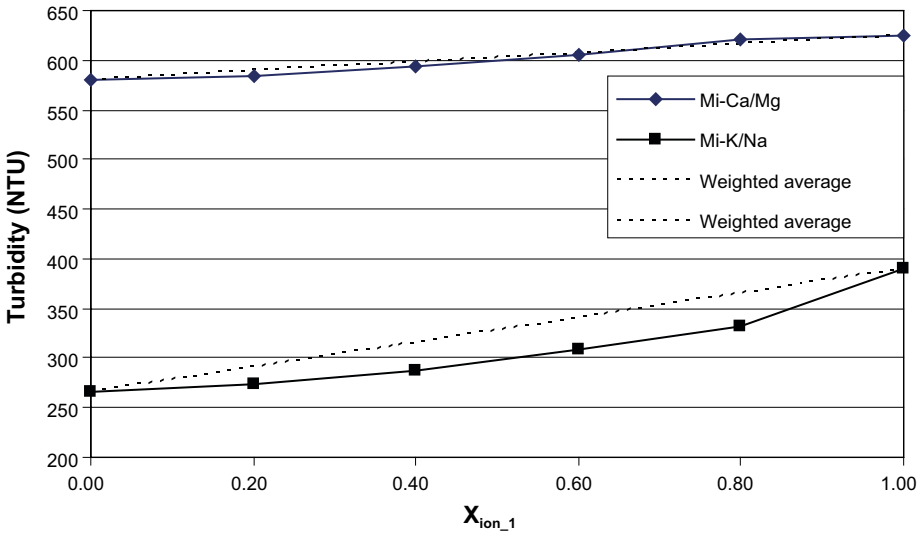

Figure 2-2. *Turbidity of mixed Mi-Ca/Mg respective mixed Mi-K/Na dispersions at a concentration of 1 g/l. The measured turbidities for divalent counterions follow closely the weighted average, Equation (2-5), while the measured turbidities for Mi-K/Na are slightly below Equation (2-5).*

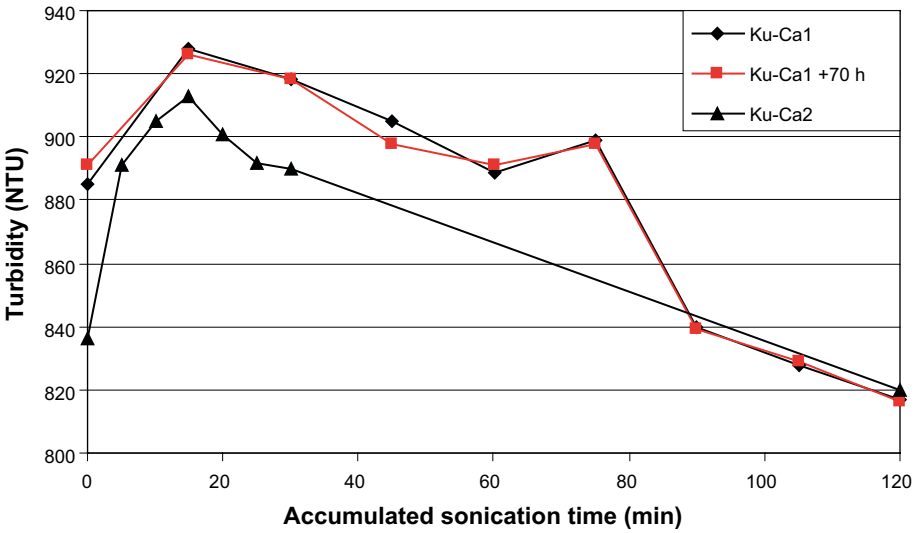

Figure 2-3. *Turbidity vs accumulated sonication time for two Ku-Ca suspensions (1.5 g/l). Ku-Ca1 + 70 h is the same suspension as KuCa1 but measured 70 h later.*

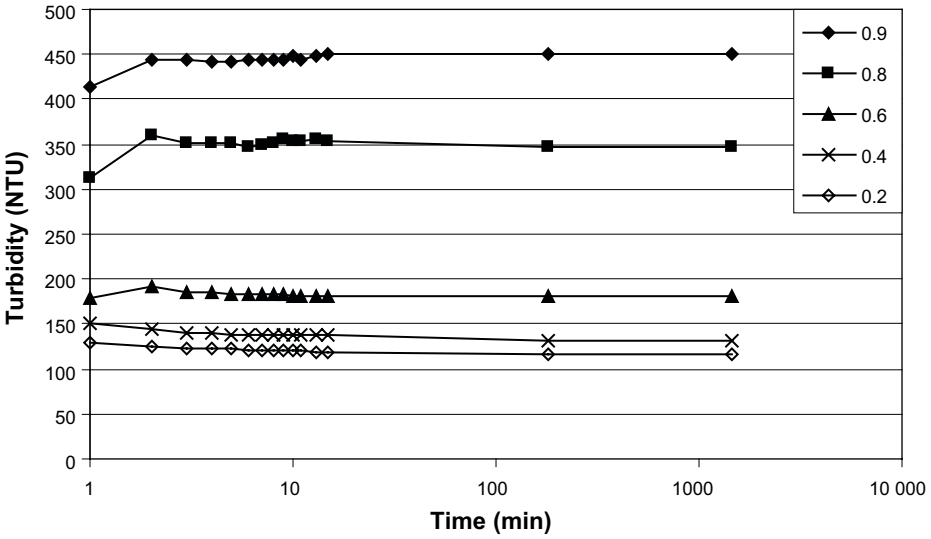

Figure 2-4. *Turbidity of mixed 1 g/l Wy-Ca/Na suspensions (X_{Ca} from 0.9 to 0.2) as a function of time after mixing.*

The transition to a pronounced Na-montmorillonite behaviour for mixed Ca/Na-montmorillonite at $X_{Ca} \leq 0.6$ is even more obvious in the series of plots in Figure 2-5 to Figure 2-7. Each plot shows the turbidity variation with X_{Ca} for Ku-, Mi- and Wy-montmorillonite at the same concentration, (0.5 g/l in Figure 2-5, 1.0 g/l in Figure 2-6). In Figure 2-7, the concentration is 2 g/l for Wy-Ca/Na, while for both Ku-Ca/Na and Mi-Ca/Na the concentration was chosen 1.5 g/l in order to not exceed the turbidity limit of the turbidimeter (1000 NTU). The experiments were done in duplicate (marked as (1) or (2) in the legends of each figure) and the results were highly reproducible. All three montmorillonites behaved similarly and up to $X_{Ca} = 0.6$ the turbidity remained close to the value for the respective homoionic Na-montmorillonite. Obviously the mixing of Ca- and Na-montmorillonite led to a break-up of the Ca-montmorillonite tactoids into an almost complete delamination, which is reflected in the turbidity. Contrast this with the relatively minor effect on the tactoid size of Ku-Ca after two hours of sonication. Turbidities were generally below Equation (2-5), even at $X_{Ca} = 0.9$ in the case of Mi-Ca/Na. Wy-Ca/Na had similar turbidity dependence as the Milos montmorillonite with a slight exception at $X_{Ca} = 0.9$ where the turbidity were close to Equation (2-5) (one value slightly above and the other slightly below at each concentration). The similarity is between Mi- and Wy-montmorillonite becomes even more apparent if the turbidity is normalized according to $\tau_{norm}(X_{Ca}) = (\tau(X_{Ca}) - \tau(0))/(\tau(1) - \tau(0))$ as shown in Figure 2-8. Both CEC and charge distribution between the tetrahedral and octahedral

sheets are alike in Wy- and Mi-montmorillonite (Karnland et al. 2006), hence it is reasonable that their turbidity curves would follow a similar pattern. Homoionic Ca-montmorillonite is aggregated due to attractive correlation forces that become dominant over osmotic repulsion in the case of polyvalent counterions (Guldbrand et al. 1984). Inclusion of monovalent counterions in the interlayers weakens the correlation attraction. Thus it is expected that the tactoid size distribution for montmorillonite with mixed di- and mono-valent ion population in the interlayer would shift towards smaller size. Up to $X_{Ca} = 0.6$, repulsion outweigh correlation attraction to such extent that almost complete delamination prevails. Monte Carlo simulations of the interaction between two charged layers with both di- and mono-valent counterions in the interlayer space show that attractive interactions dominate at $X_{Ca} = 0.9$ but a lowering of divalent content to 0.8 gave a van der Waals loop in the pressure vs. layer separation curve (Jönsson et al. 2009). The presence of such loop means that the short ~19 Å basal distance could coexist with a much longer layer separation according to the Maxwell construction (Atkins and de Paula 2006, Hedström et al. 2011). With increasing CEC, i.e., increasing layer charge, theory predicts stronger correlation forces. The Kutch montmorillonite has higher CEC as well as a larger proportion of the charge in the tetrahedral sheet, than the other two clays (Karnland et al. 2006). The plot in Figure 2-8 also shows that Ku-Ca/Na has higher normalized turbidities than Mi- or Wy montmorillonite consistent with theory.

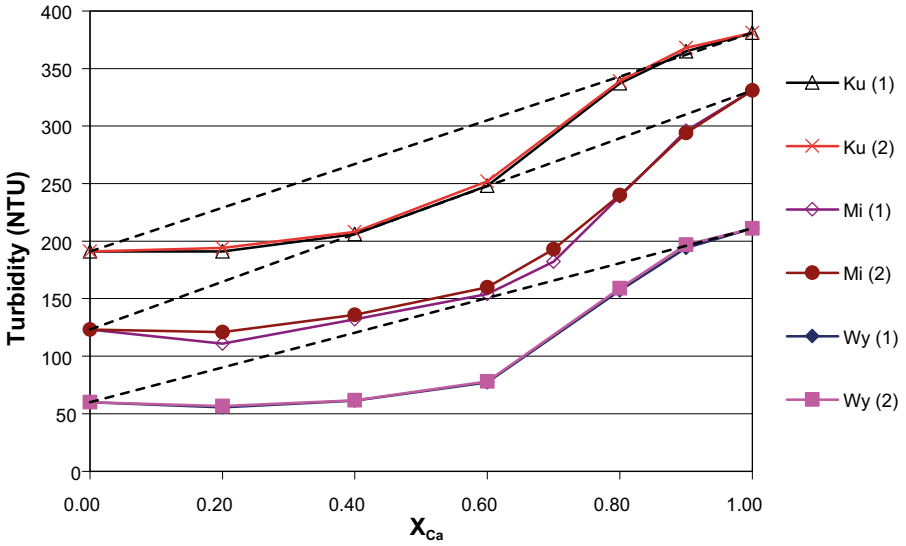

Figure 2-5. *Turbidity variation with X_{Ca} of mixed Ca/Na-montmorillonite dispersions at a concentration of 0.5 g/l. Dashed lines indicate the weighted average of Equation (2-5) for each montmorillonite.*

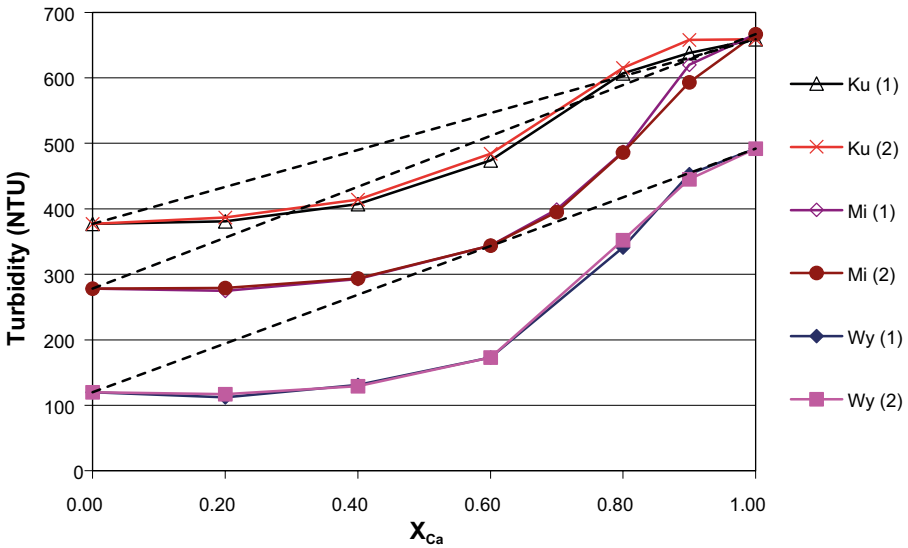

Figure 2-6. *Turbidity variation with X_{Ca} of mixed Ca/Na-montmorillonite dispersions at a concentration of 1.0 g/l. Dashed lines indicate the weighted average of Equation (2-5) for each montmorillonite.*

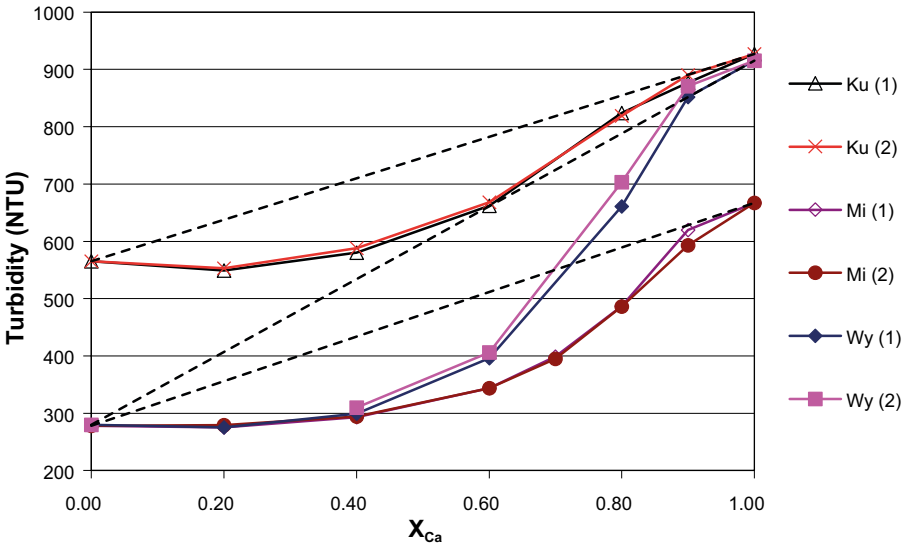

Figure 2-7. *Turbidity variation with X_{Ca} of mixed Ca/Na-montmorillonite dispersions. For Ku-Ca/Na and Mi-Ca/Na the concentration was 1.5 g/l and in the case of Wy-Ca/Na 2.0 g/l. Dashed lines indicate the weighted average of Equation (2-5) for each montmorillonite.*

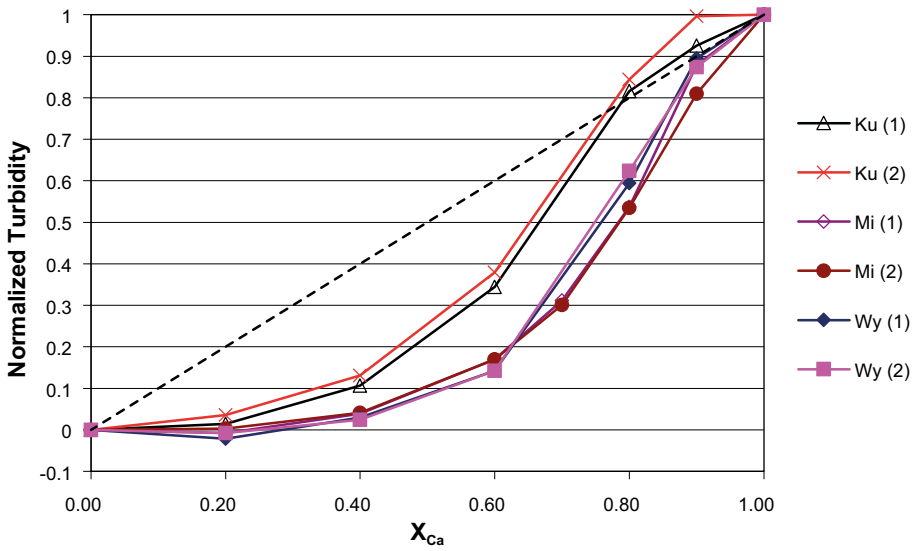

Figure 2-8. *Normalized turbidity vs X_{Ca} of mixed Ca/Na-montmorillonite dispersions at a concentration of 1.0 g/l.*

Suspensions of montmorillonite with divalent counterions (Ca^{2+} or Mg^{2+}) have similar properties as shown for Mi-Ca/Mg in Figure 2-2. Not surprisingly mixtures of Mi-Mg/Na have similar turbidity response as mixtures of Mi-Ca/Na as shown in Figure 2-9. Both Mi-Ca/Na and Mi-Mg/Na have significantly lower turbidity than the weighted average when the divalent fraction is less than 0.8 indicating break-up of tactoids.

2.4 Conclusions

It was earlier demonstrated that about 20 % sodium was sufficient to balance the correlation forces and induce break-up of Ca-montmorillonite aggregates (Birgersson et al. 2009, Hedström et al. 2011). In this study, we have investigated this break-up behaviour in further detail by mixing suspensions of Na-montmorillonite with Ca and Mg-montmorillonite, using montmorillonite from three different origins (Wyoming; Milos, Greece; Kutch region, India). For both Wy- and Mi-montmorillonite the

20 % Na^+ limit is confirmed, while the Ku-80/20 montmorillonite show less break-up than the other two. This is also in accordance with the theory for correlation effects, which are stronger, the higher the CEC. The experiments also show that the break-up process is fast: within 10 minutes the turbidities of the mixed suspensions have stabilized. Furthermore, these experiments on break-up were performed using DI water thus showing that excess ions are not needed to mix the ions. Na^+ diffuses into the interlayer of the Ca-montmorillonite tactoids and Ca^{2+} diffuses out and eventually the all clay is a mixed Ca/Na-montmorillonite. We also showed that the process is similar for Mg/Na-montmorillonite.

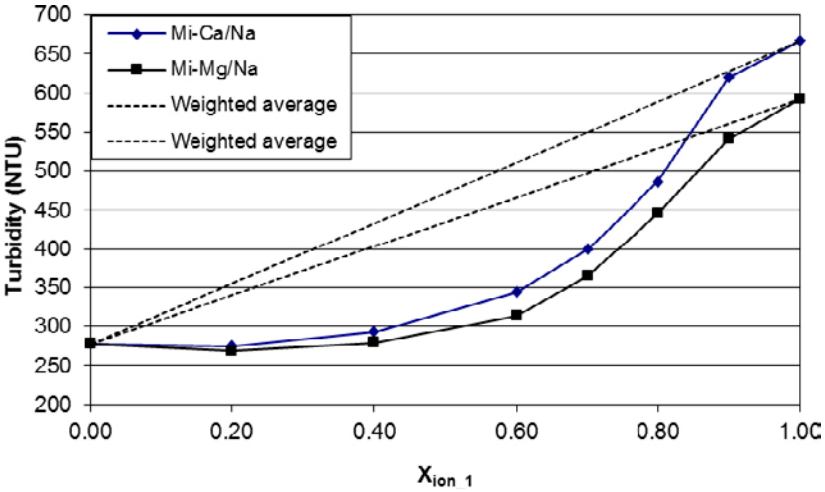

Figure 2-9. *Turbidity of mixed Mi-Ca/Na respective mixed Mi-Mg/Na dispersions at a concentration of 1 g/l.*

3 State diagrams of Wy-Na, Mi-Na and Ku-Na

3.1 Introduction

It is crucial for the integrity of a KBS-3 geological repository for spent nuclear fuel that the bentonite clay surrounding the copper canisters does not turn into a sol at the interface to the seeping groundwater, since the sol is liquid and easily transported away by flowing water. The transition to a sol may not be possible to avoid throughout the whole expected operational time of the repository. Therefore it is important to precisely know under what conditions a sol is stable, because it is under such conditions erosion may take place. It is also equally important to understand the properties of the gel phase. The gel need to be strong enough to withstand the shear forces from the seeping water, otherwise erosion may also take place at gel/groundwater interface. It is not yet fully known what clay concentrations can be obtained at interface to the seeping groundwater. This is an important question, as the clay concentration at the swelling front will have great impact on the yield stress of the buffer.

Clay particles suspended in aqueous solutions are known to exhibit a vast range of colloidal phases and phase behaviours. During the years, there have been many definitions of various colloidal clay phases such as attractive gel or glass, repulsive gel or glass, Wigner glass, sol, active or passive gel or empty liquid to mention some (Dawson 2002, Hansen et al. 2012, Mourad et al. 2008, Nishinari 2009, Ruzicka et al. 2008, 2010, Sciortino and Tartaglia 2005, Tanaka et al. 2004, Trappe and Sandkühler 2004, Zaccarelli 2007, Zhang et al. 2009, Zou and Pierre 1992). That the same type of phase or phase behaviour may by different authors be called by different names may create confusion. On the other hand, that the same name can be used for different phases/phase behaviours does not ease the situation. The issue is not helped by the fact that many colloidal phases experience aging behaviour, so one type of colloidal phase may undergo a phase transition to a different colloidal phase simply by waiting (Jabbari-Farouji et al. 2012, Ruzicka et al. 2004). This clearly shows that the method of sample preparation and testing is important in the outcome of the analysis.

Different analytical methods used in phase behaviour studies include visual observation, birefringence observation, rheological measurements, small-angle neutron scattering (SANS), small-angle light scattering (SALS), small-angle x-ray scattering (SAXS), dynamic light scattering (DLS), osmotic pressure measurements, transmission x-ray microscopy (TXM) and scanning electron microscopy (SEM) as well as environmental scanning electron microscopy (ESEM). Depending on the method of testing, the phase analyses are either performed at a macroscopic or microscopic level. Many studies are performed on a microscopic scale, while in the case of geological deep storage a more in-depth knowledge of the colloidal phase behaviour on macroscopic scale is required.

The most extensively studied clay appears to be laponite, a synthetic hectorite clay (Cummins 2007, Jabbari-Farouji et al. 2008, Mongondry et al. 2005, Mourchid et al. 1995, 1998, Ruzicka et al. 2005, 2007, 2008, 2011, Ruzicka and Zaccarelli 2011, Tanaka et al. 2004). While there are certain advantages to work with laponite, such as a more narrow size distribution as well as possibly a more clearly defined charge distribution, it is not necessarily true that the behaviour of laponite will correlate closely with the behaviour of naturally occurring montmorillonites. Whereas laponite generally have aspects ratios in the range of 30:1, the aspect ratio of montmorillonite is substantially larger, around 100:1 or more (Cadène et al. 2005, Michot et al. 2004, Ploehn and Liu 2006). A consequence from this is that the ratio of presumably positively charged edges compared with the total surface area of the montmorillonite particles is much lower than the ratio of edge charges/total surface area in laponite. This can, and most likely does, affect the ability to form interparticle bonds, i.e., edge-to-face associations. So while there may be qualitative agreement between laponite and montmorillonite state diagrams, quite likely there will be a quantitative difference. As bentonite with high montmorillonite content is considered for the construction of the buffer in the KBS-3 concept, the phase behaviour of naturally occurring montmorillonite is of the utmost importance.

Various aspects of montmorillonite phase behaviour have previously been studied by several groups (Abend and Lagaly 2000, Gabriel et al. 1996, Michot et al. 2004, Shalkevich et al. 2007). Also in our laboratory, some initial investigations concerning the montmorillonite state diagram have been conducted with emphasis on the sol-gel transition and in particular sol formation (Birgersson et al. 2009, 2011). Abend and Lagaly focused rheological experiments to estimate the conditions

for sol-gel transition. In addition to the salt concentration, they also investigated the effect various anions and cations had upon gel formation. However, while the salt concentration ranged from 1 mM to 1 M during the investigations, the clay concentration did not exceed 45 g/l (Abend and Lagaly 2000). At macroscopic levels, Shalkevich et al. identified three types of phases or systems, solid phase, liquid phase and phase-separated systems. While several types of methods were used for the study, such as visual observation and DLS, at low clay concentration (<20 g/l) and low salinity (0.01–0.1 mM NaCl) they found that only rheological investigations can differentiate between a solid and a liquid state. SANS, SALS and ESEM were used to determine the microscopic states, such as the formation of clusters or networks by either fully exfoliated particles or by clusters of particles. There techniques were also used to determine cluster size. However, Shalkevich et al. did not exceed a clay concentration of 45 g/l during their investigations either (Shalkevich et al. 2007). Michot et al. investigated the state diagram of montmorillonite up to a clay concentration of 60 g/l. Here, fractions of varying sizes of the naturally occurring montmorillonite were used during the investigations in order to study the influence of particle anisotropy. The focus was mainly on various phases at low ionic strength where the particle interactions are dominated by repulsion as is evident by the reported osmotic pressures. Thus the solid-like behaviour found in the rheological measurements is an effect of crowding or jamming rather than the formation of a continuous network. The solid state is accordingly characterized as a repulsive paste (repulsive gel). The sol-to-repulsive paste transition was studied by oscillatory stress measurements and birefringence observations to describe the macroscopic as well as the microscopic behaviour. In particular they identify an isotropic to nematic transition that not necessarily coincides with the sol-to-repulsive paste transition (Michot et al. 2004).

Similarly (Gabriel et al. 1996) identified isotropic liquids and (repulsive) gels as well as nematic (repulsive) gels in both bentonite and laponite suspensions through optical birefringence observations.

This section of the report focuses on the montmorillonite state diagram, by studying the macroscopic behaviour of montmorillonite at varying clay- and NaCl concentrations. In particular the clay concentration range is larger than in previous studies. The clay particles may very well be in a non-equilibrium state, but the resulting behaviour contains information about the initial colloidal state e.g. whether a percolated network of particles have been present or not. Whereas in many previous studies the aim has been detailed understanding of the repulsive parts of the state diagram, the present work shift the focus to the phases where attractions are crucial.

3.2 Materials and methods

Montmorillonite from three different sources, MX-80 (Wyoming, Wy) Deponit CA-N (Milos, Mi) and Asha 505 (Kutch, Ku) were extracted and converted into homoionic form as described in the report by Karnland et al. (2006).

Clay samples were prepared with specific clay- and salt concentrations at fixed volumes, according to the following protocol. Clay was dispersed in deionized water. Aqueous NaCl solution was added so that the overall sample volume as well as clay- and salt concentration were the intended ones. This salt solution was also called the internal salt solution, and the salt concentration of the internal solution was adjusted so the system would be in or near ion equilibrium with what we will term the external NaCl concentration. The determination of the internal concentration was done by solving the PB equation under the assumption/approximation that the clay particles were evenly distributed within the suspension volume initially occupied by clay (Hedström and Karnland 2012). The clay suspension was left to rest for one to four days, depending on clay before external NaCl solution was added. The volume of the clay sample was marked before external NaCl solution was added to fill the vial to the top. If the clay sample appeared to behave as a solid, the sample vial was laid down on its side. If not, the sample vial was left standing up. The clay sample was regularly checked for signs of different colloidal states by visual observation. If a sample that has been left standing up shows sign of behaving as a solid in was subsequently laid down. The preparation of a representative sample (40 g Wy-Na/l, 5 mM NaCl) is described as following: The total clay sample volume was 2 ml. Therefore, 80 mg Wy-Na was dispersed in 1 ml of deionized water. The Poisson-Boltzmann equation gives the internal NaCl concentration as 3.8 mM in order to be in equilibrium with 5 mM external solution. Therefore, 1 ml of 7.6 mM NaCl solution was then added and the sample was mixed. The 2 ml clay sample volume was marked before the external 5 mM NaCl solution was added to the sample which was then sealed and laid down on its side.

3.3 Results and discussion

During our studies of the montmorillonite state diagrams, we have come across three dominant initial state systems: gel, paste and sol. In the gel state, attractive interparticle forces govern the behaviour whereas in the paste state, repulsive interparticle forces are dominant. In the sol state, the clay particles are dispersed in a liquid phase, and it is the behaviour of this liquid phase that dominates the clay state.

In order to visually determine whether a colloidal system is a gel or a paste, one has to observe the behaviour of the phase at a longer time scale.

The state diagram shows what clay state one can expect initially, at a specific clay- and salt concentration. However, the clay systems are generally not in equilibrium, and during time, different state transitions may occur. Therefore, we also observed the behaviour of the initial clay states, both on shorter and longer time scale (> 1.5 years). During these studies, we found a variety of colloidal phase behaviours. We propose the use of the following terminology: gel, paste, sol (gaseous and liquid) and sediment.

From an initial sol state, we have observed three types of colloidal behaviours: *gaseous sol*, *liquid sol* and *sediment* (Figure 3-1).

Both gaseous and liquid sols consist of solid clay particles of colloidal size dispersed in a continuous liquid phase. However, the behaviour of the clay particles differs in the two subcategories. In a *gaseous sol* the clay particles appear not to interact with one another to any substantial extent – they tend to behave as particles in a gas. In a *liquid sol*, the clay particles are clearly interacting with one another. There is a clear boundary between the liquid phase containing colloidal particles and the liquid phase not containing or containing very few colloidal particles. In a gaseous phase, this boundary is absent or very diffuse. A liquid sol can to some extent be viewed as a gel precursor – given enough time, a continuous non-fluid colloidal network may be formed. However, this is not always necessarily true on a lab time scale, in particular if the electrolyte concentration is low. A *sediment* can be defined as clay particles that in a suspension settles under the action of gravity (Everett 1972) and we found that it is generally observed in combination with other types of colloidal behaviour.

A gel that ages appears to simply form a stronger gel. As can be expected, we have at no point observed any state transitions commencing with a gel. However, given time, a paste will either appear to swell or to “melt”, depending on the electrolyte concentration in the sample (Figure 3-2).

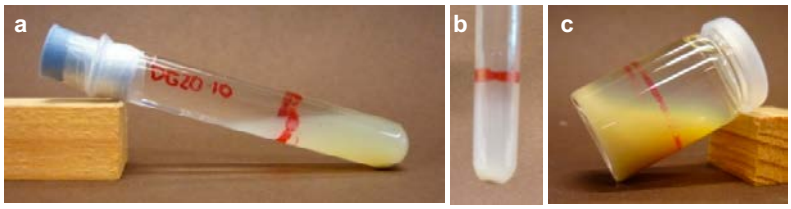

Figure 3-1. *a) Liquid sol. Exhibits flow behavior, but with a well-defined boundary between the sol and the aqueous phase without clay particles. b) Gaseous sol and sediment. The sol exhibits flow behavior, but there is no clear border towards the clear fluid. c) Gaseous and liquid sol.*

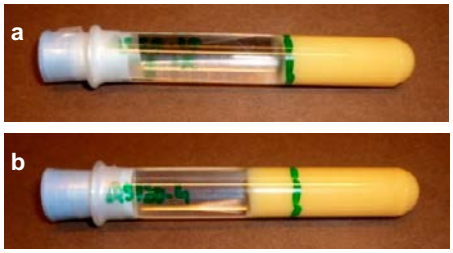

Figure 3-2. *a) Gel. No expansion past the initial sample volume. b) Swelling paste. Expansion of the initial sample volume.*

"Melt" in this context refers to the observed behaviour, a gradual disintegration of the paste beginning at the front. It is not melting in a strict thermodynamic sense although it probably reflect a paste to sol transition. During swelling of a paste the concentration of particles becomes lower and particularly near the interface to the NaCl solution. Lower clay density leads to lower repulsive forces and at one point low enough that formation of a gel network becomes possible if electrolyte concentration is above the CCC. The entire paste will gradually experience a transition into a gel as the sample continues to expand, thus lowering the clay concentration. If the electrolyte concentration is below the CCC, then the clay particles may not be able to form a network structure upon expansion of the sample. Instead, gaseous and liquid sols may form and some sedimentation may occur, and the paste appears to melt. However, in both instances, the state behaviour of the paste is the same: non-connected particles that due to osmotic pressure are forced apart until an equilibrium system is reached.

3.3.1 State diagrams

The observations of various clay states can best be described at different salinities as a function of the clay concentration. We have previously described a schematic state diagram (Figure 1-3), where at low clay concentration and salinity a sol is likely to be observed, whereas in more dense systems a paste is formed. If the salinity is sufficient high and the clay concentration is within certain limits, a gel may be formed (Birgersson et al. 2009, 2011). The dashed boundary to the sol phase at low clay concentration and higher NaCl concentrations in Figure 1-3 is an estimate regarding the percolation limit where there are not enough particles to form a network structure. Especially for slowly gelling system, this boundry is difficult to explore due to gravity that makes sedimentation competing with gelling.

These clay states, gel, paste and sol, were observed upon preparation of clay samples with varying clay- and NaCl concentration. When comparing different naturally occurring montmorillonites, it is found that the state boundaries vary. For Wy-Na, a gel state is observable first at 20 mM NaCl (Figure 3-3). As expected, the paste state is observed at higher clay concentrations, whereas a sol state is observed at low clay concentration, as well as at low salinities.

For Ku-Na, small differences in the salinity can have a great effect on the colloidal state of the system (Figure 3-4). The gel-paste state boundary is comparatively flat when one considers both the Wy-Na and the Ku-Na state diagrams. For Mi-Na, the gel-paste transition boundary is rather steep, but just as with Ku-Na, the sol-gel transition line is found far below the sol-gel transition line in the Wy-Na state diagram (Figure 3-5).

The transition boundary between sol and gel is not always easy to determine, as sometimes it appears that both a gel and a sol is present in the sample or the sol forms a gel very rapidly. For example, Ku-Na samples with a clay concentration of 10 g/l formed a gel overnight, suggesting the initial state is something in between a sol and a gel.

From the initial three colloidal clay states, a plethora of colloidal behaviour can be observed as the samples ages, as demonstrated in the following colloidal behaviour diagrams. As the colloidal states are not in equilibrium, the colloidal behaviour is continuously progressing with time. Initially, the sol state behaves as a liquid sol. With time, some sedimentation is generally observed. The initial liquid sol may remain, or experience a transition into a gaseous sol. Given enough time (> 1.5 years), most sols appears to experience a sol-gel transition, forming a very dilute gel. A paste may swell until it reaches a clay concentration where a gel can be formed, or it may "melt", forming a mixture of colloidal states.

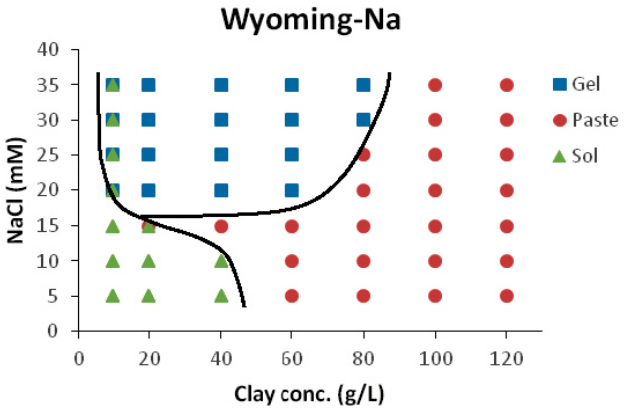

Figure 3-3. *State diagram of Wy-Na montmorillonite.*

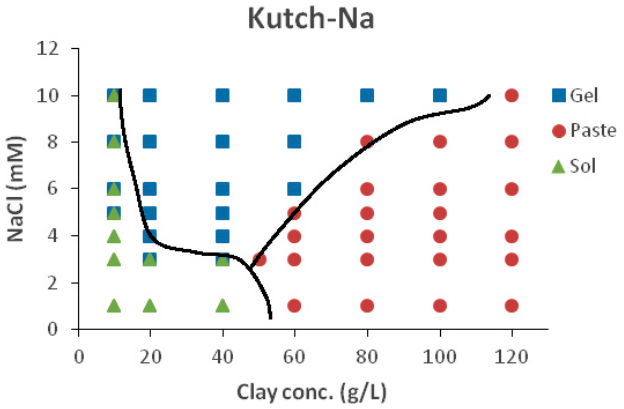

Figure 3-4. *State diagram of Ku-Na montmorillonite*

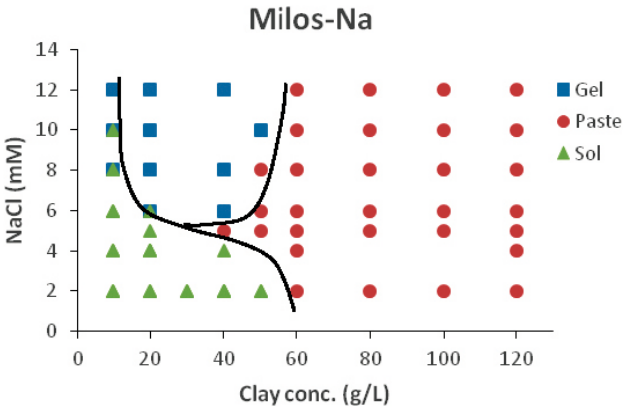

Figure 3-5. *State diagram of Mi-Na montmorillonite.*

The state behaviour diagram of Wyoming-Na shows all varieties of colloidal behaviour, as well as combinations thereof (Figure 3-6). Samples with high clay concentration initially behave as solids and should therefore be characterized as either gels or pastes. However, over time, the samples exhibit signs of expansion, which suggests the samples are pastes, not gels. At NaCl concentrations above 20 mM (CCC) the paste swells, and below 20 mM the paste appears to melt. 20 mM NaCl also appears to be a requirement for gel formation. Above 20 mM swelling of the paste is observed because at the front next to the external electrolyte a gel is formed that hinders dispersion. Below 20 mM no gel is formed at the swelling front and a rapid dispersion of clay particles occurs, giving the appearance of melting. Often, in the case of Wy-Na, the gel is not formed instantly, a day or two is usually required. Generally, the lower the clay concentration, the longer the gelation process. At a clay concentration of 10 g/l, gelation does eventually occur. However, the gelation process is markedly slower than the gelation of samples of a higher clay concentration, even 20 g/l. Therefore, in addition to gel formation, some of the samples have ample time to sediment during the process. Sedimentation is also observed for almost all samples below 60 g/l clay and 20 mM NaCl (with the exception of the 40 g/l clay sample at 15 mM NaCl). As sedimentation lowers the clay concentration in the gel, we know that a sample with the initial clay concentration 10 g/l will form a gel eventually, but we will not know with certainty what the concentration of this gel will be as the actual clay concentration will depend on the extent of sedimentation. In addition to gels and pastes, at low clay- and NaCl-concentrations, we also see sol phases, both liquid and gaseous sols.

Also with Kutch-Na, a paste is found at high clay concentrations (Figure 3-7). At NaCl concentrations at or above 4 mM, this paste swells, whereas below 4 mM NaCl it appears to melt. At lower clay concentrations, a gel state is found. Unlike for example Wyoming-Na and Milos-Na montmorillonite, Kutch-Na has a tendency to display a stable gel the moment the air interface is replaced by a liquid interface. However, at low clay concentrations the clay-rich phase behaves more as a liquid sol. Upon standing (~18 h) this liquid sol gelates. Unlike Wyoming-Na, there are no signs of sedimentation at this part of the state behaviour diagram, possibly due to the relatively rapid gelation even at a clay concentration of 10 g/l. However, when both the clay and the NaCl concentrations are low, sedimentation does occur. With one exception, these samples form either gaseous sols, liquid sols or both.

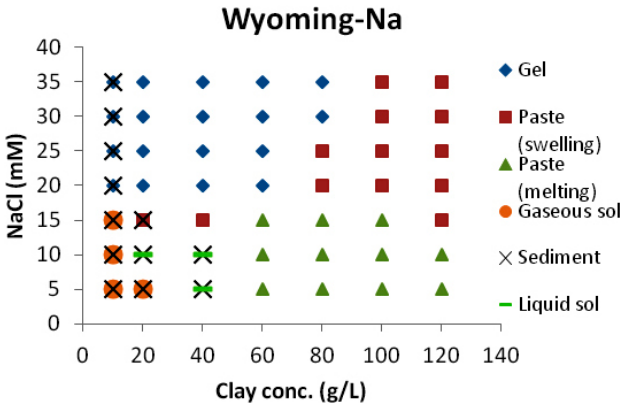

Figure 3-6. Behavioural state diagram of Wy-Na montmorillonite.

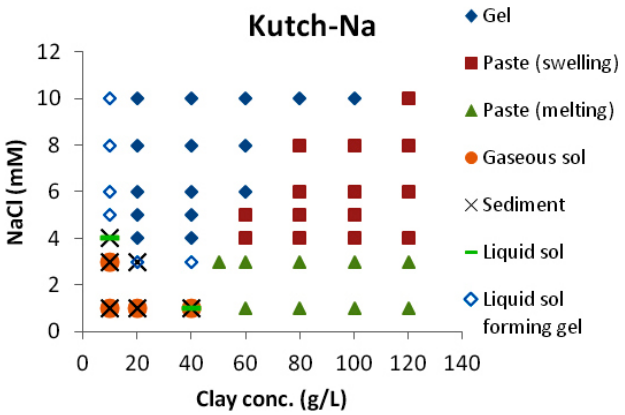

Figure 3-7. Behavioural state diagram of Ku-Na montmorillonite.

The general state behaviour diagram looks similar for Milos-Na, although there are a few differences in addition to changes in clay- and salt concentrations (Figure 3-8). Here, a combination of gel and liquid sol in the same clay samples is found at low clay concentration. It is also possible to see just a liquid sol in a clay sample, without either gaseous sol or sediment present.

3.3.2 Discussion

During this investigation, we have established the state boundaries with respect to clay concentration and salinity. It has become clear that while the same trends are observable for all the tested montmorillonites, the conditions during which a specific colloidal state can be observed varies as the state boundaries are dependent on the specific type of montmorillonite.

Table 3-1. CCC for the various montmorillonite and the highest clay concentration of gels at the CCC. This clay concentration represents the border between paste and gel.

Montmorillonite	CCC, NaCl [mM]	Gel-paste border at CCC [g/l]
Wy-Na	20	60
Mi-Na	6	40
Ku-Na	4	40

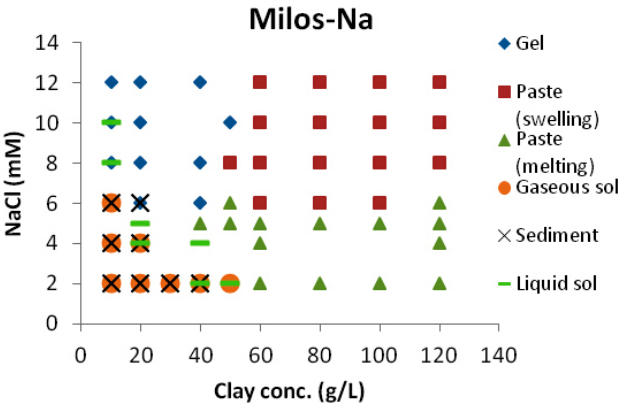

Figure 3-8. *Behavioural state diagram of Mi-Na montmorillonite.*

For example, the NaCl concentration required for the formation of a gel is 20 mM for Wy-Na but only 4 mM for Ku-Na (3 mM for a gel that is not instantly formed) and 6 mM for Mi-Na. At this boundary, the sol-gel transition boundary, a gel can be formed up to 60 g/l for Wy-Na, but at 80 g/l a paste is formed instead. For a Ku-Na clay, the paste is obtained already at 60 g/l, and for Mi-Na clay the paste is obtained at 50 g/l (Table 3-1). But also the steepness of the gel-paste transition boundary differs between the montmorillonites. For Wy-Na, an increase in the salinity by 10 mM, from 20 mM to 30 mM NaCl, increases the gel-paste transition boundary by about 20 g/l. For Ku-Na, an increase in salinity from 6 mM to 10 mM increases the gel-paste transition boundary by about 40 g/l. This shows that one montmorillonite is not identical or exchangeable with the next, not even after homo-ionization. This suggests that the known variations in properties such as the charge density, and the distribution of charges in the tetrahedral and octahedral layers (Table 2-1) most probably are responsible for the variation of the state boundaries of the various montmorillonites (Hetzel and Doner 1993). Another factor that may be of importance is the particle size distribution of the various montmorillonites. Here Wy-Na seemingly stands out as having both a broader distribution and a larger mean-weighted equivalent diameter than other tested clays (Cadène et al. 2005, Delavernhe et al. 2015). Wy-Na has also the highest CCC of the clays studied here also including FEBEX-Na that has a similar CCC to Mi-Na as shown in chapter 4.

A phenomenon that has been observed during this study is the rich behaviour of colloidal clay states. Many colloidal types of clay in aqueous solution experience aging behaviour, so one type of colloidal state may experience a transition to a different colloidal state. In addition to gel, we have observed sedimentation, liquid and gaseous sols and “melting” pastes as well as swelling pastes.

Of particular interest during our studies is the behaviour of the swelling paste. Swelling pastes are generally found in the higher concentration ranges of the state diagrams, sometimes as low as 60 g clay/l but often at higher clay concentrations (especially at higher salinities). As particles move away from one another, a gel is formed at the aqueous interface, locking the sample in place and preventing it from “melting” or disintegrating. It seems reasonable that a density gradient starts to form in the sample. However, the paste itself continues to expand until a gel has been formed throughout the sample, causing the clay concentration to become lower. When gels have been formed throughout the samples, the clay concentrations of the samples are the same as the clay concentrations of the gel samples with the highest clay concentrations. At this point the expansion of the clay samples ceases. This suggests that, provided the electrolyte concentration is above the limit for gelation, when starting with a highly compacted clay sample, the lowest possible clay concentration that can be obtained in the sample is the same clay concentration as the highest possible clay concentration for gel formation in a sample. Of course, the larger the sample, the longer this process will take. But it seems reasonable that once a sample has a clay concentration that permits gel formation at the specific concentration, expansion should cease.

Also the state behaviour varies depending on the montmorillonite. The sol-gel transition boundary has been mentioned previously. This boundary is generally also the NaCl concentration required for the formation of a swelling paste rather than a melting paste (as expected, as a gel forms at the edges of a paste in a paste that appears to swell rather than melt).

3.4 Conclusions

The method used in this investigation was particularly chosen to be able to accurately determine the gel-paste boundary since it is of importance in judging risks concerning the integrity of bentonite barriers in geological storages of spent nuclear fuel. When a gel is formed it is straightforward to judge what constitutes external electrolyte and what constitutes gel since the gel creates its own membrane. If no swelling is detected one knows that the clay concentration and external electrolyte concentration are such that the gel state is stable. When swelling occurs the initial state exerts a swelling pressure and is thus dominated by repulsions, which we term a paste. The method is less accurate when determining the actual equilibrium states below the CCC. Again from the bentonite barrier application point of view the CCC or the gel-sol line still represent the NaCl concentration where eventual loss of bentonite may occur, either through further swelling into fractures or transported away by flow.

These investigations suggest that, provided the ionic strength of the groundwater is above the CCC, the highly compacted clay in engineered barriers will act as a swelling repulsive paste and expand. Once the lowest clay concentration at the swelling front is below the clay concentration required for paste formation, the clay will form a gel. The lowest limit appears to be about 60 g/l, although it can be higher depending on the type of montmorillonite as well as the salinity in the surrounding system. With a layer of gel outside the highly compacted paste, the risk of sol formation is very low and loss of clay will probably be attributed to shear loss. However, if the salinity of the groundwater is below the electrolyte concentration required for gelation, it is likely the paste may melt rather than swell, forming gaseous and liquid sol particles which may easier be lost from the system due to groundwater flow.

Furthermore, we would like to stress the point that one montmorillonite simply is not exchangeable for another. Differences in charge density as well as most likely differences in the distribution of tetrahedral and octahedral charges affect the sol-gel transition boundary as well as the gel-paste transition boundary, which not only vary in clay concentration between montmorillonites, but also varies in steepness depending on which montmorillonite is being investigated. Particle size distribution is another factor that may influence the gel-sol and gel-paste boundaries, as it has been demonstrated that this factor influences the paste-sol boundary (Michot et al. 2004). In this, and most likely during other types of studies involving montmorillonite, one cannot investigate the generic “montmorillonite state diagram” and assume that the behaviour of one montmorillonite is identical with the behaviour of another montmorillonite.

4 Behaviour of smectite gels upon heating

4.1 Introduction

Although it is well known that colloidal clay suspensions can form gels, the gel structure is not known nor is the mechanism that holds the particles together fully understood or agreed upon (Angelini et al. 2014, Jönsson et al. 2008, Lagaly and Ziesmer 2003, Mongondry et al. 2005, Mourchid et al. 1998, Shahin and Joshi 2010). While gelling of smectite clay may be an undesired feature in many industrial applications (Goh et al. 2011), it is of utmost importance for the use of bentonite in nuclear waste management applications. In the absence of gel formation, a possible scenario for the long-term safety assessment of a geological disposal of spent nuclear fuel is loss of bentonite buffer material through contact with dilute groundwater at a transmissive fracture interface (Posiva 2012, SKB 2011). The aim of the present study is to further investigate the nature of the interactions responsible for gelling and their magnitude.

It has been argued that at relatively low ionic strength, electrostatic forces between negatively charged clay faces and presumably positively charged clay edges are the main bonding forces in the gel (Goh et al. 2011, Martin et al. 2002, Mongondry et al. 2004). The strongest indication favouring such mechanism is the large influence of tetrasodium pyrophosphate or sodium hexametaphosphate on the aggregation of clays. The addition of these polyphosphate ions to a smectite clay dispersion increases the CCC of Na^+ by more than an order of magnitude in most cases. For example, a 0.025 wt% sodium beidellite dispersion was found to coagulate at a NaCl concentration of 6 mM, which was increased to 230 mM in the presence of 1.25 mM tetrasodium pyrophosphate (Lagaly and Ziesmer 2003). Similar behaviour was observed for laponite, a synthetic hectorite (Martin et al. 2002, 2006, Mongondry et al. 2004) as well as montmorillonite (Lagaly and Ziesmer 2003).

The effectiveness of pyrophosphate to prevent gelling stems from its ability to bind to the positive edge charges of the clay particles (Mongondry et al. 2004). A sodium smectite with negative edge charges could only form a gel when the van der Waals attraction dominates the system (Jönsson et al. 2008), which would require NaCl concentrations of the order 200 mM or higher to efficiently screen the electrostatic repulsions originating from both faces and edges. The DLVO theory gives a CCC in excess of 1 M NaCl when applied to two parallel surfaces of typical montmorillonite surface charge density and using a representative Hamaker constant for handling the van der Waals interaction (Evans and Wennerström 1999).

At sufficiently low ionic strength, sodium smectite clays do not form gels and several studies have shown that sodium montmorillonite completely delaminate (Cadène et al. 2005, Michot et al. 2004, Ploehn and Liu 2006), suggesting that under such conditions inter-particle repulsion dominates.

Seemingly, the positive edge is not discernible to the negative faces at electrolyte concentrations below the CCC. This observation has been interpreted in terms of a spillover of the negative potential of the particle face into the edge region. By numerically solving the Poisson-Boltzmann equation for a thin disc, mimicking the aspect ratio and the edge and face charge densities of montmorillonite, it was found that the spillover of the negative potential depends strongly on the NaCl concentration (Secor and Radke 1985). Above the CCC the spillover is reduced to such extent that the potential emanating from the edge region is positive and thereby attraction with the negative surface of a second clay particle becomes possible. However, electrostatic screening also influences the attraction between positive and negative charges so at some ionic strength further above the CCC the smectite gel is expected to get weaker.

In this study, we attempt to study the strength of gels by means of observing their behaviour under heating. We record the temperature T_y where yield occurs (if it occurs), for investigating variations in the inter-particle bond strength of the gels as a function of NaCl concentration. Using this method we were able to confirm the qualitative behaviour deduced from the Poisson-Boltzmann theory and thereby offer new evidence supporting the idea that electrostatic edge-to-face attractions are responsible for gelling. Similar variation in interaction energy with ionic strength has also recently been discussed in a combined experimental and theoretical study on the attractions between proteins (Li et al. 2015), another system that, similar to clays display patchy interactions (Corezzi et al. 2009, Sciortino and Zaccarelli 2011).

There are many suggestions in the literature that smectite clays form percolation gels (Martin et al. 2002, Ruzicka et al. 2011, Shalkevich et al. 2007), and the notion of a three-dimensional cross-linked network is an appealing description of the gel shown in Figure 1-5. Based in part on the observation of such structures we have also perceived the gels as percolation gels (Birgersson et al. 2009) and in this study we attempt to further test that view.

Eldridge and Ferry (1954) conducted a seminal study on the thermoreversible behaviour in gelatin gels. From the melting point variation with respect to gelatin concentration, the enthalpy of cross-link formation in gelatin gels could be determined, using concepts from percolation theory (Flory 1941, Stockmayer 1943). Similarly, we tested their idea by recording the yield-point temperature as a function of clay concentration, C_{clay} while keeping the salinity constant, which allowed for evaluating the enthalpy of formation of the edge-to-face linkage in clay gels. Furthermore, the fact that clay gels and gelatin gels behave similarly further strengthen the view that clays form percolation gels under the conditions in the present study.

We have also employed our method to study aging effects on the clay gel. Our findings generally confirm the increase in gel strength with aging, as found in other studies using different techniques (Baghdadi et al. 2008, Jabbari-Farouji et al. 2012, Knaebel et al. 2000, Labanda and Llorens 2008, Mongondry et al. 2005, Ruzicka et al. 2004, Shahin and Joshi 2010).

4.2 Theory

4.2.1 Yield temperature vs ionic strength

As we already discussed in the introduction above, the spillover effect (Secor and Radke 1985) is the cause behind the emergence of a CCC. Without spillover of the negative potential from the clay layer face to the edge region, one could expect gelation at much lower ionic strength as long as there are positive charges on the edge. With the spillover theory as starting point we realize that gradual increase in ionic strength above the CCC initially should lead to increased binding energy as the negative potential from the particle face withdraw further. This process cannot continue for all ionic strengths as the Debye screening also influence the electrostatic attraction. Thus, theory suggests that there ought to be a maximum binding strength at an intermediate ionic strength. This should be reflected in a non-monotonous relation between T_y and ionic strength in experiments performed at constant clay concentration. In the case that van der Waals interaction is responsible for gelation, increasing ionic strength would only influence repulsion, thus giving a monotonous increase of T_y with ionic strength.

4.2.2 Binding enthalpy

Assuming that the gel is a percolation gel. For such a gel to be stable requires that the fraction of bonds is above a critical value. Heating the gel induces bond breaking and the gel becomes unstable and starts to yield when the bond fraction of edge-to-face linkages falls below a critical fraction g_y. Let K be the equilibrium coefficient for the clay edge (e) to face (f) association, $e + f \rightleftharpoons e \cdots f$, then (Atkins and de Paula 2006)

$$K = \frac{[e \cdots f]}{[e][f]} = \exp(-(\Delta H - T\Delta S)/RT), \tag{4-1}$$

where R is the gas constant, [ ] denotes concentration ΔH and ΔS are the enthalpy and entropy, respectively, for the reaction. We assume that that $[e \cdots f] \propto C_{\text{clay}} \cdot g$ where g is the fraction of reacted edge-to-face associations. Regarding the concentration of 'unreacted' edges and faces we further assume that both $[e]$ and $[f]$ are proportional to $C_{\text{clay}} \cdot (1-g)$ which allows us to write $K \propto g / C_{\text{clay}} \cdot (1-g)$. Increasing the temperature of a gel cause breakage of edge-to-face linkages and at T_y only a critical fraction g_y (presumably independent or only weakly dependent on C_{clay}) remains and the gel starts to yield. Under these assumptions, Equation (4-1) relates C_{clay} to T_y and after taking the logarithm one obtains

$$\ln C_{\text{clay}} = \Delta H / RT_y + \text{constant}, \tag{4-2}$$

from which ΔH can be evaluated (Eldridge and Ferry 1954, Liu and Pandey 1996).

4.3 Experimental

4.3.1 Material

Smectite extracted from two types of bentonite have been used in these investigations, Kutch-type obtained from the Indian bentonite Asha 505 (Ashapura Minechem Co.) and FEBEX-type from bentonite excavated in Cabo de Gata, Spain (Huertas et al. 2001). The smectites from both localities consist essentially of montmorillonite which were purified and ion-exchanged to homoionic sodium form according to the procedure described in Karnland et al. (2006). The purified smectite/montmorillonite is referred to as Ku-Na or FEBEX-Na.

4.3.2 Gel sample preparation

Na-montmorillonite clay was dispersed in 5 ml DI water. 5 ml NaCl solution (of double concentration of the final sample) was added after which the sample vial was vigorously shaken. After 30 min, additional NaCl solution (final concentration) was added, with care taken to avoid disturbing the clay dispersion, in order to create a liquid-liquid (or gel-liquid) interface rather than a liquid-air interface. As an example, to prepare a gel at final NaCl concentration of 5 mM, 5 ml of clay suspension prepared in DI water was mixed with 5 ml 10 mM NaCl (aq). After 30 min the additional 5 mM NaCl solution was added. The age of the samples was considered from the time when the final solution was added. The samples were left for at least 18 h, during which the clay suspension for samples of sufficient clay- and salt concentrations formed a gel. For all gels in the study the attractive forces are strong enough to balance the osmotic pressure. Thus, the addition of excess electrolyte does not cause any expansion (nor contraction) of the gel, i.e. the gel show no tendency to incorporate additional solution (cf. Figure 3-2 a). Thus we deem that adding additional NaCl solution to the gel causes negligible modification to the gel structure or gel concentration.

4.3.3 Transition temperature determination

The sample vial containing gel was lowered and placed on its side in a beaker with 0.5 l NaCl solution of the same ionic strength as the sample. Having liquid on top of the gel reduces the disturbance to the gel when lowering the vial into the beaker. Also the gel needs the support of the buoyancy of the surrounding electrolyte (see further section 5.1). The age of the gels was normally 18 h except in the test where the influence of aging was monitored. Gels of sufficient strength would at this stage show no signs of deformation or flow. The beaker was placed in a water bath, which was slowly heated to 75 °C. The temperatures of both the water bath and the NaCl solution were continuously measured, and the clay gel was checked for signs of phase transition with five degree intervals. The measurements for determining the binding enthalpy (Eldridge and Ferry 1954) were done by monitoring the transition temperature every degree Celsius. The transition or yield-point temperature, T_y was determined as the temperature when the first signs of deformation of the gel appeared.

4.4 Results

4.4.1 Temperature response

Melting temperatures for pure crystalline substances can normally be determined within a very narrow interval, while for substances with impurities melting occurs over a larger temperature span. For the clay gels in this study, complete melting did not take place at a specific temperature, which was anticipated as natural clay particles are polydisperse and gels are not crystalline. When melting occurred, the process appeared to be continuous and ceased if the temperature was not constantly raised. This was observed mainly at low ionic strength. Gels formed at high ionic strength did not melt after initial yield. Nevertheless, both at low and high ionic strength, the gels underwent an observable yield upon heating and the temperature where yield started was recorded as the transition or yield-point temperature, T_y.

For Ku-Na montmorillonite with C_{clay} = 10 g/l and ionic strengths below 10 mM, an initial gel deformation or yield was observed followed by melting of the sample, that is, as the temperature was raised, the sample started increasingly behaving as a liquid rather than a soft solid (Figure 4-1 a and b). For some samples, the melting was almost complete at 75 °C with the clay particles forming a thin layer at the bottom of the beaker. However, the clay particles did not lose all inter-particle

bonds during the heating. While a liquid may be formed, there was no gaseous-like sol formation where clay particles would give a diffuse boundary between the denser liquid and the surrounding electrolyte. At ionic strengths above 40 mM, we observed yield, but soon afterwards the gel seemed stabilised and did not melt upon further heating. The transition, while explicit, was not as pronounced as at lower ionic strengths. At even higher ionic strength no yield was observed (Figure 4-1 c).

4.4.2 Testing the spillover hypothesis

The observed variation of T_y with ionic strength for Ku-Na is shown in Figure 4-2. For clay gels with C_{clay} = 10 g/l aqueous solution, three tests series were done and the repeatability was found to be satisfactory with a measuring accuracy of ± 5 °C, except at 40 mM where the variation among the three samples was larger. Below a NaCl concentration of 10 mM the observed T_y increased with increasing ionic strength, while at 10 mM NaCl the gels in the three tests showed no signs of yield or other change during heating to 75 °C. However, at 40 mM NaCl, yield was once again observed in two of the samples. Further increasing the NaCl concentration to 70, 100 and 200 mM caused a lowered T_y, indicating a weakening of the structure. When the NaCl concentration reached 300 mM, no transition could be observed, most likely related to van der Waals interactions being dominant at higher salinity. These observations are in direct agreement with the spillover hypothesis (Secor and Radke 1985) and overall electrostatic screening.

Increased C_{clay} gave increased T_y. At low salt concentrations, T_y was markedly higher at C_{clay} = 20 g/l compared with the value at C_{clay} = 10 g/l (Figure 4-2). At C_{clay} = 20 g/l, yield was only observed at 4 and 5 mM NaCl. At salt concentrations of 6 mM and above the gels remained unchanged on the macroscopic scale during heating (Figure 4-1 c). At C_{clay} = 40 g/l, no change upon heating was observed at any tested salt concentration. It should also be noted that none of the gels, even at 40 g/l, expanded during the experiment indicating that the attractive forces withstand the osmotic repulsion.

Figure 4-3 shows the transition temperature variation with salinity for FEBEX-Na gels (10 g/l) together with the averaged results for Ku-Na gels for comparison. The behaviour of T_y is similar for the two clays, but as these are natural materials a complete overlap of the data cannot be expected. Also for FEBEX-Na, at low salinities, the initially low T_y caused the gels to melt to varying extents.

Figure 4-1. *Three gels after rapid heating to 75 °C. (a) Ku-Na gel (10 g/l) in 5 mM NaCl solution. The gel underwent almost complete melting transition during heating to 75 °C and solidified as the temperature was lowered. (b) Ku-Na gel (10 g/l) in 6 mM NaCl-solution. The gel experienced large deformation (partial melting) during heating to 75 °C. (c) Ku-Na gel (20 g/l) in 200 mM NaCl-solution. The gel showed no sign of change.*

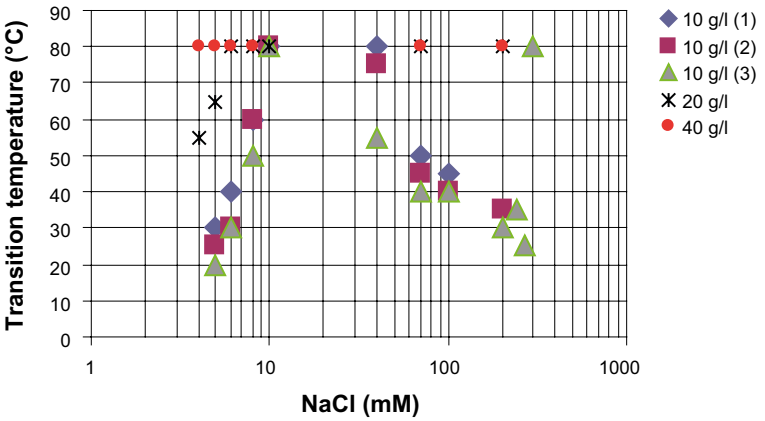

Figure 4-2. *Transition temperatures of Ku-Na gel (10–40 g/l) at varying salinity. Samples that showed no change upon heating to 75 °C (the maximum temperature in the test) are plotted at 80 °C.*

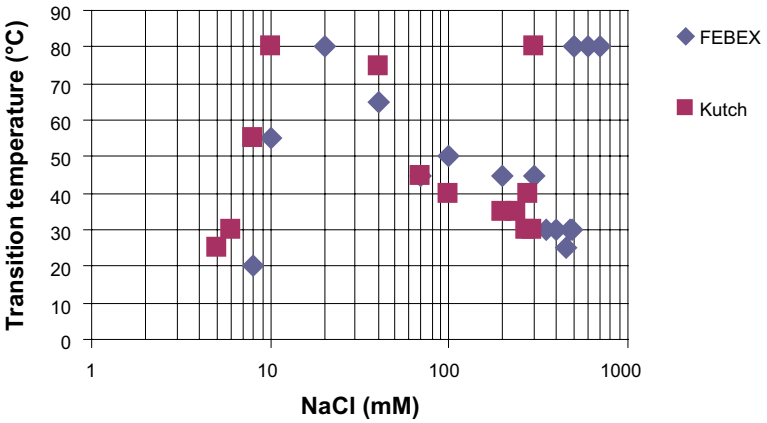

Figure 4-3. *Comparison of the transition temperatures of Ku-Na and FEBEX-Na gels (10 g/l) at varying salinity. Samples that showed no change upon heating to 75 °C are plotted at 80 °C.*

For example, at 5 mM NaCl, the melting was complete akin to the Ku-Na gel in Figure 4-1 a. In 20 mM NaCl solution heating did not induce any visible change of the gel. However, also for FEBEX-Na, yield was again observed when the ionic strength was further increased. For gels formed in NaCl solutions of 40 mM and above, T_y decreased until the concentration was 400–450 mM. At even higher NaCl concentrations, 500 mM and above, FEBEX-Na gels showed no visible change during heating to 75 °C.

4.4.3 Fusion of clay gel pieces

To illustrate thermoreversible behaviour in these systems we tested if gels cut in pieces could be recovered. Two Ku-Na samples with C_{clay} = 20 g/l and with 4 and 5 mM NaCl solution, respectively, were initially heated to 75 °C, at which point the gels had started to deform and melt. Upon cooling to room temperature the gel state returned. The newly formed gels were then sectioned. The gel pieces were placed in standing vials and rapidly heated to 75 °C and then left to cool. The sample with 4 mM NaCl concentration had formed a gel that showed no signs of being the result of fusion of several fragments. With 5 mM NaCl concentration, the gel had fused into one entity, but it was clearly visible that the gel had consisted of several pieces. Without increasing the temperature, gel pieces put together did not fuse. This suggests that the clay particles at the gel surface find a local energy minimum configuration and heat transfer is needed to reform bonds with particles on a neighbouring gel surface.

4.4.4 Aging behaviour

FEBEX-Na samples with C_{clay} = 10 g/l and NaCl concentration of 8 mM were prepared, and at different times after preparation T_y was measured (Figure 4-4). At two and seven hours after sample preparation, T_y could not be measured as the particle network was not yet strong enough to support the yield forces arising in the samples when the vials were placed horizontally. At 18 and 24 hours after preparation, T_y was 20 °C, confirming the earlier measurement (Figure 4-3). A slightly increased T_y of 20–25 °C was measured for samples that had rested 2 to 5 days. For longer aging times, T_y rose conspicuously, with 35 and 45 °C for 6 and 7 days waiting time, respectively. While T_y continued to increase after the initial week, the rate of increase declined somewhat. Clearly, aging increases the strength of dilute clay gels, confirming the results of earlier studies (Baghdadi et al. 2008, Jabbari-Farouji et al. 2012, Knaebel et al. 2000, Labanda and Llorens 2008, Mongondry et al. 2005, Ruzicka et al. 2004, Shahin and Joshi 2010). The increased transition temperatures of gel samples suggest that while a gel can be formed fairly rapidly (<24 h), the initially formed network is not necessarily the most stable. Furthermore, it suggests that even after clay particles have been locked in a network, there is still enough movement for the particles to adjust to a thermodynamically more favourable arrangement. Similar tests on 10 g/l FEBEX-Na and 350 mM NaCl concentration indicated no correlation of T_y with aging of the samples (Figure 4-4). Here T_y showed a narrower spread: While the highest value being 45 °C, they were generally around 30–40 °C. However, upon heating the more aged samples, they slowly started breaking down with visible aggregates breaking off the gel. This behaviour was not observed in the test with 8 mM NaCl.

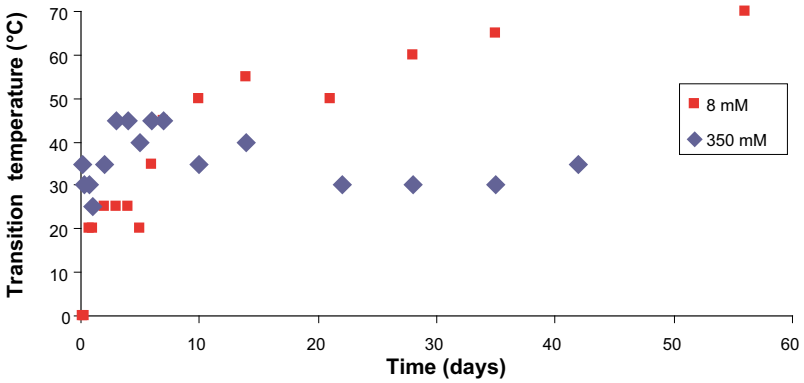

Figure 4-4. *Transition temperatures of FEBEX-Na gel (10 g/l clay, 8 and 350 mM NaCl) at specific time intervals after sample preparation. Samples that immediately yielded under their own weight are placed at 0 °C.*

A possible explanation to these observations, in particular the lack of influence on T_y with sample age for the high salinity gel, could be that inter-particle bond formation occurred rapidly at the higher salinity because of reduced repulsions. At 350 mM, DLVO theory for face-to-face orientation (Evans and Wennerström 1999) predicts a secondary minimum of 16 k_BT for clay platelets with radii of 100 nm, using a Hamaker constant of 5 k_BT. Consequently, it is reasonable to assume that under these conditions there is a competition between edge-to-face and face-to-face orientations leading to smaller aggregates of comparatively strongly connected particles, that form the units in a more heterogeneous gel or glass structure (Angelini et al. 2014, Tanaka et al. 2004). According to DLVO theory for parallel clay layers at 8 mM the secondary minimum is absent. Thus at this low salinity a more homogeneous gel structure of edge-to-face bonds is expected to develop over time.

4.4.5 Effect of heating upon gel volume

Vials with 5 ml Ku-Na gel, with the gel level marked, were placed upright in beakers containing 0.5 l NaCl solution and heated to 75 °C. The temperature was kept for 2–5 hours before returning to room temperature. This test was performed for Ku-Na gels with C_{clay} = 8 g/l in 6 mM NaCl solution, C_{clay} = 10 g/l in 6, 70 and 300 mM NaCl solutions, and C_{clay} = 20 g/l in 6 mM NaCl solution. In all tests the gel volume was unchanged after the heating and cooling cycle. The fact that these gels can be formed at the same volume fraction but at different salinities shows that the gels are not in the energy ground states. For example, at 300 mM the screening of the electrostatic repulsion should allow for a much more compact gel structure than at 6 mM. The unchanged gel volume upon heating shows that the gels are dynamically arrested structures that are not easily transferred to the ground state. Similarly, aging did not cause any volume change. The increased T_y with aging then suggest an optimization of bonds rather than an optimization of global structure.

4.4.6 Evaluation of binding enthalpy for edge-to-face junctions

For percolation gels the binding enthalpy can be determined from a linear relation between the logarithm of the concentration of the gelling substance and the reciprocal temperature of melting (Eldridge and Ferry 1954). The binding enthalpy evaluation was done for Ku-Na gels at a NaCl concentration of 5 mM in order to cover the largest possible temperature range, as seen in Figure 4-2. Two test series were done with C_{clay} from 10 to 16 g/l. As before, when the gel showed the first signs of yield, the transition temperature was recorded. From the results plotted in Figure 4-5 and Equation (4-2) the evaluated enthalpy of formation for edge-to-face junctions is -11.5 ± 0.7 kJ/mol, which is equivalent to -4.6 ± 0.3 k_BT at room temperature. The small scatter of data around the linear regression line in Figure 4-5 strongly indicates that the approximations and assumptions made in the derivation of the relation between C_{clay} and T_y are justified.

4.5 Discussion

In the present work we have presented new evidence that dilute smectite clay gels are formed through electrostatic edge-to-face attractions. In contrast to earlier experimental work advocating this mechanism (Goh et al. 2011, Martin et al. 2002, Mongondry et al. 2004) our experiments do not require any

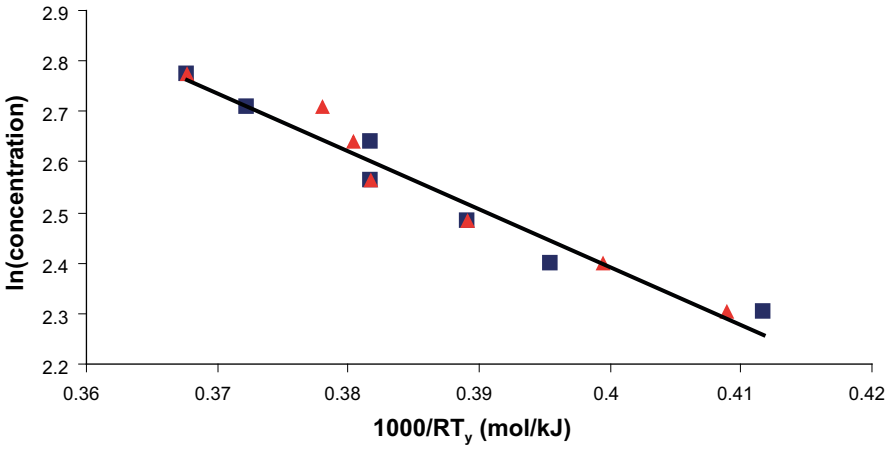

Figure 4-5. *Relation between ln (clay concentration) vs inverse transition temperature for Ku-Na montmorillonite at NaCl concentration of 5 mM. Regression analysis of the data from both test series gave the enthalpy of formation of edge-to-face junctions to −11.5 ± 0.7 kJ/mol corresponding to −4.6 ± 0.3 k_BT at room temperature.*

modification of the clay edge with polyphosphate ions, but rely solely on the measured variation of T_y with NaCl concentration. Once the ionic strength was above a critical value for gel formation (5 mM at or near room temperature), T_y was found to increase with ionic strength until it reached a maximum. This is because of increased screening of the negative potential that spills over to the edge region (Secor and Radke 1985) which in turn led to increased strength of the edge–face interaction. With further increase in ionic strength, screening would eventually weaken the electrostatic attraction, which in the experiments was seen as a decrease of T_y with ionic strength. The observed non-monotonic variation of T_y with ionic strength demonstrates that gelling in dilute smectite clay suspensions are primarily of electrostatic nature and van der Waals attraction, while always present, is less crucial. It is important to note that if van der Waals forces were the only attractive component in the system, T_y would increase monotonically with ionic strength since salt in such scenario can only screen repulsion.

While simulations have been of great value for identifying different possible phases that may exist depending on the boundary conditions and assumptions regarding face and edge charges (Angelini et al. 2014, Delhorme et al. 2012a, b, Jönsson et al. 2008), the coarse-graining assumptions necessary to perform these simulations cause large uncertainty regarding the actual values for the binding energies.

Here we have done a first attempt to obtain realistic binding enthalpies relevant for gelation. Based on ideas from percolation theory (Eldridge and Ferry 1954), we used our method of determining T_y to evaluate the enthalpy for the edge-to-face linkage in Ku-Na gels. In 5 mM NaCl solution, the "binding" enthalpy for Ku-Na gels 18 h after preparation was −4.6 ± 0.3 k_BT. This enthalpy can be viewed as a lower limit since 5 mM is just above the critical concentration for forming Ku-Na gels. We have also in agreement with previous work (Baghdadi et al. 2008, Jabbari-Farouji et al. 2012, Knaebel et al. 2000, Labanda and Llorens 2008, Mongondry et al. 2005, Ruzicka et al. 2004, Shahin and Joshi 2010) demonstrated that aging had strong influence on the gel strength at low salinity. If the observed increase in strength is related to reorganization of the bonds or to an increase in ΔH with time still remains to be investigated. As the gels are formed in aqueous NaCl solutions, T_y values possibly located above the boiling point cannot be measured, which somewhat limits the method to the study of only the weakest gels. Nevertheless, we believe that our results can form the basis for further studies into clay gel stability using for example rheology. We expect that yield strength would show similar variation with salinity as T_y in the present study. The combination of the present method and rheology could also allow for estimating the binding enthalpy at higher salinities, longer aging times, and at higher clay concentrations. The present results also show that in order to model the phase diagram of smectite clay and ultimately the evolution of a bentonite buffer in a nuclear waste repository, attractive edge-to-face interactions need be included besides the ordinary DLVO forces. Also below the CCC the edge-to-face interaction is found to be important as found in simulations (Angelini et al. 2014) as well as discussed in our earlier work as an explanation for the sedimentation rates found in Na-montmorillonite sols (Birgersson et al. 2009). This proposes that the present results also have relevance for improving modelling below the CCC.

5 Rheology

Understanding rheological properties of montmorillonite/bentonite is important for assessing the fate of clay in a geological repository for spent nuclear fuel, especially under dilute groundwater conditions. Smectite clays such as montmorillonite have complicated phase diagrams with several arrested states, especially different kinds of repulsive phases as well as various sol states. To simplify the picture somewhat, we only consider gel, repulsive paste, and sol. The gel consists of a volume-spanning network of connected clay particles that is formed when the clay particle concentration is above the percolation threshold and the salinity is higher than a critical concentration value. The gel has yield strength and the attractive particle-particle forces withstands the osmotic pressure so the gel does not expand in contact with excess electrolyte. Sols are by definition liquid colloidal systems. In very dilute sols, the clay particles can be treated as non-interacting, and sometimes this system is referred to as a gas or gaseous sol. But the phase as a whole is liquid since the clay particles are suspended in an aqueous solution. At higher clay concentration (volume fraction) the clay particle may interact, but the phase is still liquid, i.e. a sol. At sufficiently high clay concentration, the osmotic repulsion (overlapping double layer) forces may dominate giving the system solid-like properties. This is conventionally termed repulsive gel (Abend and Lagaly 2000), albeit direct particle-particle contact may be absent. Thus we prefer the term repulsive paste or simply paste as stated in section 1.2.

Erosion studies using artificial fracture systems show that when a gel is formed at the swelling front, the penetration of the clay into the fracture is limited and erosion is below detection limit (section 6.2.3). Thus erosion of bentonite in a repository is only expected when conditions are such that a sol can be formed. Yield stress measurements, reported here, on gelled structures confirms that such gels are expected to withstand the shear stresses from the flowing water. Similarly, work on repulsive pastes and sols, using Wyoming montmorillonite extracted from MX-80 bentonite, shows that mechanical erosion of the repulsive paste at the paste-sol interface is highly unlikely (Eriksson and Schatz 2015). Thus, erosion under dilute water conditions is a matter of repulsive paste-to-sol transition and the removal rate of the sol.

5.1 Phenomenological description of montmorillonite gels of relevance for rheological measurements

A clay gel is defined by a volume-spanning network of connected clay platelets through attractive forces. The network forces are strong enough to withstand the osmotic repulsion. Thus a gel does not expand in contact with excess electrolyte. Figure 5-1 shows the behaviour of a suspension at 20 g/l of Ku-Na montmorillonite (Na^+ homo-ionized montmorillonite from Asha 505 bentonite, Kutch district, India) in contact with air (left) and in contact with excess electrolyte (right), respectively. The NaCl concentration in the suspension and in the excess electrolyte was the same: 20 mM. In contact with air the suspension appears liquid-like, while in contact with excess electrolyte the gel characteristics become evident. These seemingly contradicting behaviours of the Ku-Na suspension occur in the same sample and depends only on the boundary between the clay-rich phase and the surrounding. The gel-like property transpires immediately after the interface with air is removed by adding extra electrolyte. As it is unlikely that the addition of further electrolyte would instantaneously cause network bond formation, we must conclude that the volume-spanning network of clay platelets was already present. This clay-particle network has low yield strength and cannot support its own weight unless it is also supported by the buoyancy of water. Thus when the gel borders air, tilting of the vial causes rupture of the gel structure and the system appears liquid (Figure 5-1, left). When the gel borders excess electrolyte, the buoyancy of the surrounding liquid gives the needed support and the gel behaviour is clearly manifested (Figure 5-1, right). In this study we will examine the shear stress as a function of strain to determine the yield stress of Asha 505 montmorillonite at NaCl concentrations above the critical coagulation concentration.

Homo-ionic Ku-Na montmorillonite forms gels at NaCl concentrations as low as 4 mM, while at 3 mM gels form only slowly, causing substantial sedimentation (Figure 3-7 in section 3.3.1).

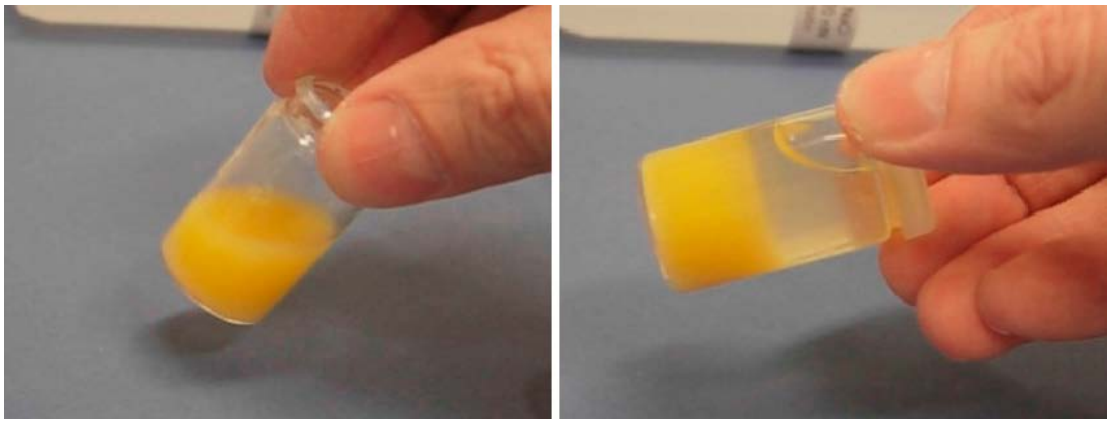

Figure 5-1. *Ku-Na montmorillonite, 20 g/l, in 20 mM NaCl. Left: Behaviour of the suspension when the interface is air. Right: The same suspension with 6 ml 20 mM NaCl(aq) added on top of the suspension to give an interface to a liquid.*

5.2 Experimental

5.2.1 Material

Raw (as received) Asha505 bentonite was dispersed in DI water (10 g/l) and sonicated for 15 minutes. Then the suspensions were left on magnetic stirrer overnight. The <2µm fraction, which essentially consists of montmorillonite, was extracted from the bentonite suspension using centrifugation. The suspension containing the <2µm fraction was placed in 60 °C oven until the water had evaporated (approximately 3 days). The oven-dried montmorillonite was subsequently milled to a fine powder. Note that the montmorillonite is not homo-ionized. A previous determination of exchangeable ions showed that the montmorillonite fraction of Asha 505 contains Mg^{2+} (28 %), Ca^{2+} (31 %), Na^{+} (40 %), and K^{+} (1 %) (Karnland et al. 2006). Since the origin of Asha bentonite is the Kutch district in India we hereafter refer to the montmorillonite (<2µm fraction) as Ku-mmt.

5.2.2 Sample preparation

Stock dispersions (20 g/l and 40 g/l) of Ku-mmt were prepared by mixing the montmorillonite powder with DI water using magnetic stirrer. After ~20h the dispersions appeared homogeneous and smooth. After ~24h the dispersions were added to NaCl solutions. Each sample cup was filled with 15 ml of NaCl(aq) (double strength) and 15 ml of Ku-mmt stock dispersion was added. The sample was capped and vigorously shaken 50 (5 and 10 mM final ionic strength) or 100 times (50 and 100 mM final ionic strength) and left to rest (1 day or 1 week) before the rheology tests. After examining the yield-stress results from the first series of experiment, we decided to also perform tests on Ku-mmt in 20 mM NaCl(aq). Those samples were neither prepared from the same stock dispersion, nor by the same person.

5.2.3 Yield-stress measurements

Yield stress was measured with rotating vane rheometry (Barnes and Nguyen 2001) using a Brookfield DV II + Pro LV viscometer and the V-73 vane spindle. The vane was lowered into the clay sample and the measurement was started immediately. The yield-stress measurement was conducted at a low constant rotational rate of 0.05 rpm for 500–800 s. The yield stress is taken as the peak value in the stress-time curve (equivalent to stress-strain curve).

5.3 Results

Figure 5-2 display the appearance of a Ku-mmt gel after a yield stress measurement. The vane spindle has clearly cut out a cylinder in the gel. The dimensions of the V-73 vane spindle are 25.35 mm in height and 12.67 mm in “diameter”. The remaining pattern is stable and the gel does not spontaneously

reform on a “laboratory” timescale. This suggests that when the gel is broken, the clay particles at the gel surfaces arrange themselves into new local energy minima. Thus there is a barrier for the clay particles to reconnect with particles on the neighbouring surface. Figure 5-2 represents yet another strong evidence that these systems really are gels. In Figure 5-2 the gel is covered with excess electrolyte to ensure buoyancy to avoid collapse at the top surface, which would ruin the pedagogical point of the photo. In the actual measurements behind the data in this report, no excess electrolyte were added. Also the spindle was “properly” immersed until the gel reached the mark at the middle of the shaft (the mark is visible at the water surface in Figure 5-2).

All measurements in this study were made in triplicates, except for the non-gelled samples without any added NaCl (duplicates). The results for Ku-mmt at 10 g/l and 24 h rest time are shown in Figure 5-3. With no added salt, the shear stress was constantly below measurement threshold. The samples prepared in NaCl(aq) had all developed yield strength. Furthermore, the agreement among the triplicate samples was very good, both in terms of the general shape of the shear stress vs time curves and the variation of the maximum value. The largest relative variation in Figure 5-3 is for the 10 mM samples where the maximum stresses differ by 14 % between the largest and smallest values. The effect of salinity on the maximum stress (here chosen as the yield stress) is particularly high at the lower concentrations: the value of ~1.5 Pa at 10 mM is more than three times larger than the value at 5 mM, ~0.5 Pa. The yield stress curves seem to converge at the two highest NaCl concentrations. The increase in NaCl concentration from 10 to 50 mM gave an increase in yield stress from ~1.5 to ~2.5 Pa (see also Table 5-1). There is also a pronounced increase in shear modulus with increasing NaCl concentration, in line with the increase in yield stress.

It is well known that aging can have profound effect on rheological properties. This is illustrated by comparing Figure 5-3 and Figure 5-4. Letting clay samples rest for a week gives a significant increase in both shear modulus and yield stress. The effect is larger for gels formed at lower salt concentrations, which is logical: weaker bonds need less thermal agitation to explore configuration space, thus the effect of optimizing the overall gel structure is detectable on a shorter timescale.

Increasing the solids content has an even larger effect on yield stress than aging. Figure 5-5 shows the shear stress curves obtained after 24 h for Ku-mmt at a concentration of 20 g/l. Again, without the addition of NaCl the shear stress was below detection. The largest effect of increasing clay concentration is seen for the samples at 5 mM, where the average yield stress has increased to 4.4 Pa, which is eleven times larger than the value at 10 g/l (Figure 5-3 and Table 5-1). At the other NaCl concentrations the increase in yield stress is about a factor of 3.5 which is still significant. For dispersions with weak attractions the yield strength σ_y can be expected to approximately vary with the particle volume fraction ϕ_c as $\sigma_y \propto \phi_c$ (Russel et al. 1992). Thus one would assume σ_y to increase by a factor of four when the clay concentration is doubled. In Figure 5-5 we also show results obtained at 20 mM NaCl. These samples appear to have higher yield stress than the 50 mM samples. It should be noted however, that the 20 mM samples were prepared at a later occasion using a different Ku-mmt stock solution.

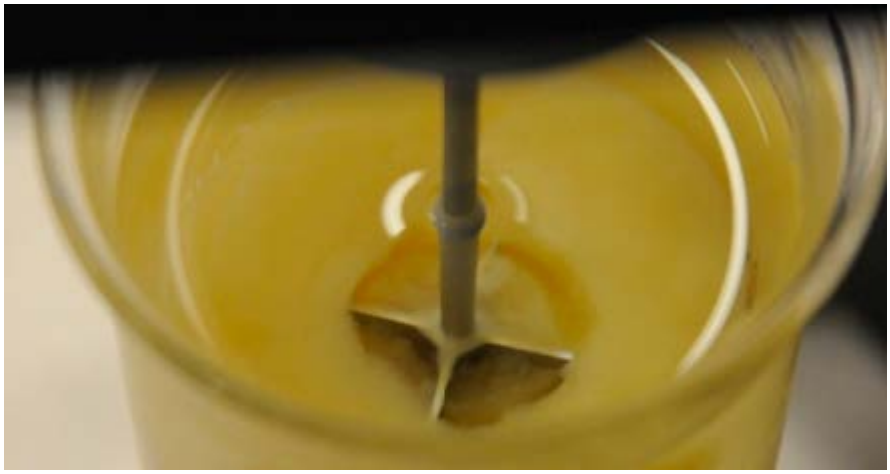

Figure 5-2. *Ku-mmt, 20 g/l in 20 mM NaCl(aq) after a yield stress measurement.*

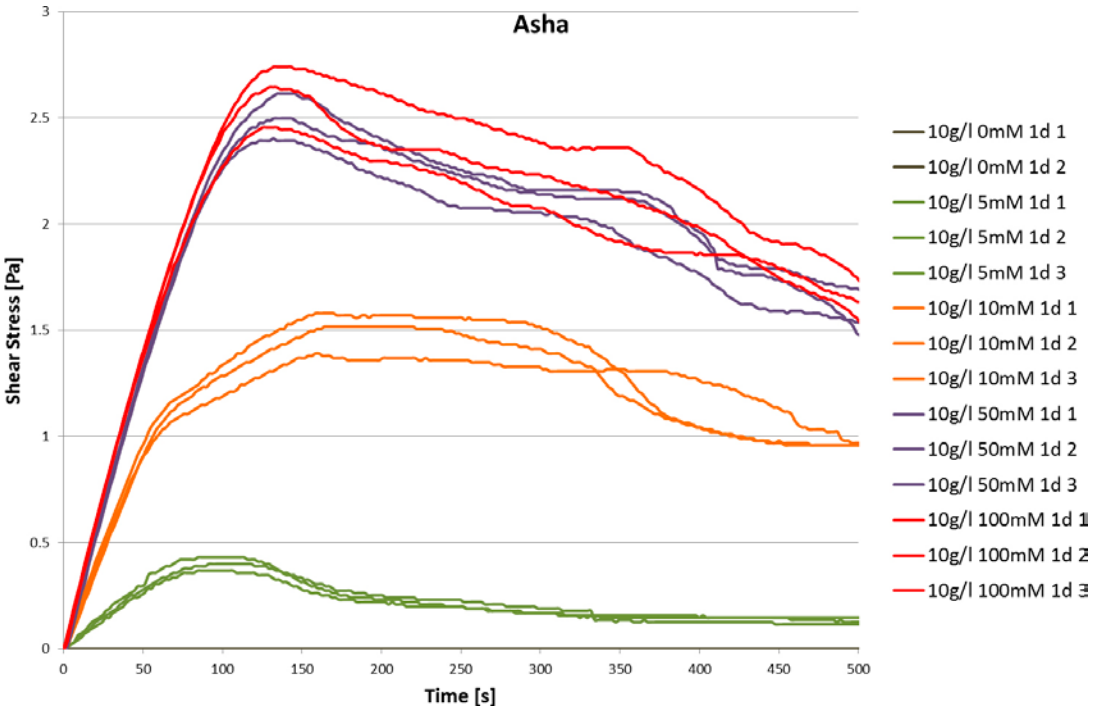

Figure 5-3. *Shear stress vs time for Ku-mmt at a concentration of 10 g/l and different NaCl concentrations 24 hours after preparation. Note that without extra NaCl, denoted 0mM in the legend, the suspension has no yield stress at all, and the two curves coincide with the x-axis.*

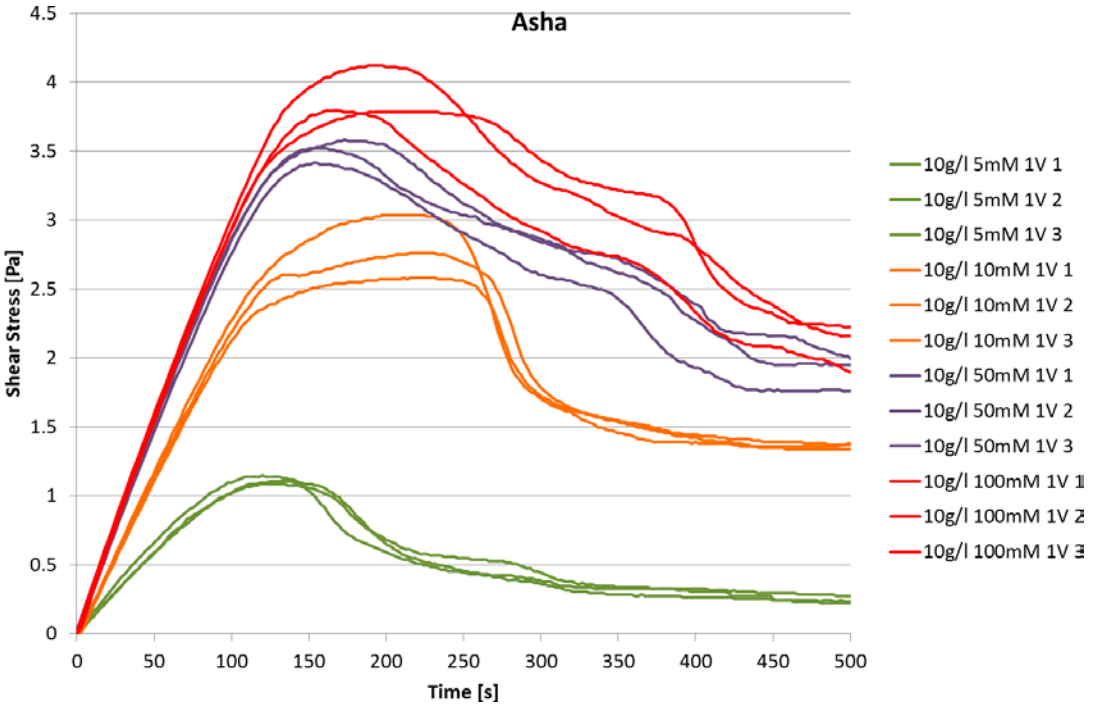

Figure 5-4. *Shear stress vs time for Ku-mmt at a concentration of 10 g/l and different NaCl concentrations 1 week after preparation.*

It is thus premature to suggest that this non-trivial variation of yield-stress with salinity is related to the observations of yield-point temperatures in chapter 4. One should also bear in mind that the rheology tests are done on Ku-mmt which is not homo-ionized, whereas the yield-point temperature study was carried out using Ku-Na. One week aging caused the 100 mM samples to have yield stress above the measuring range so tests were performed by inserting the vane halfway. Unfortunately that did not give reliable values as can be seen from the scatter in Figure 5-6.

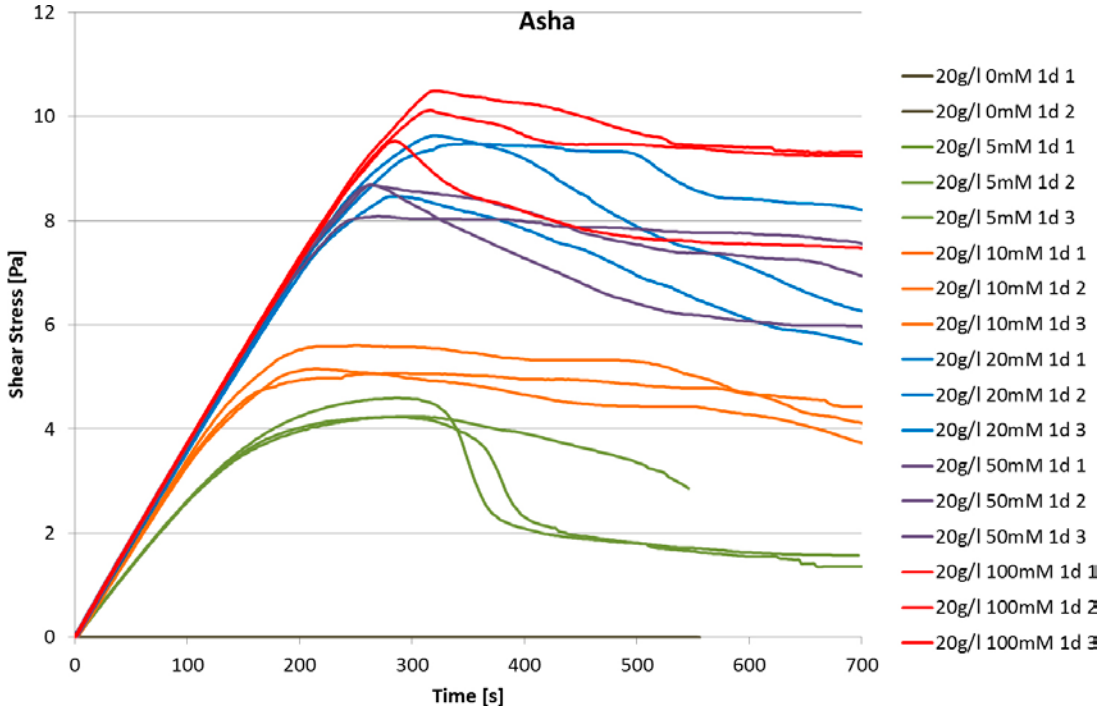

Figure 5-5. *Shear stress vs time for Ku-mmt at a concentration of 20 g/l and different NaCl concentrations 24 hours after preparation. Note that without extra NaCl, denoted 0mM in the legend, the suspension has no yield stress at all, and the two curves coincide with the x-axis.*

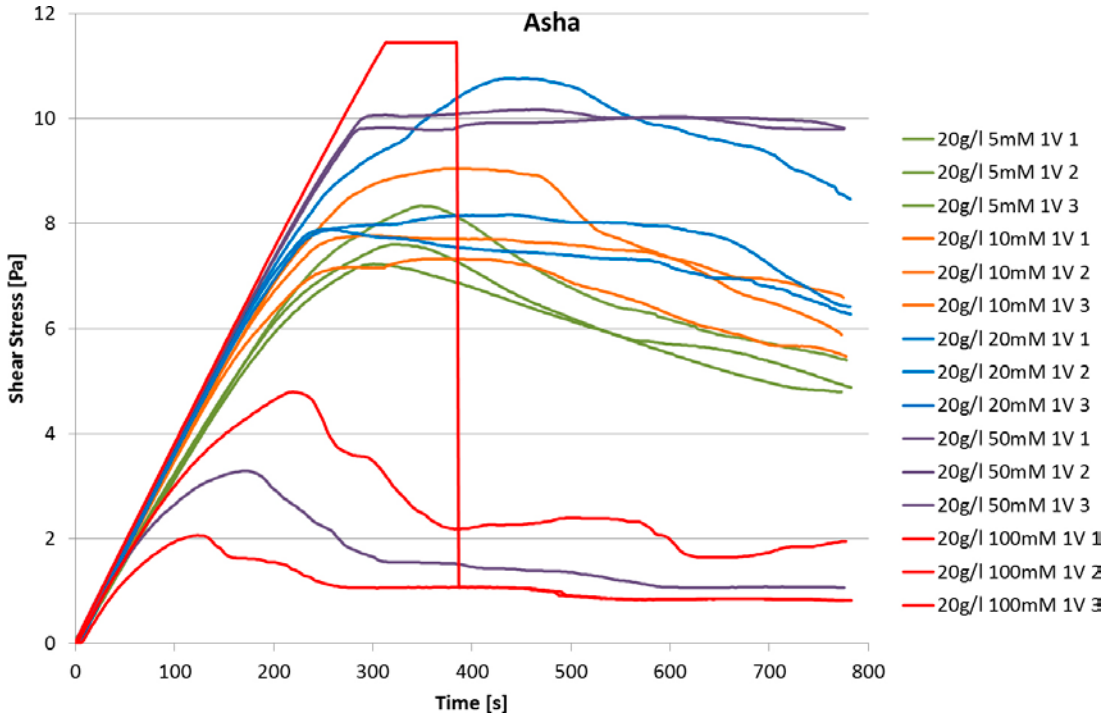

Figure 5-6. *Shear stress vs time for Ku-mmt at a concentration of 20 g/l and different NaCl concentrations 1 week after preparation. Note that for the 100 mM sample the stress is higher than instrument measuring range. Therefore tests were done by inserting the vane spindle only halfway into the gel (the lowest two 100 mM and lowest 50 mM curves).*

Table 5-1. Average maximum yield stress from the rheological measurements in Figure 5-3 to Figure 5-6.

	Average maximum yield stress (Pa)				
[NaCl]	C_{mmt}	10 g/l, 24 h	10 g/l, 1 week	20 g/l, 24 h	20 g/l, 1 week
5 mM		0.4	1.1	4.4	7.7
10 mM		1.5	2.8	5.3	8.0
20 mM		–	–	9.2	8.9
50 mM		2.5	3.5	8.5	–
100 mM		2.6	3.9	10.0	–

The 5 mM samples showed similar increase in yield stress upon aging as for the 10 g/l samples. In fact there are 5 mM curves in Figure 5-6 showing higher yield stress than some of the measurements on 10 and 20 mM samples. Possibly there are artefacts making the aged samples at higher salinity to show too low shear stress. The results from immersing the vane spindle halfway into the gel, reported in Figure 5-6 suggest that the gels do not have an even density but get thicker with depth. If the gels were homogeneous, immersing the vane halfway should give half the response compared to a fully immersed vane. The response is clearly much less than half of the values obtained with a fully immersed vane. The more aged the sample, the more influence of gravity to redistribute mass. It was also noticed during preparation that air bubbles tended to be trapped inside the stronger gels. We would expect the air bubbles to cause a weakening of the gel. However, their effect on yield stress in the aged samples is unclear. For the next series of experiments even more efforts will be made to increase the homogeneity of the gels. In order to also measure higher stresses a smaller vane spindle has been obtained.

5.4 Conclusions and considerations for geological disposal

Gel formation is the only smectite-specific mechanism that can prevent erosion of clay at a transmissive fracture. The present tests show strong sensitivity to the salinity of the external water. For Ku-mmt a NaCl concentration of ~5 mM is needed to form a gel. However, even at such low concentration the present tests show that the yield stress is significant. In fact, all tested gels have yield stresses several orders of magnitude higher than the anticipated drag force of the flowing water in a repository (Eriksson and Schatz 2015). The yield stress also shows strong dependence on clay concentration. This dependence is even stronger than that on salinity. The highest clay concentration in this study is 20 g/l, but at a repository one may expect higher clay concentrations at the repulsive paste-to-gel border adjacent to the groundwater, cf. the Ku-Na state diagram in Figure 3-4. In the present study we also reconfirm the effect of aging. One week of resting produce significantly stronger gels than those tested after 24 hours. At installation of the buffer bentonite in a future repository, the groundwater conditions are such that a gel will be formed at the swelling front and strongly limit penetration of bentonite into water-bearing fractures.

6 Swelling and erosion in artificial fractures

6.1 Materials and methods

6.1.1 Material

The erosion studies reported here have been performed using Wyoming-type (Wy) montmorillonite extracted from MX-80 bentonite (American Colloid Co.). The montmorillonite was purified and ion-exchanged with NaCl or $CaCl_2$ to the homo-ionic form according to the procedure described in Karnland et al. (2006). The purified montmorillonite is referred to as Wy-Me, where Me is the counter ion.

Most experiments in this study have been conducted using Wy-Na. There are two major reasons for working with Wy-Na: First, Na-montmorillonite show essentially unlimited swelling below the critical coagulation concentration (CCC), i.e. it turns into a sol, which is the reason for studying the erosion process under dilute conditions in the first place. Second, Wy-Na has the highest CCC (~20 mM NaCl) of all the clays investigated in chapter 3. Thus erosion rates obtained using Wy-Na are pessimistic estimates, compared to the conceivable future conditions in a high-level waste (HLW) repository.

Wy-Ca, on the other hand, is not sol-forming (Birgersson et al. 2009) so in this study, erosion experiments using Wy-Ca have not been performed. However, mixed Ca/Na-montmorillonite was found to form sol and erode in DI water when the Na^+ content was >20 % of the CEC (Birgersson et al. 2009, Hedström et al. 2011) in line with earlier findings (Shainberg and Kaiserman 1969). A Wy-Ca/Na montmorillonite prepared from mixing equal amount of powdered Wy-Ca and Wy-Na montmorillonite is therefore included in the present study. In this montmorillonite 50 % of CEC is compensated by Ca^{2+} and 50 % by Na^+. In the following this clay will be referred to either as Wy-Ca/Na or as Wy-50/50.

6.1.2 Equipment

The artificial fractures, made of poly(methyl methacrylate), were square with inside dimensions 21 cm by 21 cm. In the set of experiments reported here, two apertures, 120 μm and 240 μm have been used. Based on measurements using steel feeler gauge strips the aperture is within 10 μm of nominal value. The artificial fracture is equipped with an inlet and outlet, allowing us to flow various solutions through the cell (Figure 6-1).

Both on the inlet and outlet side there is a trench or narrow slot. On the outlet side some of the eroded material may gather there so the outlet slot is equipped with an additional inlet and outlet. This allows for flushing the outlet slot ensuring that all eroded material can be gathered. At the centre of the fracture system there is room for a clay disk of diameter 35 mm and thickness ~10 mm. The clay is contacted to water only via the slit.

The amount of eroded montmorillonite was evaluated from the turbidity of the effluent, using a portable turbidimeter (TN-100, Eutech Instruments). At low clay concentrations (<5 g/l), the turbidity response have been found to be linear. The mass of eroded clay particles can thus be calculated through the equation $m_{clay}=(N \cdot V)/114$ where m_{clay} is the mass of the eroded clay (g), N is the turbidity (NTU) and V is the volume of the suspension (L) (Birgersson et al. 2009). Below turbidities of 20 NTU the instrument resolution is 0.01 NTU. All measured turbidities in erosion tests are well within this high-resolution range.

6.1.3 Method

The montmorillonite was dried *in vacuo* overnight, followed by saturation with DI water in a test cell similar to the ones used by Clay Technology AB for measuring swelling pressures (Karnland et al. 2006). The initial dry density of the montmorillonite is 1257 kg/m^3 which gives a water-saturated density of 1800 kg/m^3. The water-saturated clay disk was transferred to the artificial fracture, with care taken not to allow the clay to dry. The fracture was closed and filled with degassed DI water.

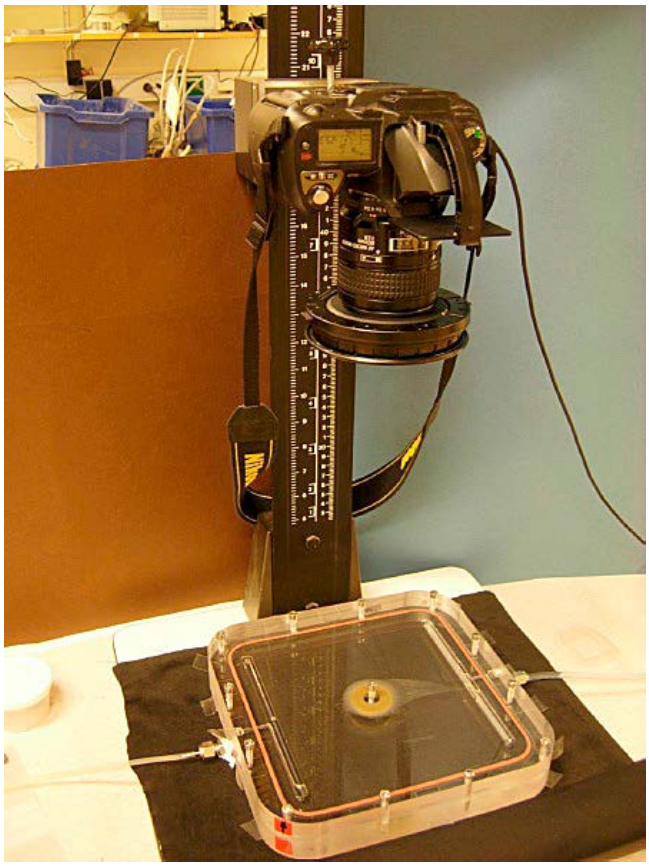

Figure 6-1. *Experimental set-up.*

During free swelling experiments, the artificial fracture was filled with either degassed DI water or saline solution prepared from degassed DI water, after which the clay was allowed to swell into the fracture. This was photographically documented, with pictures taken at suitable intervals depending on the rate of expansion.

During erosion measurement experiments, aqueous solution, also prepared from degassed DI water, was flowed through the artificial fracture. The start- and end times of the erosion measurement were recorded. When the flow was stopped, the collected suspension was weighted. The outlet slot was flushed with degassed DI water to collect eroded material which had gathered in the outlet slot, and the flushed-through suspension was also weighted. Turbidity measurements were used to determine the amount of eroded colloidal clay particles in both water volumes.

6.2 Results and discussion

6.2.1 Free swelling – deionized water

The free swelling behaviour was investigated at two different fracture apertures, 120 μm and 240 μm, in DI water. Initially, the swelling into the fracture progressed rapidly at both 120 μm and 240 μm. While the swelling progressively slows down, during the experimental time scale it does not cease completely. At 120 μm, closest to the clay disk we find a repulsive paste, quite well-defined and thick enough to appear very bright in colour (scattered light from the camera flashes) (Figure 6-2 a). This paste is strong enough that as it expands, it pushes air bubbles in the fracture ahead of itself, rather than surrounding them. Further out, there is a sol of possibly varying clay concentration. (In the case of Wy-Ca/Na the average clay concentration in the erodible sol was found to be ~30 g/l.) At the interface between the sol and the DI water a fingering instability occur, akin to the Rayleigh-Taylor instability (RTI) that occurs when a denser liquid is placed on top of a less dense liquid and is pulled down by gravity. The RTI fingers are particularly well resolved in the thinner fracture Figure 6-2 a. In this case it is not gravity that is the driving force for the RTI but osmotic water transport into the clay.

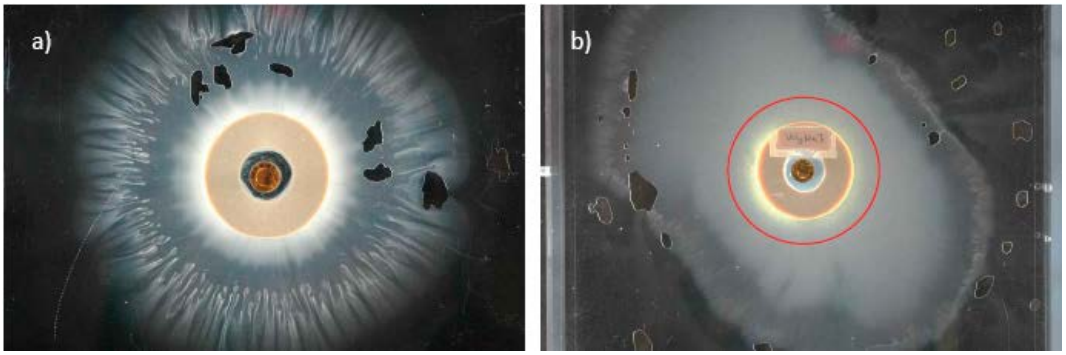

Figure 6-2. *Free swelling in deionized water after 30 days at a) 120 µm aperture and b) 240 µm aperture. The red circle in b) shows the extent of extrusion (swelling) of paste (the brighter area outside the montmorillonite disk in a) into the fracture at 120 µm for comparison. When there is a rather high flow through the cell, all clay outside the brighter paste, is transported away.*

The same phases, the thick paste and the sol, are found during free swelling at an aperture of 240 µm (Figure 6-2 b). Also RTI can be found, although the fingers are less well-resolved at the broader aperture. As in the case of 120 µm aperture, the paste is sufficiently thick to push air bubbles ahead during swelling rather than encompassing them. For comparison, the edge of the corresponding paste is outlined in Figure 6-2 b, which gives an idea of the difference in swelling capability at different apertures.

The paste, i.e., the thicker clay phase closest to the disk, is found to withstand the shear forces and not erode under our conditions, even at the highest flow rates. However, as swelling is a continuous process, particles that disperse from the paste to form a sol are easily flowed away into the fracture. Both in free-swelling tests and in the tests with flowing aqueous solution the paste (the bright region of about 1 cm radial extrusion from the emplaced clay into the fracture as seen in Figure 6-2 a) have never been seen to extend beyond ca 1 cm extrusion when the fracture aperture is 120 µm.

6.2.2 Free swelling – 25 mM NaCl-solution

The free swelling behaviour in a solution with higher salinity was also investigated. When setting up this experiment, clay happened to be mechanically extruded into the fracture when the fracture was closed, thus initially the clay in the fracture had the same density as in the disk. This point constitutes the starting point for swelling, and has been outlined with a red circle in Figure 6-3. During the initial 48 h, some swelling (1–2 mm) was evident. Despite this, after the first two days no more swelling took place and the clay appeared to have formed a stable gel (at the interface to the solution), which does not release clay particles into the fracture. Even with a flow of 25 mM NaCl-solution, there were no signs of erosion. In fact, decreasing the salinity to 20, 15 or 10 mM NaCl still caused no erosion during flow (Figure 6-4). In order to see any sign of erosion, the salinity of the solution had to be decreased to 5 mM NaCl. This suggests the presence of some sort of hysteresis, which might affect the montmorillonite loss in the actual HLW repository.

6.2.3 Erosion measurement Wy-Na

Initial erosion measurements were performed at a fracture aperture of 120 µm (Figure 6-5). The measurements commenced at 5 mM NaCl (aq). As expected, since CCC is in the vicinity of 20 mM, the erosion rate was found to increase with increasing flow rate. After 14 days the salinity was increased to 10 mM NaCl (aq) which gave a decreased erosion. However, it was still increasing with flow rate. The tests with various flow rates using 10 mM NaCl (aq) was conducted over 25 days. After increasing the salinity to 15 mM NaCl (aq), the erosion during the first 48 h was roughly half the erosion at the corresponding flow rates at 10 mM NaCl.

Within a week, erosion had completely ceased or was below the detection limit. The salinity was further increased to 20 mM NaCl, as 20 mM NaCl is close to the CCC of Wyoming montmorillonite clay as reported in chapter 3. As expected, there were no signs of erosion. The erosion rate vs flow velocity is reasonably well captured with a power law for the lowest two NaCl concentrations with R^2 equal to 0.95 and 0.94 in the case of 5 mM and 10 mM, respectively.

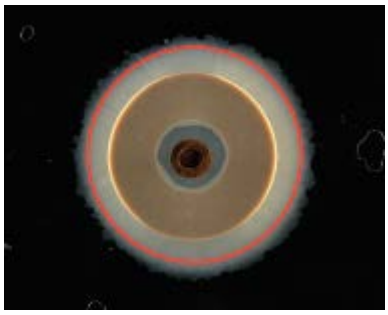

Figure 6-3. *Free swelling in 25 mM NaCl-solution at an aperture of 120 µm. The saturated density of the montmorillonite is 1800 kg/m³.*

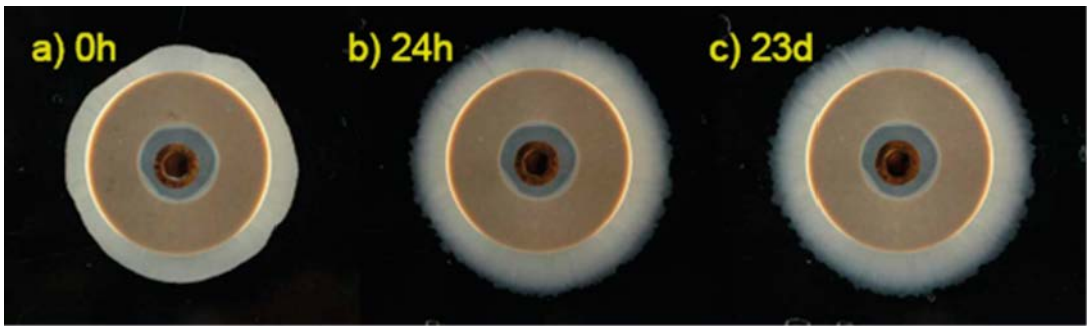

Figure 6-4. *Top view of a 1 cm thick Na-montmorillonite disc that swells into a 120 µm fracture. The diameter of the disc (darker grey) is 35 mm. a) Initial condition. The initial extrusion of clay gel is mechanical and happened when the fracture top was mounted and thus not caused by swelling. The fracture is filled with 25 mM NaCl solution adjusted to pH > 9. b) After 24h swelling. Swelling is completed and a gel is formed at the outer rim of the clay that prevents further expansion. For 10 days the solution was left stagnant. Then we let the solution flow through the fracture at various velocities. During the flowing phase the NaCl concentration in the external solution was gradually lowered. c) After 23 days. The NaCl concentration had at this time been 15 mM for 24 hours.*

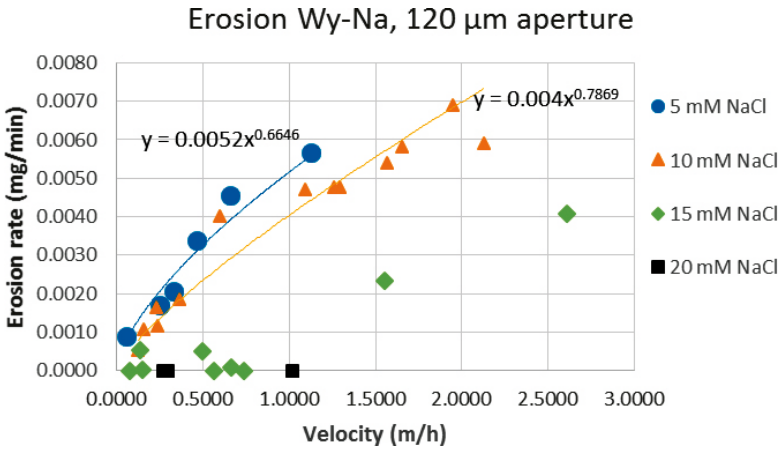

Figure 6-5. *Erosion of Wy-Na in an artificial fracture with aperture 120 µm. Salinity of the flowing solution was increased from 5 mM NaCl to 20 mM NaCl.*

After the salinity had been increased from 5 mM NaCl to 20 mM NaCl, we decided to test if erosion would commence at 10 mM NaCl as previously erosion ceased upon increasing the salinity from 10 mM NaCl to 15 mM NaCl. The salinity of the aqueous solution was first decreased to 15 mM NaCl before erosion measurements at 10 mM NaCl was started. Despite the fact that the erosion measurements were performed during a month's time, which is ample time for the clay to reach a new

Donnan equilibrium with the new solution (Birgersson and Karnland 2009, Hedström and Karnland 2012, Hsiao and Hedström 2015), there were no signs of erosion during any of the measurements. Therefore, the salinity was decreased to 5 mM NaCl. Yet again, there were no signs of erosion during the initial measurements. However, after 16 days, erosion commenced. The erosion measurements were continued during two months, in order to investigate whether erosion during this time period reaches the erosion at the initial 5 mM NaCl-measurements. Despite this, the erosion did not appear to approach the earlier erosion levels (Figure 6-6). It is of course possible that given enough time, the erosion will be similar whether the NaCl-concentration is increased from DI water, or decreased from a higher NaCl-concentration, but it is not obvious on this time scale. Consequently, there appears to be a considerable hysteresis effect, where the history of the clay sample play a significant role in the erosion of montmorillonite clay. This illuminates the difficulty in reaching conclusions as to the CCC, the phase behaviour or the erosion susceptibility of montmorillonite.

6.2.4 Comparison of erosion at different fracture apertures

Erosion measurements at an aperture of 240 µm commenced with DI water. When shifting to 5 mM NaCl solution, the change in erosion rate at low flows was marginal. Changing to 10 mM NaCl solution gave a noticeable reduction in erosion rates (Figure 6-7).

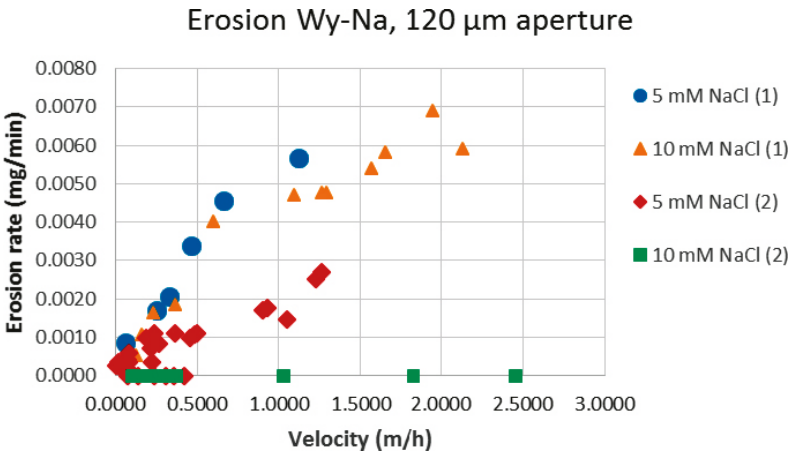

Figure 6-6. *Erosion rates vs flow velocity for the case where first the NaCl concentration in the flowing solution was increasing (1). After reaching 20 mM NaCl the concentration in the flowing solution was decreased (2).*

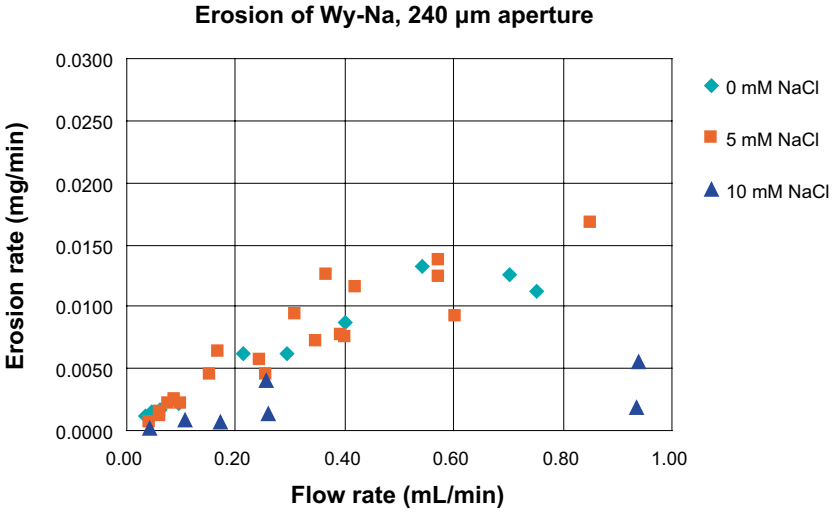

Figure 6-7. *Erosion of Wy-Na in an artificial fracture with aperture 240 µm. Salinity was increased from 0 mM NaCl to 10 mM NaCl.*

When we compare the erosion at different fracture apertures, we find that the erosion depends on the fracture aperture as well as salinity. One has to take into account that in Figure 6-8 the erosion rate is plotted against flow rate given as volume per time, thus at the same flow rate the flow velocity at the larger aperture is lower. Without any clay present the velocity would be precisely a factor two lower in the 240 µm fracture compared to the 120 µm fracture at the same flow rate. Due to larger extrusion of clay in the wider fracture (cf. Figure 6-2) the ratio in flow rate must be less than a factor two. The results in Figure 6-8 show that at 5 mM, erosion rate is larger in the wider fracture also taking velocity into account. However at 10 mM NaCl the erosion rates vs flow velocity are more or less the same for the two apertures. The extensive swelling in the case of 240 µm aperture (Figure 6-2) makes comparisons with the smaller aperture difficult. To have similar flow conditions in the both cases would require larger lateral dimensions of the artificial fracture at the larger aperture.

6.2.5 Erosion from Wy-Ca/Na (Wy-50/50)-horizontal fracture

The mixed Wy-Ca/Na was water saturated in a test cell over a period of 9 days after which the montmorillonite disk was transferred to the artificial fracture setup (aperture 120µm). The montmorillonite was contacted to DI and degassed water and was left to swell for 36 days under stagnant water conditions. The general free-swelling behaviour of Wy-50/50 is similar to Wy-Na (Figure 6-2), with the development of RTI fingers at interface to the water. After the free-swelling period DI water was flushed through the fracture to remove the sol. Then measurements of erosion under flowing conditions started using saline water with ionic strength from 1 mM to 20 mM. The ionic strength was set by NaCl but in order to avoid ion-exchange a small amount of $CaCl_2$ was added (1µM to 10 µM depending on the NaCl concentration).

The results for ionic strength up to 4 mM are presented in Figure 6-10. For ionic strengths up to 3 mM the erosion rates behave similarly with erosion increasing with flow velocity. At 4 mM the erosion is generally lower at all flow velocities. Furthermore, there is no trend between flow velocity and erosion rate. There are three outliers in the 4 mM results (flow velocity ~1.5 m/h and erosion rates ~0.009 mg/min). Those measurements were made in the beginning after switching from 3 mM to 4 mM solution and most likely reflects the behaviour of Wy-Ca/Na at 3 mM and are not representative for the equilibrium conditions at 4 mM. In general, the erosion rates at 4 mM scatter around 0.001 mg/min which are close to the lowest measured rates for Wy-Na at 5 and 10 mM NaCl (Figure 6-5), but in contrast to the results for Wy-Na the dependence on flow velocity is absent.

The erosion did not stop at 4 mM so further tests at higher ionic strengths were conducted. Most measured erosion rates at ionic strengths between 5 and 20 mM were about a factor of two lower than the rates at 4 mM, but not showing any clear trend with increasing ionic strength (Figure 6-11).

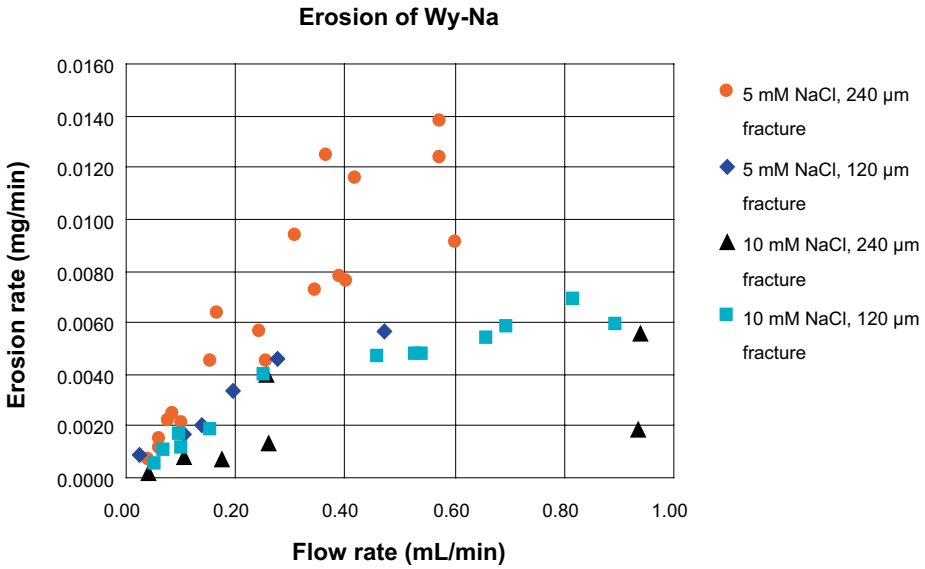

Figure 6-8. *Comparison of erosion rates of Wy-Na in artificial fractures with apertures 120 µm and 240 µm. Salinity was increased from 0 mM NaCl to 10 mM NaCl.*

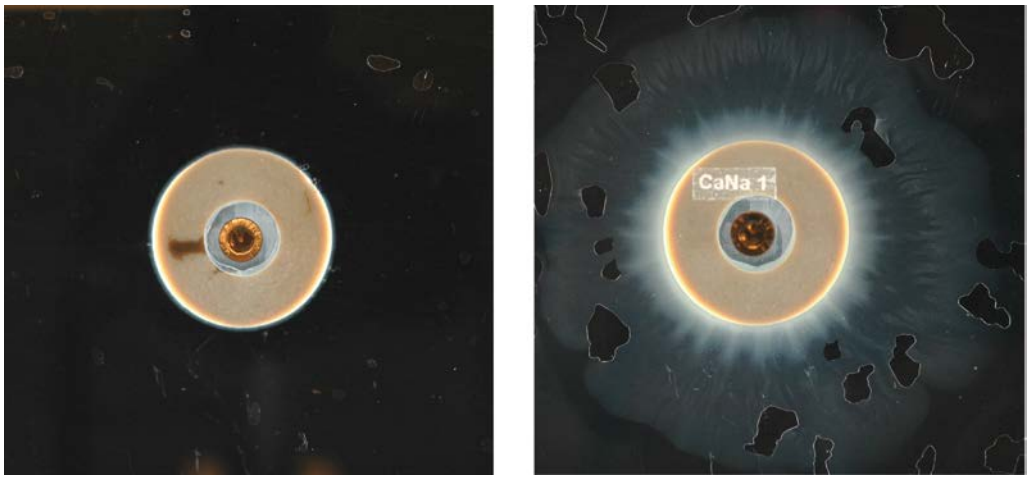

Figure 6-9. *Free swelling of Wy-50/50 in deionized water and aperture of 120 µm. Left: Initial state. Right: The state after 36 days. The gas bubbles visible in the right picture presumably originate from gas that was trapped around (above and under) the montmorillonite disk at installation.*

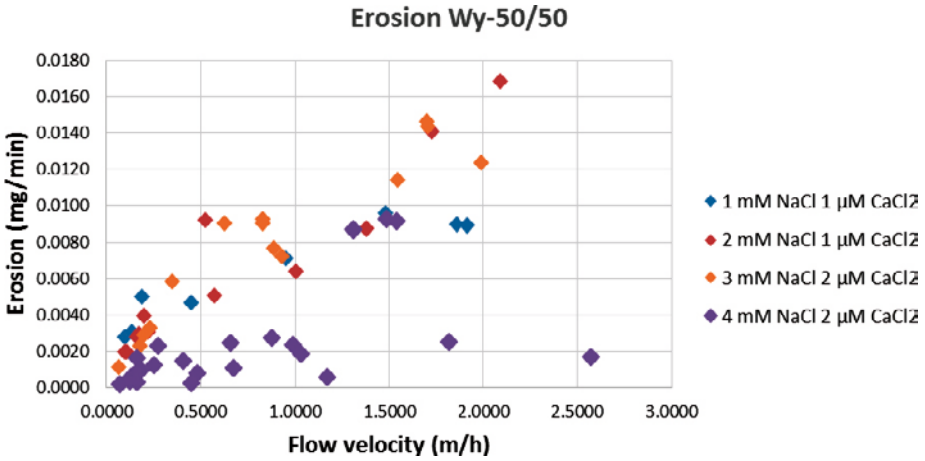

Figure 6-10. *Erosion of Wy-Ca/Na in an artificial fracture with aperture 120 µm. Salinity was increased from 1 mM NaCl to 4 mM NaCl. A small µM $CaCl_2$ concentration is included to prevent ion exchange during the tests.*

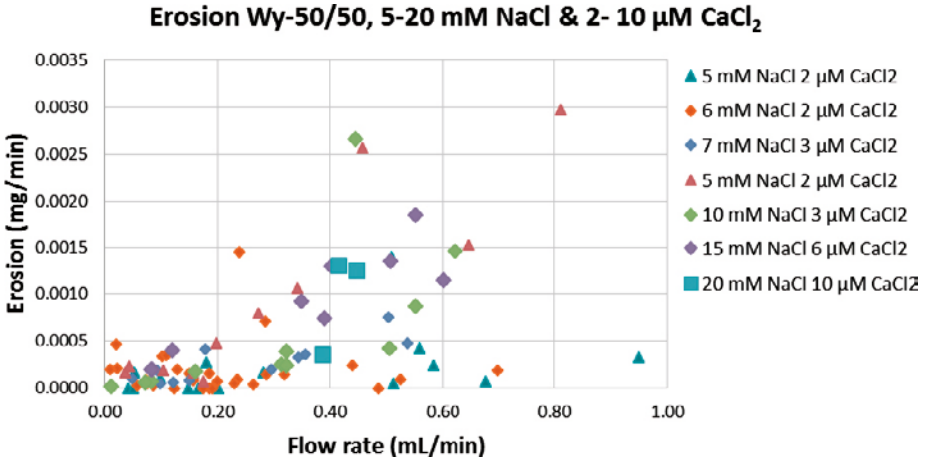

Figure 6-11. *Erosion of Wy-Ca/Na in an artificial fracture with aperture 120 µm. Salinity was changed according to the order in the legend. The lowest salinity was 5 mM and the highest 20 mM. A small µM $CaCl_2$ concentration is included to prevent ion exchange during the tests.*

Possibly, there is a tendency that erosion increases for ionic strengths beyond 7 mM. After the erosion measurements at 7 mM were completed the ionic strength was lowered to 5 mM. The erosion rates measured at 5 mM after this change were higher than the erosion rates measured after ionic strength was increased from 4 to 5 mM. After the second period of erosion measurements at 5 mM the ionic strength was increased to 10, 15 and finally 20 mM. Interestingly, erosion did not stop even at 20 mM NaCl and 10 µM $CaCl_2$.

At the lowest flow rates <0.2 ml/min (velocity ~0.5m/h) all the erosion measurements in Figure 6-11 gave erosion rates below 0.0005 mg/min. With a diameter of the clay paste (initial disk + extruded zone) of 6 cm the above erosion rates correspond to a unit erosion rate of 3.7×10^{-7} kg/m$^2 \cdot$ s. Under the assumption of a fracture aperture in the repository of 1 mm and a diameter of the clay paste of 2 m, the above unit erosion rate corresponds to an erosive mass loss <0.08 kg/yr. The highest erosion rate in Figure 6-11 is 0.003 mg/min, i.e., six times larger than the erosion rates for velocities below 0.5m/h.

Returning to the erosion rates at NaCl concentrations from 1 to 4 mM, further insights can be gained by re-evaluating the data underlying the plot in Figure 6-10. In Figure 6-12 the variation of clay concentration in the effluent with flow velocity is shown. The clay concentration decreases with increasing velocity. This suggests that the paste-to-sol transition rate limits the erosion rate. At the higher flow velocities the concentration drops as the transfer of clay from paste to sol cannot keep up with the increased flow.

One may estimate the amount of eroded material per unit time, R_{ero}, as

$$R_{ero} = vdaC_{clay}, \qquad (6\text{-}1)$$

where v is the flow velocity, d is the diameter of the clay region, a the fracture aperture and C_{clay} the clay concentration in the effluent volume that is limited by d (Figure 6-13). It is reasonable to assume that flowlines originating outside d do not interact with the clay, hence do not carry clay particles. Then that portion of the flow just dilute the clay concentration that is measured in the effluent. Thus C_{clay} is larger than the measured values (e.g., Figure 6-12) and can be obtained by multiplying the measured concentration by the lateral dimension (perpendicular to the flow) of the artificial fracture divided by d. In the case of 1 mM NaCl and the lowest velocity (0.097 m/h=850 m/year) in Figure 6-12, the diameter of the clay region, including the extruded portion, is 60 mm whereas the test cell width is 210 mm. C_{clay} is thus obtained multiplying the concentrations in Figure 6-12 by 21/6=3.5. At the lowest velocity the calculated C_{clay} is 0.24g/l. The unit erosion rate is evaluated to 65 kg/(m$^2 \cdot$ year). As seen in Figure 6-12 the clay concentration variation with flow velocity is well described with a power law. In the following we will argue that the calculated unit erosion rate is a pessimistic estimate as it is evaluated at a velocity that is at least an order of magnitude larger than realistic flow velocities in a repository during/after a glaciation.

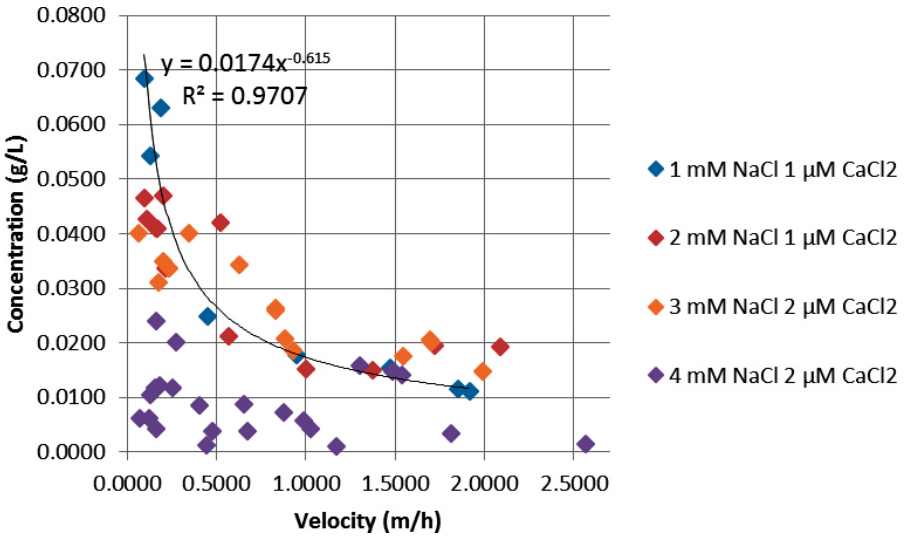

Figure 6-12. *Clay concentration in effluent as a function of flow velocity.*

When the flow velocity is reduced the clay concentration in the effluent is not increased by the same amount. For example assume the velocity is reduced by a factor of 100 the increase in clay concentration is just a factor of 16. R_{ero} in Equation (6-1) could in this case only remain unchanged provided that the diameter d is increased about six times. In the present set-up, the swelling into the fracture is about 1 cm and it is reasonable to assume that when the system is scaled-up to repository dimensions the swelling into the fracture is similar as in the small scale test, i.e., on the order of centimetres. At a flow velocity of 850 m/year the anticipated diameter of the clay paste surrounding the canisters is around 2 m. For the erosion rate to be unchanged the diameter must increase to 12 m. The tests presented here never show any expansion of the denser region (that appear bright in the photographs in Figure 6-2 and Figure 6-9) beyond 10–15 mm into the 120 µm fracture. In the case of stagnant Grimsel water simulant and horizontal fracture the clay loss due to expansion into the fracture was the same after 12 days as after 6 days suggesting that the swelling process slows down significantly (see below). An additional factor not taken into account in the discussion above is the viscosity increase of the sol with increasing concentration. This would further reduce erosion.

Hitherto, the clay concentration of the sol has been unknown. This concentration is not equivalent to C_{clay} above, because C_{clay} refers to the concentration in the effluent. To determine the clay concentration of the sol, which in this case refers to the erodible phase, Wy-Ca/Na were left to free-swell in DI water for 7 (two tests) to 9 (1 test) days and after each free-swelling period the fracture was flushed and the amount of eroded montmorillonite measured. By estimating the difference in area of the clay before and after flushing the fracture the volume of the eroded sol could be calculated (Figure 6-14). The three swelling-flushing sequences gave the sol concentrations 31, 32, and 34 g/l.

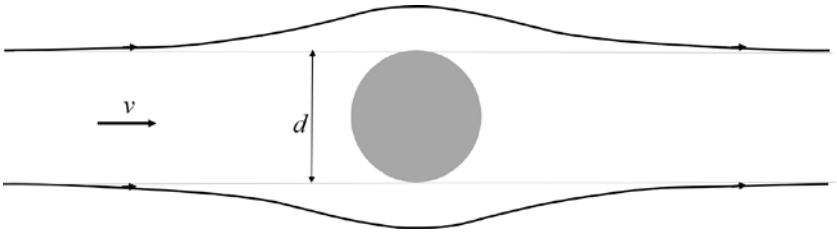

Figure 6-13. *Flowlines around a circular clay region. Presumably flowlines originating outside the diameter, d, do not interact with the clay.*

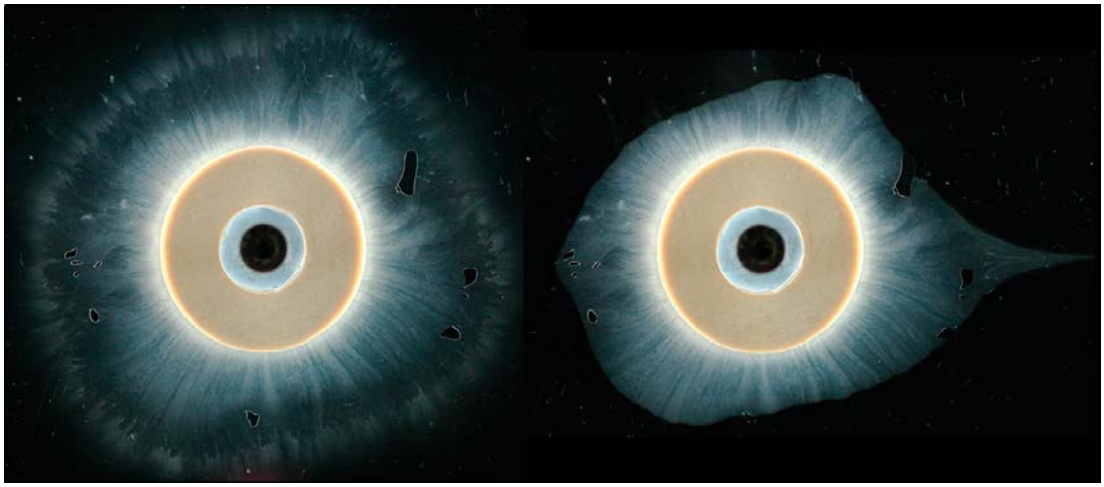

Figure 6-14. *Before (left) and after (right) flushing a Wy-Ca/Na that had been swelling in stagnant DI water for 6.75 days. The flushing lasted 14 minutes and 200 ml DI water flowed through the fracture.*

6.2.6 Wy-Ca/Na in contact with Grimsel water simulant in horizontal and sloped fractures

We let Grimsel water (0.7 mM NaCl and 0.14 mM $CaCl_2$ in this study) represent glacial/post glacial conditions. Figure 6-15 shows the results from erosion tests using Grimsel water together with the results from 1 mM NaCl. The erosion rates using Grimsel water and a horizontal fracture are comparable to the previous findings for 1 mM NaCl. The results at zero flow velocity were obtained in stagnant water over a period of several days. The eroded amount represent the sol surrounding the paste, and this material was collected by flushing the fracture for 15–30 minutes using high flow. The erosion rate at zero velocity was calculated by dividing the eroded mass with the time of free "expansion" (rather paste-to-sol transition). The total amount was ~8 mg both after 6 days of swelling and after 12 days. This suggests that the paste-to sol transition only progresses as long as the sol is removed. In stagnant water the sol is only diluted which is a diffusive process and therefore slow.

For a sloped fracture, the sol is constantly removed due to gravity. Note that the sol is a liquid phase of higher density than water and gravity acts on this liquid. This gives in the case of a 45 degree slope angle an erosion rate of an order of magnitude higher than the one measured after 12 days under stagnant conditions in a horizontal fracture. Specifically the unit erosion rate becomes 170 kg/(m^2 · year). Using the example above of a clay paste with diameter of 2 m and a fracture aperture of 1 mm, the erosion from a sloped fracture (slope angle 45 degrees) amounts to approximately 1 kg/yr under glacial water conditions. Perhaps an aperture of 50 µm would be a more realistic case for a repository. Then the buffer clay loss would be 20 times less, which over a 10 000 year period of glacial meltwater conditions would amount to 500 kg. In the above example the circumference was calculated using the equation for a circle to compare to the horizontal case. But if a fracture intersects a deposition hole at 45 degree angle then the minor axis is the same as that of the circle, i.e. 2 m while the major axis is $2\sqrt{2}$ m. This gives a circumference 1.2 times longer than that of the circle. Correcting the estimated buffer loss for this increase in circumference gives 600 kg over the 10 000 year period.

6.3 Conclusions

For Wy-Na we have confirmed the connection between the flow rate and the erosion, when the NaCl concentration is well below the CCC. As the salinity increases, erosion decreases. At an aperture of 120 µm, the erosion eventually ceases when the salinity in the system is 15 mM NaCl. For the aperture of 240 µm the test has not yet been performed above 10 mM but the tests at 10 mM NaCl indicate a clear reduction in erosion rate. In fact the erosion rates vs flow velocity are the same for 120 and 240 µm apertures at 10 mM NaCl, possibly indicating the formation of stable structures at that salinity. However, more data are needed to verify this and to rule out other explanations.

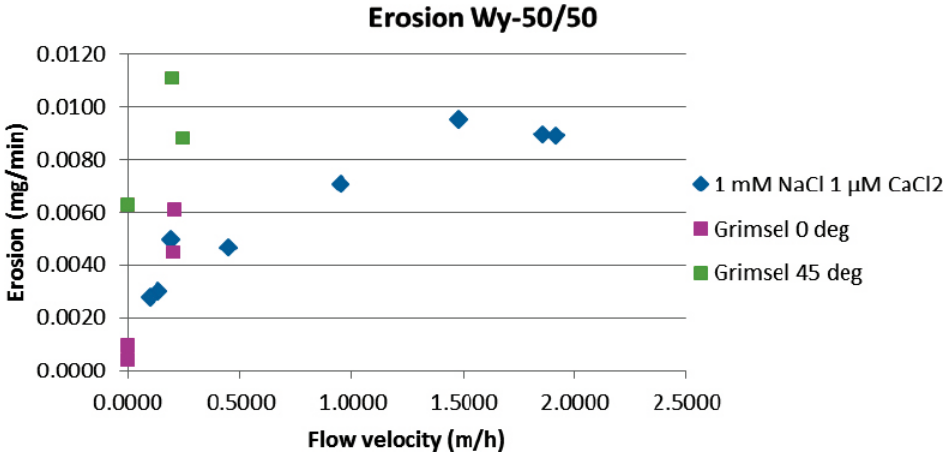

Figure 6-15. *Erosion of Wy-Ca/Na in an artificial fracture with aperture 120 µm. Grimsel water has ionic strength of 1.12 mM which is comparable to 1 mM NaCl.*

Furthermore for Wy-Na, we see a hysteresis effect present, that is, the history of the clay will affect the erosion capability of the clay. That means that a montmorillonite clay that erodes at a salinity of 10 mM NaCl, might be completely stable against erosion, if it has previously had a higher salinity present, during which the clay particles at the clay-solution interface could form a gel. This suggests that not only is control of the boundary conditions of importance for evaluating erosion rates; awareness of the system's history seems also crucial. An important finding in the present study is that swelling of Wy-Na into a 120 µm aperture fracture is limited when the fracture is filled with 20 or 25 mM NaCl(aq), i.e., at or above the concentration where a gel is formed. The extent of radial swelling was just 1–2 mm when the dry density of the emplaced montmorillonite was 1257 kg/m^3. This limited swelling is in line with modelling results based on empirical data of the relation between the density of MX-80 and the swelling pressure, the shear strength and the friction against a fracture surface (Birgersson et al. 2009).

Erosion in sloped fractures showed an order of magnitude larger erosion rates compared to those obtained using horizontal fractures. As long as the sol is removed from the paste-sol interface, erosion was found to progress under glacial water conditions. The erosion rate obtained using Wy-50/50 montmorillonite was found to be approximately 170 kg/(m^2 · year) in the case of stagnant conditions but 45 degree slope angle. Under horizontal conditions and a flow of 850 m/year the unit erosion rate was found to be 65 kg/(m^2 · year).

However, the extent of radial swelling over, e.g. a period of 10 000 years in a repository is uncertain. The tests presented here have never showed any expansion of the clay paste beyond 10–15 mm into the 120 µm fracture, even when the facture is filled with DI water. Based on these findings, we deem it justified to assume that the swelling in to the fracture in a repository would also be on the centimetre rather than metre scale. Therefore the diameter is taken to be 2 m in all the up-scaled estimates. Implicit in this assumption is that the density of the paste falls fairly steeply when it penetrates into the fracture so that the results obtained here with a montmorillonite dry density of ~ 1260 kg/m^3 will also be relevant to the actual buffer density. Models with (Birgersson et al. 2009) or without (Neretnieks et al. 2009) explicit friction between bentonite and fracture will arrive at rather different conclusions regarding the extent of swelling. Since the up-scaled erosion rates are proportional to the circumference of the paste-sol interface, gaining even more information regarding the extent of radial swelling with for example clay dry density is important if one wants to use lab-scale data for predicting erosion at the repository scale.

7 Overarching conclusions

In this report several studies aiming at understanding the phase behaviour of montmorillonite are reported. From the colloid erosion perspective, understanding the phase behaviour is central. Of the three main montmorillonite phases (paste, gel, and sol), colloid erosion is only likely to occur when the montmorillonite turn into a sol, which is liquid, and the transformation to a sol is linked to the aqueous chemistry of the groundwater. For homoionic Na-montmorillonite the sol phase is possible when the ionic strength (NaCl concentration) is below the CCC. For homoionic Ca-montmorillonite the sol phase is absent due to correlation forces. It was earlier demonstrated that about 20 % sodium was sufficient to balance the correlation forces and induce a break-up of Ca-montmorillonite aggregates (Birgersson et al. 2009, Hedström et al. 2011). In this study, we have further investigated this break-up behaviour by mixing suspensions of Na-montmorillonite with Ca and Mg-montmorillonite, using montmorillonite from three different origins (Wyoming; Milos, Greece; Kutch region, India). For both Wy- and Mi-montmorillonite the 20 % Na^+ limit is confirmed, while the Ku-80/20 montmorillonite show less break-up than the other two. This is also in accordance with the theory for correlation effects, which are stronger, the higher the CEC. The experiments also show that the break-up process is fast: within 10 minutes the turbidities of the mixed suspensions have stabilized. Furthermore, these experiments on break-up were performed using DI water thus showing that excess ions are not needed to mix the ions. Na^+ diffuses into the interlayer of the Ca-montmorillonite tactoids and Ca^{2+} diffuses out and eventually the all clay is a mixed Ca/Na-montmorillonite. We also showed that the process is similar for Mg/Na-montmorillonite.

A large part of the study has been devoted to increase the understanding of the gel state. From a theoretical perspective we have shown that standard DLVO theory for parallel layers is not applicable to smectite clays in low ϕ_c region where gels are formed. The van der Waals interaction (using a relevant Hamaker constant and a representative clay layer area) becomes weaker than thermal fluctuations at $\phi_c \approx 1/17$, while we herein have presented gels formed at $\phi_c \approx 1 \times 10^{-4}$. The only plausible force responsible for gelation of montmorillonite is electrostatic edge-to-face attraction. In order for modelling work on bentonite erosion under low salinity conditions to be relevant, this interaction must be included. Models based on DLVO for parallel layers cannot explain, e.g., the low CCC values that are found in experiments or the complex behaviour of the phase diagram.

We present new evidence that support the notion of positive edge charges and the spillover model, which states that at low salinity the spillover of the negative potential from the face to the edge creates a barrier for edge-to-face interaction. Above the CCC this barrier is overcome and the positive edge of one clay layer is discernible to a second clay layer.

Based on ideas from percolation theory we devised a heating experiment from which the enthalpy of edge-to-face bond formation was estimated. While no theory yet exists for how to incorporate edge-to-face interactions into a general model for bentonite expansion and erosion, knowing the magnitude of the "binding energy" could serve as a guideline for a simplified model beyond the parallel-layer DLVO treatment.

Rotating vane rheometry measurements on Kutch (Asha 505) gels show that the yield strengths are substantially higher than required to withstand the assumed shear stresses from flowing water in a repository. It is also important to note that these experiments were done on quite thin gels, 10 and 20 g montmorillonite per litre. The experimental phase diagrams presented in chapter 3 show that at the CCC, the repulsive paste-to-gel border is located between 40 to 60 g clay per litre. Between 10 and 20 g/l the yield strength seemed to approximately follow a ϕ_c^2 relation. Thus in a repository where the gel at the swelling front would be denser (at least 40 to 60 g/l) a significantly higher yield strength is expected than the ones for the 10 and 20 g/l gels. Our study also confirm the findings by others that aging increases the gel strength.

Combined with the study on repulsive Wy-Na and Wy-Ca/Na (50/50) pastes (Eriksson and Schatz 2015) we may conclude that mechanical erosion is not likely to occur from neither repulsive pastes nor gels. However, below the CCC there is a transition from the repulsive paste to sol which is exposed to erosion.

Erosion experiments using artificial fractures also demonstrate that material is lost when the ionic strength is below the CCC. This erosion occurs both under flowing conditions (horizontal fracture) or under stagnant water conditions provided that the fracture is sloped (in this study 45 degrees). The tests using Wy-Ca/Na (50/50) gave an order of magnitude larger erosion rates using sloped fracture compared to horizontal fracture. Assuming that the results from the laboratory tests can be scaled up (0.1 mm aperture and clay radius 3 cm) to repository condition (1 mm aperture and radius 1 m) the bentonite loss due to colloidal sol formation is approximately 1 kg/yr. As long as the sol is removed from the repulsive paste/sol interface the transition from paste to sol progresses and erosion continues. A factor that may lessen the impact of gravity would be accumulation of clay aggregates in uneven fractures. This has not been addressed with the planar fractures used in this study. Furthermore the rheological properties of an accumulation aggregates is unknown as well as the intrinsic stability of individual aggregates. The latter property is related to the strength of edge-to-face bonds as discussed in section 4.5.

The sol that is in quasi equilibrium with the repulsive paste appear as a dense liquid which is why it is so readily affected by gravity. The emergence of a Rayleigh-Taylor instability in the swelling tests under stagnant conditions is another manifestation of the liquid qualities of the sol. From observing this instability, there appears to be an interfacial tension between the sol and the DI water (this must also be a question of observation timescale since we know that clay and water is miscible and could form what we in chapter 3 term a gaseous sol). Clearly the montmorillonite layers in the dense sol interact. Presumably the interaction is again related to the positive edge charge, further highlighting the need to extend the theoretical study beyond regular DLVO based models. If low ionic strength (Grimsel like) is a possible future scenario, large bentonite loss due to colloidal sol formation cannot be ruled out. As suggested by this study, the rate-limiting factor for erosion is the repulsive paste to sol transfer rate and the rate by which the sol is removed. A deeper understanding of the paste/sol equilibrium appears to be crucial for a credible assessment of the erosion process under dilute water conditions.

Above the CCC there is no detectable erosion. This observation is also made under high pH conditions. The lowest CCC value found in this study was ~4 mM NaCl for Ku-Na, followed by 6 to 8 mM for Mi-Na. In contrast, the highest CCC value was found for Wy-Na at 20 mM NaCl. Presumably, under most of the operational time of the repository the aqueous conditions are above the CCC.

Acknowledgements

The research leading to these results has received funding from the European Atomic Energy Community‘s Seventh Framework Programme (FP7/2007-2011) under Grant Agreement no295487, the BELBaR project.

References

SKB's (Svensk Kärnbränslehantering AB) publications can be found at www.skb.com/publications.

Abend S, Lagaly G, 2000. Sol–gel transitions of sodium montmorillonite dispersions. Applied Clay Science 16, 201–227.

Alemán J V, Chadwick A V, He J, Hess M, Horie K, Jones R G, Kratochvíl P, Meisel I, Mita I, Moad G, Penczek S, Stepto R F T, 2007. Definitions of terms relating to the structure and processing of sols, gels, networks, and inorganic-organic hybrid materials (IUPAC Recommendations 2007). Pure and Applied Chemistry 79, 1801–1829.

Angelini R, Zaccarelli E, de Melo Marques F A, Sztucki M, Fluerasu A, Ruocco G, Ruzicka B, 2014. Glass–glass transition during aging of a colloidal clay. Nature Communications 5. doi:10.1038/ncomms5049

Atkins P W, de Paula J, 2006. Atkins' physical chemistry. 8th ed. Oxford: Oxford University Press.

Avena M J, Mariscal M M, De Pauli C P, 2003. Proton binding at clay surfaces in water. Applied Clay Science 24, 3–9.

Baghdadi H A, Parrella J, Bhatia S R, 2008. Long-term aging effects on the rheology of neat laponite and laponite–PEO dispersions. Rheologica Acta 47, 349–357.

Barnes H A, Nguyen Q D, 2001. Rotating vane rheometry – a review. Journal of Non-Newtonian Fluid Mechanics 98, 1–14.

Birgersson M, Karnland O, 2009. Ion equilibrium between montmorillonite interlayer space and an external solution – Consequences for diffusional transport. Geochimica et Cosmochimica Acta 73, 1908–1923.

Birgersson M, Börgesson L, Hedström M, Karnland O, Nilsson U, 2009. Bentonite erosion. Final report. SKB TR-09-34, Svensk Kärnbränslehantering AB.

Birgersson M, Hedström M, Karnland O, 2011. Sol formation ability of Ca/Na-montmorillonite at low ionic strength. Physics and Chemistry of the Earth, Parts A/B/C 36, 1572–1579.

Bratko D, Jönsson B, Wennerström H, 1986. Electrical double layer interactions with image charges. Chemical Physics Letters 128, 449–454.

Brindley G W, Brown G (eds), 1980. Crystal structures of clay minerals and their x-ray identification. London: Mineralogical Society.

Cadène A, Durand-Vidal S, Turq P, Brendlé J, 2005. Study of individual Na-montmorillonite particles size, morphology, and apparent charge. Journal of Colloid and Interface Science 285, 719–730.

Corezzi S, De Michele C, Zaccarelli E, Tartaglia P, Sciortino F, 2009. Connecting irreversible to reversible aggregation: time and temperature. Journal of Physical Chemistry B 113, 1233–1236.

Cummins H Z, 2007. Liquid, glass, gel: the phases of colloidal laponite. Journal of Non-Crystalline Solids 353, 3891–3905.

Dawson K A, 2002. The glass paradigm for colloidal glasses, gels, and other arrested states driven by attractive interactions. Current Opinion in Colloid & Interface Science 7, 218–227.

Delavernhe L, Steudel A, Darbha G K, Schäfer T, Schuhmann R, Wöll C, Geckeis H, Emmerich K, 2015. Influence of mineralogical and morphological properties on the cation exchange behavior of dioctahedral smectites. Colloids and Surfaces A: Physicochemical and Engineering Aspects 481, 591–599.

Delhorme M, Jönsson B, Labbez C, 2012a. Monte Carlo simulations of a clay inspired model suspension: the role of rim charge. Soft Matter 8, 9691–9704.

Delhorme M, Labbez C, Jönsson B, 2012b. Liquid crystal phases in suspensions of charged platelike particles. Journal of Physical Chemistry Letters 3, 1315–1320.

Dubois M, Zemb T, Belloni L, Delville A, 1992. Osmotic pressure and salt exclusion in electrostatically swollen lamellar phases. Journal of Physical Chemistry 96, 2278–2286.

Duc M, Gaboriaud F, Thomas F, 2005. Sensitivity of the acid–base properties of clays to the methods of preparation and measurement: 1. Literature review. Journal of Colloid and Interface Science 289, 139–147.

Eldridge J E, Ferry J D, 1954. Studies of the cross-linking process in gelatin gels. III. Dependence of melting point on concentration and molecular weight. Journal of Physical Chemistry 58, 992–995.

Eriksson R, Schatz T, 2015. Rheological properties of clay material at the solid/solution interface formed under quasi-free swelling conditions. Applied Clay Science 108, 12–18.

Evans D F, Wennerström H, 1999. The colloidal domain: where physics, chemistry, biology, and technology meet. 2nd ed. New York: Wiley-VCH.

Everett D H, 1972. Manual of symbols and terminology for physicochemical quantities and units, Appendix II: Definitions, terminology and symbols in colloid and surface chemistry. Pure & Applied Chemistry 31, 577–638.

Flory P J, 1941. Molecular size distribution in three dimensional polymers. I. Gelation. Journal of The American Chemical Society 63, 3083–3090.

Forsman J, 2004. A simple correlation-corrected Poisson–Boltzmann theory. Journal of Physical Chemistry B 108, 9236–9245.

Forsman J, 2009. Density functional theories of surface interactions in salt solutions. The Journal of Chemical Physics 130, 64901. doi:10.1063/1.3071195

Gabriel J-C P, Sanchez C, Davidson P, 1996. Observation of nematic liquid-crystal textures in aqueous gels of smectite clays. Journal of Physical Chemistry 100, 11139–11143.

Garcia-Lopez A C, Garcia-Rubio L H, 2008. Rayleigh-Debye-Gans as a model for continuous monitoring of biological particles: Part II, development of a hybrid model. Optics Express 16, 4671–4687.

Goh R, Leong Y-K, Lehane B, 2011. Bentonite slurries – zeta potential, yield stress, adsorbed additive and time-dependent behaviour. Rheologica Acta 50, 29–38.

Goodwin J W, 2009. Colloids and interfaces with surfactants and polymers. 2nd ed. Chichester: Wiley.

Greene-Kelly R, 1953. Irreversible dehydration in montmorillonte. Clay Minerals Bulletin 2, 52–56.

Grosberg A Y, Nguyen T T, Shklovskii B I, 2002. Colloquium: The physics of charge inversion in chemical and biological systems. Reviews of Modern Physics 74, 329–345.

Guldbrand L, Jönsson B, Wennerström H, Linse P, 1984. Electrical double layer forces. A Monte Carlo study. The Journal of Chemical Physics 80, 2221–2228.

Hackley V A, Ferraris C F, 2001. The use of nomenclature in dispersion science and technology. Washington, DC: U.S. Dept. of Commerce, Technology Administration, National Institute of Standards and Technology. (NIST Special Publication 960–3)

Hamley I W, 2007. Introduction to soft matter: synthetic and biological self-assembling materials, Rev. ed. Chichester: Wiley

Hansen E L, Hemmen H, Fonseca D M, Coutant C, Knudsen K D, Plivelic T S, Bonn D, Fossum J O, 2012. Swelling transition of a clay induced by heating. Scientific Reports 2. doi:10.1038/srep00618

Hedström M, Karnland O, 2011. Ca/Na selectivity coefficients from the Poisson–Boltzmann theory. Physics and Chemistry of the Earth, Parts A/B/C 36, 1559–1563.

Hedström M, Karnland O, 2012. Donnan equilibrium in Na-montmorillonite from a molecular dynamics perspective. Geochimica et Cosmochimica Acta 77, 266–274.

Hedström M, Birgersson M, Nilsson U, Karnland O, 2011. Role of cation mixing in the sol formation of Ca/Na-montmorillonite. Physics and Chemistry of the Earth, Parts A/B/C 36, 1564–1571.

Hetzel F, Doner H E, 1993. Some colloidal properties of beidellite; comparison with low and high charge montmorillonites. Clays and Clay Minerals 41, 453–460.

Hsiao Y-W, Hedström, M, 2015. Molecular dynamics simulations of NaCl permeation in bihydrated montmorillonite interlayer nanopores. The Journal of Physical Chemistry C 119, 17352–17361.

Huertas F J, Carretero P, Delgado J, Linares J, Samper J, 2001. An experimental study on the ion-exchange behavior of the smectite of Cabo de Gata (Almería, Spain): FEBEX bentonite. Journal of Colloid and Interface Science 239, 409–416.

Iwata S, Tabuchi T, Warkentin B P, 1994. Soil–water interactions: mechanisms and applications. 2nd ed. New York: M. Dekker.

Jabbari-Farouji S, Tanaka H, Wegdam G H, Bonn D, 2008. Multiple nonergodic disordered states in laponite suspensions: a phase diagram. Physical Review E 78, 61405. doi:10.1103/PhysRevE.78.061405

Jabbari-Farouji S, Wegdam G H, Bonn D, 2012. Aging of rotational diffusion in colloidal gels and glasses. Physical Review E 86, 41401. doi:10.1103/PhysRevE.86.041401

Jenny H, Reitemeier R F, 1935. Ionic exchange in relation to the stability of colloidal systems. Journal of Physical Chemistry 39, 593–604.

Jönsson B, Labbez C, Cabane B, 2008. Interaction of nanometric clay platelets. Langmuir 24, 11406–11413.

Jönsson B, Åkesson T, Jönsson B, Meehdi S, Janiak J, Wallenberg R, 2009. Structure and forces in bentonite MX-80. SKB TR-09-06, Svensk Kärnbränslehantering AB.

Kahn A, 1958. The flocculation of sodium montmorillonite by electrolytes. Journal of Colloid Science 13, 51–60.

Karnland O, Olsson S, Nilsson U, 2006. Mineralogy and sealing properties of various bentonites and smectite-rich clay material. SKB TR-06-30, Svensk Kärnbränslehantering AB.

Kjellander R, 1988. Inhomogeneous Coulomb fluids with image interactions between planar surfaces. II. On the anisotropic hypernetted chain approximation. The Journal of Chemical Physics 88, 7129–7137.

Kjellander R, Marčelja S, 1984. Correlation and image charge effects in electric double layers. Chemical Physics Letters 112, 49–53.

Kjellander R, Marčelja S, Quirk J, 1988. Attractive double-layer interactions between calcium clay particles. Journal of Colloid and Interface Science 126, 194–211.

Kjellander R, Lyubartsev A P, Marčelja S, 2001. McMillan–Mayer theory for solvent effects in inhomogeneous systems: calculation of interaction pressure in aqueous electrical double layers. The Journal of Chemical Physics 114, 9565–9577.

Knaebel A, Bellour M, Munch J-P, Viasnoff V, Lequeux F, Harden J L, 2000. Aging behavior of laponite clay particle suspensions. Europhysics Letters (EPL) 52, 73–79.

Labanda J, Llorens J, 2008. Effect of aging time on the rheology of laponite dispersions. Colloids and Surfaces A: Physicochemical and Engineering Aspects 329, 1–6.

Lagaly G, Ziesmer S, 2003. Colloid chemistry of clay minerals: the coagulation of montmorillonite dispersions. Advances in Colloid and Interface Science 100–102, 105–128.

Li W, Persson B A, Morin M, Behrens M A, Lund M, Zackrisson Oskolkova M, 2015. Charge-induced patchy attractions between proteins. Journal of Physical Chemistry B 119, 503–508.

Liu Y, Pandey R B, 1996. Sol–gel phase transitions in thermoreversible gels: onset of gelation and melting. The Journal of Chemical Physics 105, 825–836.

Martin C, Pignon F, Magnin A, Meireles M, Lelièvre V, Lindner P, Cabane B, 2006. Osmotic compression and expansion of highly ordered clay dispersions. Langmuir 22, 4065–75.

Martin C, Pignon F, Piau J-M, Magnin A, Lindner P, Cabane B, 2002. Dissociation of thixotropic clay gels. Physical Review E 66, 21401. doi:10.1103/PhysRevE.66.021401

Messina R, 2009. Electrostatics in soft matter. Journal of Physics: Condensed Matter 21, 113102. doi:10.1088/0953-8984/21/11/113102

Michot L J, Bihannic I, Porsch K, Maddi S, Baravian C, Mougel J, Levitz P, 2004. Phase diagrams of Wyoming Na-montmorillonite clay. Influence of particle anisotropy. Langmuir 20, 10829–10837.

Mongondry P, Nicolai T, Tassin J-F, 2004. Influence of pyrophosphate or polyethylene oxide on the aggregation and gelation of aqueous laponite dispersions. Journal of Colloid and Interface Science 275, 191–196.

Mongondry P, Tassin J F, Nicolai T, 2005. Revised state diagram of laponite dispersions. Journal of Colloid and Interface Science 283, 397–405.

Mourad M C D, Byelov D V, Petukhov A V, Lekkerkerker H N W, 2008. Structure of the repulsive gel/glass in suspensions of charged colloidal platelets. Journal of Physics: Condensed Matter 20, 494201. doi:10.1088/0953-8984/20/49/494201

Mourchid A, Delville A, Lambard J, LeColier E, Levitz P, 1995. Phase diagram of colloidal dispersions of anisotropic charged particles: equilibrium properties, structure, and rheology of laponite suspensions. Langmuir 11, 1942–1950.

Mourchid A, Lécolier E, Van Damme H, Levitz P, 1998. On viscoelastic, birefringent, and swelling properties of laponite clay suspensions: revisited phase diagram. Langmuir 14, 4718–4723.

Neretnieks I, Liu L, Moreno L, 2009. Mechanisms and models for bentonite erosion. SKB TR-09-35, Svensk Kärnbränslehantering AB.

Newman A C D, Brown G, 1987. The chemical constitution of clays. In Newman A C D (ed). Chemistry of clays and clay minerals. Harlow: Longman, 1–128.

Nishinari K, 2009. Some thoughts on the definition of a gel. In Masayuki T, Nishinari K (eds). Gels: structures, properties, and functions. Berlin: Heidelberg. (Progress in Colloid and Polymer Science 136), 87–94.

Norrish K, 1954. The swelling of montmorillonite. Discussions of the Faraday Society 18, 120–134.

Pashley R M, Israelachvili J N, 1984. Molecular layering of water in thin films between mica surfaces and its relation to hydration forces. Journal of Colloid and Interface Science 101, 511–523.

Permien T, Lagaly G, 1994. The rheological and colloidal properties of bentonite dispersions in the presence of organic compounds III. The effect of alcohols on the coagulation of sodium montmorillonite. Colloid and Polymer Science 272, 1306–1312.

Ploehn H J, Liu C, 2006. Quantitative analysis of montmorillonite platelet size by atomic force microscopy. Industrial & Engineering Chemistry Research 45, 7025–7034.

Posiva, 2012. Safety case for the disposal of spent nuclear fuel at Olkiluoto – Performance Assessment 2012. Posiva 2012-4, Posiva Oy, Finland.

Quirk J P, Marčelja S, 1997. Application of double-layer theories to the extensive crystalline swelling of Li-montmorillonite. Langmuir 13, 6241–6248.

Russel W B, Saville D A, Schowalter W R, 1992. Colloidal dispersions. Cambridge: Cambridge University Press.

Ruzicka B, Zaccarelli E, 2011. A fresh look at the laponite phase diagram. Soft Matter 7, 1268–1286.

Ruzicka B, Zulian L, Ruocco G, 2004. Routes to gelation in a clay suspension. Physical Review Letters 93, 258301. doi:10.1103/PhysRevLett.93.258301

Ruzicka B, Zulian L, Ruocco G, 2005. More on the phase diagram of laponite. Langmuir 22, 1106–1111.

Ruzicka B, Zulian L, Ruocco G, 2007. Ageing dynamics in laponite dispersions at various salt concentrations. Philosophical Magazine 87, 449–458.

Ruzicka B, Zulian L, Angelini R, Sztucki M, Moussaïd A, Ruocco G, 2008. Arrested state of clay-water suspensions: gel or glass? Physical Review E 77, 20402. doi:10.1103/PhysRevE.77.020402

Ruzicka B, Zulian L, Zaccarelli E, Angelini R, Sztucki M, Moussaïd A, Ruocco G, 2010. Competing interactions in arrested states of colloidal clays. Physical Review Letters 104, 85701. doi:10.1103/PhysRevLett.104.085701

Ruzicka B, Zaccarelli E, Zulian L, Angelini R, Sztucki M, Moussaïd A, Narayanan T, Sciortino F, 2011. Observation of empty liquids and equilibrium gels in a colloidal clay. Nature Materials 10, 56–60.

Sciortino F, Tartaglia P, 2005. Glassy colloidal systems. Advances In Physics 54, 471–524.

Sciortino F, Zaccarelli E, 2011. Reversible gels of patchy particles. Current Opinion in Solid State and Materials Science 15, 246–253.

Secor R B, Radke C J, 1985. Spillover of the diffuse double layer on montmorillonite particles. Journal of Colloid and Interface Science 103, 237–244.

Segad M, Jönsson B, Cabane B, 2012. Tactoid formation in montmorillonite. The Journal of Physical Chemistry C 116, 25425–25433.

Shahin A, Joshi Y M, 2010. Irreversible aging dynamics and generic phase behavior of aqueous suspensions of laponite. Langmuir 26, 4219–4225.

Shainberg I, Kaiserman A, 1969. Kinetics of the formation and breakdown of Ca-montmorillonite tactoids. Soil Science Society of America Journal 33, 547–551.

Shalkevich A, Stradner A, Bhat S K, Muller F, Schurtenberger P, 2007. Cluster, glass, and gel formation and viscoelastic phase separation in aqueous clay suspensions. Langmuir 23, 3570–3580.

SKB, 2006. Long-term safety for KBS-3 repositories at Forsmark and Laxemar – a first evaluation. Main report of the SR-Can project. SKB TR-06-09, Svensk Kärnbränslehantering AB.

SKB, 2011. Long-term safety for the final repository for spent nuclear fuel at Forsmark. Main report of the SR-Site project. SKB TR-11-01, Svensk Kärnbränslehantering AB.

Smith D E, Wang Y, Chaturvedi A, Whitley H D, 2006. Molecular simulations of the pressure, temperature, and chemical potential dependencies of clay swelling. The Journal of Physical Chemistry B 110, 20046–20054.

Stockmayer W H, 1943. Theory of molecular size distribution and gel formation in branched-chain polymers. The Journal of Chemical Physics 11, 45–55.

Swartzen-Allen S L, Matijevic E, 1976. Colloid and surface properties of clay suspensions. III. Stability of montmorillonite and kaolinite. Journal of Colloid and Interface Science 56, 159–167.

Tanaka H, Meunier J, Bonn D, 2004. Nonergodic states of charged colloidal suspensions: repulsive and attractive glasses and gels. Physical Review E 69, 31404. doi:10.1103/PhysRevE.69.031404

Thießen P A, 1947. Kennzeichnung submikroskopischer Grenzflächenbereiche verschiedenartiger Wirksamkeit. Zeitschrift für anorganische Chemie 253, 161–169.

Tombácz E, Szekeres M, 2004. Colloidal behavior of aqueous montmorillonite suspensions: the specific role of pH in the presence of indifferent electrolytes. Applied Clay Science 27, 75–94.

Trappe V, Sandkühler P, 2004. Colloidal gels – low-density disordered solid-like states. Current Opinion in Colloid & Interface Science 8, 494–500.

Van Olphen H, 1977. An introduction to clay colloid chemistry: for clay technologists, geologists and soil scientists. 2nd ed. New York: Wiley.

Verwey E J W, Overbeek J T G, 1948. Theory of the stability of lyophobic colloids: the interaction of sol particles having an electric double layer. New York: Elsevier.

Wang Z, Liu L, Neretnieks I, 2011. A novel method to describe the interaction pressure between charged plates with application of the weighted correlation approach. The Journal of Chemical Physics 135, 244107. doi:10.1063/1.3672001

Wennerström H, Jönsson B, Linse P, 1982. The cell model for polyelectrolyte systems. Exact statistical mechanical relations, Monte Carlo simulations, and the Poisson–Boltzmann approximation. The Journal of Chemical Physics 76, 4665–4670.

Witten T A, Pincus P A, 2010. Structured fluids: polymers, colloids, surfactants. Oxford: Oxford University Press.

Zaccarelli E, 2007. Colloidal gels: equilibrium and non-equilibrium routes. Journal of Physics: Condensed Matter 19, 323101. doi:10.1088/0953-8984/19/32/323101

Zhang T H, Groenewold J, Kegel W K, 2009. Observation of a microcrystalline gel in colloids with competing interactions. Physical Chemistry Chemical Physics 11, 10827–10830.

Ziman J M, 1979. Principles of the theory of solids. 2nd ed. Cambridge: Cambridge University Press,.

Zou J, Pierre A C, 1992. Scanning electron microscopy observations of "card-house" structures in montmorillonite gels. Journal of Materials Science Letters 11, 664–665.

Arkitektkopia AB, Bromma, 2016

SKB is tasked with managing Swedish nuclear and radioactive waste in a safe way.

skb.se